Journal of Science & Technology in the Tropics

Volume 2 Number 1 June 2006

JOSTT

DEDICATED TO THE ADVANCEMENT OF SCIENCE AND TECHNOLOGY RELATED TO THE TROPICS

Journal of Science & Technology in the Tropics

AKADEMI SAINS MALAYSIA

COSTAM

Volume 2 Number 1
June 2006
ISSN 1823-5034

Journal of Science & Technology in the Tropics Volume 2 Number 1 2006

CONTENTS

Journal of Science and Technology in the Tropics (2006) **2**: 9-15

Determination of vitamin E and fatty acid contents in food served at an army training centre

S. Suzana[1], L. Saptuyah[1], H. Hasnah[1], M. S. Siti Zuraini[2], S. Norshafarina[2], M. Jamaludin[2] and K. Sundram[3]

[1]Department of Nutrition and Dietetics, Faculty of Allied Health Sciences, Universiti Kebangsaan Malaysia, Jalan Raja Muda Abdul Aziz, 50300 Kuala Lumpur, Malaysia

[2]Department of Biomedical Sciences, Faculty of Allied Health Sciences, Universiti Kebangsaan Malaysia, Jalan Raja Muda Abdul Aziz, 50300 Kuala Lumpur, Malaysia

[3]Division of Nutrition, Malaysian Palm Oil Board, Bandar Baru Bangi, 43000 Kajang, Selangor, Malaysia

Abstract A study was conducted to determine the vitamin E content and fatty acids composition in foods served in a cafeteria of an army training centre in Malaysia. A total of 22 food samples from a one day menu in July and October was purposely sampled and analysed for their vitamin E and fatty acid contents using High Performance Liquid Chromatography and Gas Chromatography methods, respectively. The adequacy of dietary intake of these nutrients among 84 trainees was also assessed from a one-day food record. The vitamin E and fatty acid intake derived from the food analysis was compared to values obtained from the food composition tables (FCT). The content of vitamin E in the food samples varied from 0 mg in cooked rice to 11.76 mg in 'asam pedas' fish (mackerel). The predominant saturated fatty acid (SFA), monounsaturated fatty acid (MUFA) and polyunsaturated fatty acid (PUFA) in the food samples were palmitic, oleic and linoleic acids, respectively. Percentage of SFA, MUFA and PUFA as calculated using food analysis to total energy intake was 6.2%, 6.0% and 2.0%, respectively.. The comparative figure estimated using FCT was 12.1%, 8.3% and 3.0%, respectively. These figures did not meet the Recommended Nutrient Intake (RNI). The vitamin E intake was 11.68 mg/d (food analysis) and 8.37 mg/d (FCT). Approximately 20% and 85% of subjects did not meet the RNI for vitamin E, based on food analysis and FCT, respectively. In conclusion, the intake of both vitamin E and fatty acids of the subjects were not satisfactory. Furthermore, vitamin E intake may be underestimated if based on the food composition alone.

Keywords fatty acids – vitamin E – dietary intake – army trainees

INTRODUCTION

Vitamin E is a lipid-soluble, chain breaking antioxidant that prevents the propagation of free radical reaction and lipid peroxidation [1]. Fatty acids play an important role as the major component in human cells and as a source of energy during strenuous exercises [2]. Vitamin E with other mineral like zinc is important for sustaining the soldiers during metabolic stress [3]. Intensive exercise or heavy physical activity can induced lipid peroxidation and lead to oxidative stress that will damage the body tissue and cells [4]. A study conducted among Thai soldiers showed that supplementation of antioxidant at high dosage was beneficial in reducing the lipid peroxidation in red blood cells and also plasma [4]. In Malaysia, antioxidant status among soldiers has not been reported, however, sub-clinical vitamin E deficiency has been detected among rural elderly Malays (27%), especially men [5]. Fatty acids act as energy source during intensive and heavy physical activity that leads to the reduction in free fatty acids in plasma [6]. The amount and the quality of fats consumed from diet are related to several disorders and diseases such as coronary heart disease [7], obesity [8] and certain cancers [9].

In Malaysia, a few studies have been carried out among army trainees to determine physical activity level, basal metabolic rate and energy requirement [10], but not vitamin E and fatty acids intake. Studies on determination of fatty acid compositions and vitamin E in food are rather limited. Furthermore, the Malaysian Food Composition Tables [11] do not have values for vitamin E and only provide composition of fatty acids for only 44 types of foods. Therefore, this study was aimed to determine the content of vitamin E and fatty acid contents in selected foods and to assess the adequacy of intake among army trainees.

MATERIALS AND METHODS

Study design

A total of 84 army trainees from a training centre in Port Dickson, Malaysia were invited to participate in the study. The inclusion criteria were aged 18 to 30 years, healthy with no known chronic diseases, physically active and participate in the training programme at the centre. Individuals who smoked, drank alcohol, took vitamin and mineral supplement and herbal or traditional medicine were excluded from the study. Subjects were asked to fill up a standard questionnaire on socio-demographic and health status. Data on dietary intake was obtained through a one-day food record. In addition, the anthropometric indices such as weight, height and body composition using body impedance (Maltron 916, UK) were also measured. The study is part of a larger study to determine the efficacy of antioxidant supplementation on red blood cells and plasma among army trainees. The study has been approved by the Research and Ethical Committee of the Medical Faculty, Universiti Kebangsaan Malaysia (FF-022-2003).

Food sampling

Twenty-two food samples served at the training centre's cafeteria were collected in triplicates and stored at -20 °C prior to analysis, but some samples were in duplicates from a one-day menu. The food samples were classified into six groups namely, cereal and cereal products, fats, eggs and poultry, fish, vegetable and fruit and miscellaneous. The samples were analysed for their vitamin E and fatty acids compositions.

Preparation of sample

Total lipid was extracted by refluxing with chloroform-methanol 2:1 (v/v) according to the method of Folch *et al.* [12]. For the determination of vitamin E, 1 mL of hexane was added into the lipid extract weighing ± 0.1g and vortexed. Hexane (5 mL) was added into the lipid extract weighing 0.2-0.5g and vortexed. Vortexed sample (1 mL) was pipetted into microtube and centrifudged for 2 minutes at 3000 rpm. Upper layer (1 mL) of the centrifudged sample was pipetted into the vial autosampler. About 20-50 L sample from the vial was injected into the HPLC system. For determination of fatty acids compositions, 100 uL of lipid extracts was diluted with 1mL of hexane in a microtube. 5M Natrium methylate (100 uL) was added into the solution to produce fatty acids methyl ester (FAME) and centrifudged at 3000 rpm for 2 minutes. About 1 mL from the upper layer of solution was pipetted into the vial and placed in the autosampler GC. GC was programmed to inject a volume of 1 uL into the GC system.

Determination of total fat, fatty acids and vitamin E

The following nutrients were quantified: total fat, saturated fatty acids (SFA): C8-C22; monounsaturated fatty acids (MUFA): C16:1-C20:1; polyunsaturated fatty acids (PUFA): C18:2-C18:3, tocopherol and tocotrienols isomer. Fatty acid compositions in food samples were analysed by gas chromatography (GC) using capillary columns following the AOCS Official Method Ce 1-62 [13]. The analyses were performed using a Perkin Elmer Autosystem and Shimadzu model 2010 (Shimadzu, Japan) with FID detector. The Perkin Elmer Autosystem (Perkin Elmer, Inc. USA) with Turbochrome software equipped with capillary column of 105 m x 0.25 mm x 0.20 µm (Restex corp., USA) and helium as carrier gas. Whereas, Shimadzu chromatograph equipped with 30 mm x 0.25 mm x 0.20 µm (Supelco) (Shimadzu, Japan) capillary column and the carrier gas was nitrogen. GC parameters: Column (Oven) temperature programme (100 - 160 °C, Rate 3°C/minute, 160 - 240 °C, Rate 3°C/ minute) injection 250 °C, detector 260 °C, split on 100:1 and carrier gas pressure was 40 psi. Identification was based on the retention times of the following references oils AOCS RM3, AOCS RM6, 19 and 37 components FAME Mix (Supelco, USA). Quantification was based on percent of peak area.

Vitamin E (tocopherol and tocotrienol) were analyzed using chromatographic system, HPLC, Agilent Technoloies model 1100 with Chemstation software based on the AOCS Official Method Ce 8-89 [14]. Two

normal phase columns connected in series. The columns are Zorbax RX-Sil; 250 x 4.6 mm, 5 micron from Agilent Technologies (Agilent Technologies M, Corp, USA) and using a fluorescent detector. Mobile phase used was isocratic-hexane:IPA in a ratio of 99.5:0.5 using flow rate at 2 mL/minute. Peaks shown on chromatograms of test samples were identified by matching their retention times against standards and reference mix. Tocopherol standards were purchased from Merck KgaA (Germany) and Sigma Co. (St. Louis, USA). MPOB's tocotrienol-rich fraction was used as a reference for tocotrienols.

Assessment of daily fatty acids and vitamin E intake

Dietary assessment was carried out using a one-day dietary record filled up by the subjects on the same day when the food samples being taken. The subjects were instructed to estimate the food portions using household measurements. The food portions in the dietary record were converted into grams and computed for total nutrient intake using nutrient compositions derived from the food samples analysis and also those from the UK Food Composition Tables for vitamin E [15] and the Malaysian Food Composition Tables for fatty acid compositions [11]. Data obtained were analysed using the Statistical Package for Social Sciences Version 12.0.

RESULTS AND DISCUSSION

Eighty four newly recruited male army trainees, predominantly Malays (92.8%), volunteered to participate in the study. Their age were 18-23 years, body mass index (BMI) 20.9 ± 1.82 kg/m^2, percentage of body fat was 21.2 ± 3.3 % and lean body mass 46.4 ± 4.4 kg. The nutritional status was good, with 83% fell into the normal category of body weight (BMI 18.5 to 24.9 kg/m^2) [16]. The percentage of coefficient variation (CV%) for vitamin E analysis for most samples was below 10%, with the exception of eight food samples. This was probably due to the little amount of vitamin E present in those foods. The accepted values for CV% for fatty acids analysis is as follows: less than 5% if the amount of fatty acid is more than 10% from

Table 1. Composition of saturated fatty acids in selected foods.

Type of food	n	Saturated Fatty Acids (SFA) (%)							
		Caprilic C 8:0	CapricC 10:0	Lauric C 12:0	Myristic C 14:0	Palmitic C 16:0	Stearic C 18:0	Arachidic C 20:0	Behenic C 22:0
A. Cereal & grain product									
Chicken rice (rice only) (N1)	2	1.1	0.8	-	0.7	27.5	4.2	-	-
Chicken rice (N2)	3	0.05	0.05	0.7	1.0	38.8	3.7	0.2	0.04
Nasi lemak	3	1.3	1.0	9.4	3.9	20.9	4.0	0.6	0.1
White bread	2	-	-	-	0.8	42.1	8.9	0.3	-
Bun	3	0.3	0.3	6.4	2.8	37.3	3.3	0.2	0.04
Fried mee hoon	3	0.01	0.01	0.2	0.7	38.1	3.6	0.3	0.04
B. Fat									
Mix butter with jem	2	0.2	0.2	2.4	1.7	43.5	4.4	0.3	-
C. Egg & poultry									
Scramble egg	2	-	-	0.3	0.8	38.1	5.3	0.3	0.6
Fried chicken	3	0.01	0.02	0.2	0.8	28.8	4.4	0.2	0.5
Chicken kurma	3	0.02	0.02	8.3	0.8	31.4	3.8	0.3	0.1
D. Fish									
Fried mackerel with soy sauce	3	0.1	-	0.2	1.4	38.6	5.1	0.3	0.5
Fried mackerel with 'taucu'	2	-	-	0.4	1.1	40.5	4.3	0.4	-
Fried mackerel 'asam pedas'	2	-	-	0.4	1.1	40.9	4.2	0.3	-
E. Vegetables & Fruit									
Fried swamp cabbage	3	0.04	0.02	0.3	1.1	38.0	4.5	0.3	-
Bean sprouts in coconut milk	2	6.7	5.2	40.2	15.3	13.7	3.0	-	-
Mix vegetable asam pedas	2	-	-	0.4	1.1	40.7	4.3	0.3	-
Cucumber	2	-	-	-	1.0	38.2	4.5	0.3	-
Star fruit	2	-	-	-	0.7	20.1	2.5	0.5	-
F. Miscellanous									
Soy sauce	2	-	-	0.3	0.8	34.7	4.2	0.4	-
Ketchup	2	-	-	0.4	1.0	19.4	3.1	0.6	-
Soup	2	-	-	0.3	0.8	27.4	4.1	-	-

the total fat content; 5-10% if the amount of fatty acid is between 1 to 10% from the total fat content and more than 10% for fatty acid with content less than 1% from the total fat content [17]. The CV% for the fatty acids analysis in this study are close to the acceptable range, i.e. 5.46%, 7.55% and 10.72% for fatty acid content of more than 10%, 1 to 10% and less than 1%, respectively from the total fat in food samples.

As shown in Table 1, the predominant saturated fatty acid was palmitic acid (C 16:0) which existed in chicken rice (N2), white bread, scramble egg, fried mackerel cooked with soy sauce, fried mackerel cooked with 'taucu' and fried mackerel 'asam pedas', fried swamp cabbage and mix vegetable 'asam pedas' (38% - 42% of palmitic acid). Food sample of margarine and jam contained the highest amount of palmitic acid (43.5%). The high composition of palmitic acid was due to the usage of palm oil in cooking or food. Palm oil contains 43% of palmitic acid [18]. It is interesting to note that white bread also contained a substantial amount of palmitic acid, possibly due to fat source from palm oil used in its processing.

Stearic acid only accounted for 3 to 8% of fatty acid. Coconut rice (nasi lemak), chicken kurma and bean sprouts cooked in coconut milk contained a higher amount of lauric acid (C12:0) and myristic acid (C14:0) as compared in other foods. This is because coconut milk is already high in these types of fatty acids [19].

Epidemiological studies showed that palmitic, lauric and myristic acids might increase the cholesterol level in human body [20], with myristic acid being the most potent [21]. However, myristic acid was found to increase both LDL and HDL cholesterols in healthy individuals [22]. Palmitic acid would not necessarily result in hypercholesterolimic effect as it depended on the source of palmitic acid and LDL receptor's set point of individuals. Palmitic acid is neutral if the amount of cholesterol intake from the diet is less than 300 mg/day or if the LDL receptor's activity is not standardized [23, 24)

As shown in Table 2, oleic acid (C18:1) was the most dominant MUFA in all food samples. Linoleic acid (C18:2) was high in soya sauce, white bread and all fried dishes, while, the other PUFA and MUFA fatty

Table 2. Composition of monounsaturated and polyunsaturated fatty acids and vitamin E content in selected foods.

Type of food	n	MUFA (%)			PUFA (%)			Vitmain E (mg)		
		Palmitoleic C 16:1	Oleic C 18:1	Eicosenoic C 20:1	Linoleic C 18:2	Linolenic C 18:3	Unconfirmed Fatty acids	*P/S ratio	mg/ 100g	CV %
A. Cereal & grain product										
Chicken rice (N1)	2	3.8	41.4	-	19.1	0.7	0.7	0.58	0.03	2.8
Chicken rice (N2)	3	0.4	42.7	0.1	11.6	0.3	0.4	0.27	0.33	1.9
Nasi lemak	3	0.5	36.5	0.4	19.2	0.3	1.9	0.47	1.62	1.3
White bread	2	-	22.8	-	21.9	1.4	1.8	0.45	0.15	5.8
Bun	3	0.1	32.7	0.2	15.4	0.5	0.5	0.31	1.27	2.0
Fried mee hoon	3	0.1	44.0	0.1	12.2	0.2	0.4	0.29	2.05	23.4
B. Fat										
Mix butter with jem	2	-	37.3	-	9.4	0.2	0.4	0.18	3.47	69.1
C. Egg & poultry										
Scramble egg	2	0.8	39.9	-	13.5	0.3	0.1	0.30	0.51	12.6
Fried chicken	3	4.5	42.4	0.2	15.8	1.0	1.2	0.48	1.47	22.2
Chicken kurma	3	0.3	43.4	0.1	10.3	0.2	1.0	0.23	5.27	1.1
D. Fish										
Fried mackerel with soy sauce	3	1.5	40.4	0.2	7.7	0.2	3.8	0.17	1.85	0.1
Fried mackerel with 'taucu'	2	0.3	40.7	-	11.3	0.6	0.4	0.25	5.72	9.7
Fried mackerel 'asam pedas'	2	0.3	41.4	-	11.0	-	0.4	0.23	11.76	7.8
E. Vegetables & Fruit										
Fried swamp cabbage	3	0.7	42.8	0.2	10.2	0.3	1.3	0.24	1.20	2.9
Bean sprouts in coconut milk	2	-	12.1	-	3.1	-	0.7	0.04	0.02	33.3
Mix vegetable asam pedas	2	0.3	41.6	-	10.5	0.6	0.2	0.24	0.27	37.0
Cucumber	2	0.5	36.9	-	17.7	0.8	0.1	0.42	0.01	0.0
Star fruit	2	0.6	59.7	1.5	6.0	7.2	1.2	0.55	0.05	20.0
F. Miscellanous										
Soy sauce	2	0.3	32.5	-	25.1	1.3	0.4	0.65	0.01	0.0
Ketchup	2	0.6	17.3	-	54.1	2.2	1.3	2.30	0.03	33.3
Soup	2	0.1	42.3	-	15.7	1.0	2.3	0.51	0.03	60.0

acids existed in small amount (<1%). The highest ratio of polyunsaturated to saturated fatty acid (P/S) was found in ketchup of chicken rice, soy sauce, star fruit, chicken rice (rice only) and soup. This ratio was influenced by the fatty acid composition of the ingredients and the type of cooking oil used in food preparation [17].

The highest content of vitamin E (tocopherol and tocotrienol) in the food samples being analysed was mackerel 'asam pedas' (11.8 mg/100g wet weight), followed by fried fish with taucu and chicken kurma. These findings were also affected by the food preparation method [17]. Foods fried with palm oil contained a significant amount of vitamin E. The vitamin E content with this oil (33.1 mg/100g) is higher than other vegetable oils [15].

Dietary intake estimated from the one-day dietary record revealed that the mean energy intake of subjects was 2018 ± 331 kcal/d. The mean intake only met 68% of energy requirement of 2820 kcal/day for men with heavy physical activity (PAL 2.05), aged 19 to 29 year and weighing 60 kg [25]. The mean intake of fatty acids and vitamin E among army trainees is shown in Table 3. In general, fatty acids intakes estimated from the calculation using food composition tables were higher (SFA 12.1%, MUFA 8.3% and PUFA 3.0%) than those derived from food analysis (SFA 6.2%, MUFA 6.0% and PUFA 2.0%). However, for vitamin E, the findings were just the opposite. The underestimation of vitamin E content from the UK FCT [15] was due to the fact that this FCT only considers tocopherol in vitamin E values, whilst, this study analysed both tocopherol and tocotrienol. As for fatty acids, most of the FCT such as the UK [15] only provide information of total fatty acids but not a detailed composition. The Malaysian FCT [11] provides information of fatty acid compositions only for 44 food items. Thus, only eight from 22 food samples in this study can be compared fairly with the later.

The best method to estimate nutrient intake is to have a duplicate food analysis of individuals, as it reduces errors during estimation of intake [26]. However, this method is costly and requires good cooperation from subjects [26]. There is a need to update the Malaysian FCT with a more comprehensive profiling of fatty acids and vitamin E for various foods and cooked dishes.

Overall, both vitamin E and fatty acids intake of the subjects were not satisfactory when compared to the RNI [25]. Although, the mean of vitamin E intake calculated from the values obtained from food analysis (11.68 ± 1.97 mg/d) achieved 117% of RNI, 20% of subjects did not meet the RNI for vitamin E. It was however noted that the ratio of vitamin E/ PUFA from

Table 3. Comparison of fatty acids and vitamin E intake computed from Food Composition Tables and Food Analysis and percentage of intake as compared to the recommendations.

Nutrient	Calculation (n=84)	Range of calculation	Food analysis(n=84)	Range of food analysis	Recommendation
SFA					
(g/day)	26.54 ± 5.24	13.4 - 36.4	13.59 ± 2.32	8.0 - 18.2	<10% kcal[1,2]
(% kcal)	12.1 ± 3.11		6.2 ± 1.48		
(% recommendation)	121 %		62 %		
MUFA					
(g/day)	18.17 ± 3.17	11.5 - 25.4	13.03 ± 2.34	6.9 - 17.6	>10% kcal[1]
(% kcal)	8.3 ± 1.96		6.0 ± 1.46		
(% recommendation)	83 %		60 %		
PUFA					
(g/day)	6.52 ± 1.11	4.2 - 9.4	4.42 ± 0.93	2.1 - 6.4	4-6 % kcal[1]
(% kcal)	3.0 ± 0.68		2.0 ± 0.53		
(% recommendation)	60 %		40 %		
Vitamin E					
(mg/day)	8.37 ± 1.71	4.9 - 15.0	11.68 ± 1.96	6.7 - 15.5	10 mg/day[3]
(% RNI [3])	84 %		117 %		

[1] Recommendation for Malaysian adult [28]
[2] Recommendation for Adult Treatment Panel III [29]
[3] RNI vitamin E for Malaysia [25]

both estimation of FCT and food analysis for subjects was above the recommended value of 0.6 mg vitamin E per g PUFA [27]. The ratios of SFA:MUFA:PUFA for subjects from estimation of FCT (2.7:2.8:1) and food analysis (4.8:3.0:1) were closed to the ratio recommended for adults Malaysian of 2:3:1 [28], but not those suggested by the American Heart Association of 1:1:1.[29].

In conclusion, it appears that the SFA intake of the subjects was high and the intake of PUFA was low. Dietary modification with low saturated food sources such as coconut milk and increased intake of PUFA included nuts and legumes and vegetable oil are recommended for the army trainees.

Acknowledgement – The project was funded by a grant (IRPA 09-09-0049 EA 145) from the Ministry of Science, Innovation and Technology. We are indebted to the staff of Department of Nutrition and Dietetics; Division of Nutrition, Malaysian Palm Oil Board, Medical Graft Co. and the army trainees who volunteered in this study.

REFERENCES

1. Eduardo S., Hassoun G. and Pollack S. (2004) Effect of vitamin E supplementation on the regular treatment of seasonal allergic rhinitis. *Ann Allergy Asthma Immunol.* **92**: 654-658.
2. German J.B. and Dillard C.J. (2004) Saturated fats: what dietary intake? *Am J Clin Nutr.* **80**: 550-559.
3. Montain S.J. and Young A.J. (2003) Diet and physical performance. *Appetite.* **40**: 255-267.
4. Parmorn J., Kallaya K., Anadi N. and Atip L. (2002) Effect of antioxidants supplemented beverage on scavenging enzymes and lipid peroxidation in Thai soldiers. *Mahidol University Annual Research* 29.
5. Suzana S., Jane E., Hilary J.P. and Suriah A.R. (1999) Nutritional status of rural elderly Malays: Dietary and boichemical findings. *Int J Vitam Nutr Res.* **69**(4): 277-284.
6. Jones N.L., Heigenhauser G.J., Kuksis A., Matsos C.G, Sutton J.R. and Toews C.J. (1980) Fat metabolism in heavy exercise. *Clin Sci (Lond)* **59**: 469-78.
7. Demaison L and Moreau D. (2002) Dietary n-3 polyunsaturated fatty acids and coronary heart disease-related mortality: a possible mechanism of action. *Cell Mol Life Sci* **59:** 463-477.
8. Bray G.A. and Popkin B.M. (1998) Dietary fat intake does affect obesity! *Am J Clin Nutr* **68:**1157-1173.
9. Simopoulos A. (1999) Essential fatty acids in health and chronic disease. *Am J Clin Nutr* **70**:560S-569S.
10. Ismail M.N., Isa M. and Janudin A. (1996) Energy requirement of Malaysian soldiers in base camp. *Mal J Nutr* **2**:168-174.
11. Tee E.S., Ismail M.N., Mohd Nasir A. and Khatijah I. (1997) Nutrient composition Malaysian foods. Ed. ke-4. Institute of Medical Research: Kuala Lumpur.
12. Folch J.L., Lees M. and Sloane-Stanley G.H. (1957) A simple method for the isolation and purification of total lipids from animal tissues. *J Biol Chem* **226**: 497-509.
13. AOCS Official Method Ce 1-62. (2006) Fatty Acid Composition by Gas Chromatography. In: Official Methods and Recommended Practices of the AOCS, 5th ed. American Oil Chemist Society.Illinois, USA.
14. AOCS Official Method Ce 8-89. (2006) Determination of Tocopherol and Tocotrienols in Vegetable Oils and Fats by HPLC. In Official Methods and Recommended Practices of the AOCS, 5th ed. American Oil Chemist Society, Illinois, USA.
15. Holland B., Welch A.A., Unwin I.D., Buss D.H., Paul A.A., Southgate D.A.T. (1991) McCance and Widdowson's The Composition of Foods. 5th ed. *Royal Society of Chemistry, Ministry of Agriculture, Fisheries and Food (RSC/MAFF),* Cambridge, United Kingdom.
16. WHO (1997) Report of WHO Consultation on obesity: Preventing and management of the global epidemic. WHO, Geneva.
17. Heinonen M., Valsta L., Antolainen M., Ovaskainen M.-L., Hyvönen L. and Mutanen M. (1997) Comparison between Analyzed and calculated food composition data: Carotenoids, Retinoids, Tocopherol, Tocotrienols, Fat, Fatty Acids and sterols. *J Food Comp Anal* **10**:3-13.
18. Siew W.L. (2000) Analysis of palm and palm kernel oils. In Basiron Y., Jalani B.S., Chan K.W. (eds.) *Advances In Oil Palm Research.* Malaysian Palm Oil Board, Kuala Lumpur pp968-1035
19. Tee E.S., Ng T.K.W. and Chong Y.H. (1979) Cholesterol content and fatty acid composition of some Malaysian foods. *Med J Mal* **33**: 334-336.
20. Dreon D.M., Fernstrom H.A., Campos H., Blanche P., Williams P.T. and Krauss R.M. (1998) Change in dietary saturated fat intake is correlate with change mass of large low-density-lipoprotein particles in men. *Am J Clin Nutr* **67**: 828-836.

21. Kris-Etherton P.M. and Yu S. (1997) Individual fatty acids effects on plasma and lipoproteins: human studies. Am J Clin Nutr **65 (suppl):** 1628S-1644S.
22. Temme E.H., Mensink R.P. and Hornstra G. (1997) Effects of medium chain acids (MCFA), myristic, and oleic acid on serum lipoproteins in healthy subjects. *J Lipid Res* **38**: 1746-1754.
23. Hayes K.C., Pronczuk A., Lindsey S., et al. (1991). Dietary saturated fatty acids (12:0, 14:0, 16:0) differ in their impact on plasma cholesterol and lipoproteins in nonhuman primates. *Am J Clin Nutr* **53**: 491-498.
24. Ng T.K.W., Hassan K., Lim J.B. et al. (1991) Nonhypercholesterolemic effects of a palm oil diet in Malaysian Volunteers. *Am J Clin Nutr* **53**: 1015S-1020S.
25. NCCFN (2005) Recommended Nutrient Intake for Malaysia. *National Coordinating Committee on Food and Nutrition, Ministry of Health Malaysia,* Putrajaya pp207.
26. Dwyer J.T. (1994) Dietary assessment. In Shils, M.E., Olson, J.A., Shike, M. (eds.) *Modern Nutrition in Health and Disease* pp 842-860. Lea & Febigar, Philadelphia.
27. Valk E.E. and Honstra G. (2000) Relationship between vitamin E requirement and polyunsaturated fatty acid intake in man: a review. *Int J Vit Nutr Res* **70**(2): 31-42.
28. Ng T.K.W. (1995) Towards improved fat intake and nutrition for Malaysians. *Mal J Nutr* **1:** 21-30.
29. National Cholesterol Education Program (NCEP) (2002) Expert Panel on Detection, Evaluation, and Treatment of High Blood Cholesterol in Adults (Adult Treatment Panel III). Third Report of the National Cholesterol Education Program (NCEP) Expert Panel on Detection, Evaluation, and Treatment of High Blood Cholesterol in Adults (Adult Treatment Panel III) final report. *Circulation* **106:** 3143-3421.

Journal of Science and Technology in the Tropics (2006) **2**: 17-20

The restriction fragment length polymorphism patterns and the presence of outer membrane protein gene in some *Vibrio cholerae* O1 and O139 strains

N. M. Zin[1], T. Nakano[2] and K. Sano[2]
[1]Department of Biomedical Science, Faculty Allied Health Sciences, Universiti Kebangsaan Malaysia, Kuala Lumpur, Malaysia
[2]Department of Microbiology, Osaka Medical College, Takatsuki-shi, Osaka, Japan

Abstract The diarrheal disease cholera is caused by *Vibrio cholerae* belonging to the O1 or O139 serogroup and pathogenicity is based on the presence or absence of cholera toxin (CT) production. In this study, all strains of *Vibrio cholerae* were identified to be O1 and O139, either CT negative or positive. The restriction fragment length polymorphism (RFLP) pattern was determined after digestion with Not1 restriction enzyme. In addition, detection of the outer membrane protein (*ompW*) genes was carried out using the Polymerase Chain Reaction (PCR) assay. The results revealed several RFLP patterns with the O139 Ret$^-$ strains exhibiting one extra band compared to ordinary O139 strains. Nevertheless, amplification of 588-bp fragments revealed *ompW* genes in all (100%) of *V. cholerae* tested. The results showed that all *V. cholerae* strains, including the CT$^-$ strain, were positive for ompW. In conclusion, different RFLP patterns were obtained. *ompW* is not suitable to be used as a gene target in *V. cholerae* because cholera toxin producer and non-producer cannot be differentiated.

Key words *ompW* gene – PCR – PFGE – *Vibrio choleare*

INTRODUCTION

Cholera is an important disease that has killed millions of people and it continues to be major health problem worldwide [1]. The causal agent of cholera is *Vibrio cholerae* which produces cholera toxin (CT-positive). However, CT-negative *V. cholerae* O1 are also present and normally isolated from environmental waters in countries that are not endemic for cholera such as Japan [2].

Generally, expression of the CT gene (*ctx*) in *V. cholerae* is controlled in a complex manner involving transcriptional, translational and post-translational regulations. Previous studies have shown that genes partially homologous to *ompW* of *V. cholerae* are present in certain other bacteria, such as *Escherichia coli* and *Aeromonas* spp [3,4]. Several functions were proposed for the OmpW-related proteins in these bacteria, including their pore- or channel-forming [3] and colicin receptor properties [5]. Although the precise function of the OmpW protein in *V. cholerae* is not yet known, it may play a role in the adherence process, which is likely to facilitate the survival of the organism within the host or in the environment or both [6]. The genetic diversity and molecular epidemiology of *V. cholerae* O1 has been reported using various molecular techniques such as restriction fragment length polymorphism (RFLP), pulse-field gel electrophoresis (PFGE), amplified fragments length polymorphism and variants of polymerase chain reaction (PCR)-based methods [7-11]. Nevertheless, the conventional methods of classifying *V. cholerae* are biotyping, serotyping and bacteriophage typing but these methods cannot differentiate clones. Hence, the need of RFLP is crucial.

In the present study, we evaluated the use of PFGE to examine the RFLP patterns of *V. cholerae* O1 and O139 isolates. The study was extended using primer pairs targeted to a gene encoding an outer membrane protein (*ompW*), whose nucleotide sequence was first reported by Jalajakumari and

JOURNAL OF SCIENCE AND TECHNOLOGY IN THE TROPICS

NOTICE TO CONTRIBUTORS

JOSTT is a multi-disciplinary journal. It publishes original research articles and reviews on all aspects of science and technology relating to the tropics. All manuscripts are reviewed by at least two referees, and the editorial decision is based on their evaluations.

Manuscripts are considered on the understanding that their contents have not been previously published, and they are not being considered for publication elsewhere. The authors are presumed to have obtained approval from the responsible authorities, and agreement from all parties involved, for the work to be published.

Submission of a manuscript to JOSTT carries with it the assignment of rights to publish the work. Upon publication, the Publishers (COSTAM and ASM) retain the copyright of the paper.

Manuscript preparation

Manuscripts must be in English, normally not exceeding 3500 words. Type double spaced, using *MS Word*, on one side only of A4 size with at least 2.5 cm margins all round. Number the pages consecutively and arrange the items in the following order: title page, abstract, key words, text, acknowledgements, references, tables, figure legends.

Title page

Include (i) title, (ii) names, affiliations and addresses of all authors, (iii) running title not exceeding five words, and (iv) email of corresponding author.

Abstract and key words

The abstract, not more than 250 words, should be concise and informative of the contents and conclusions of the work. A list of not more than five key words must immediately follow the abstract.

Text

Original research articles should be organized as follows: Introduction, Materials and Methods, Results, Discussion, Acknowledgement, References. The International System of Units (SI) should be used. Scientific names and mathematical parameters should be in italics.

References

References should be cited in the text as numbers enclosed with square [ ] brackets. The use of names in the text is discouraged. In the reference section, the following examples should be followed:

1 Yong H.S., Dhaliwal S.S. and Teh K.L. (1989) A female Norway rat, Rattus norvegicus, with XO sex chromosome constitution. *Naturwissenschaften* **76: 387-388.**
2 Beveridge W.I.B. (1961) *The Art of Scientific Investigation*. Mercury Book, London.
3 Berryman A.A. (1987) The theory and classification of outbreaks. *In* Barbosa P. and Schultz J.C. (eds.) *Insect outbreaks* pp. 3-30. Academic Press, San Diego.

Tables

Tables should be typed on separate sheets with short, informative captions, double spacing, numbered consecutively with Arabic numerals, and do not contain any vertical lines. A table should be set up to fit into the text area of at most the entire page of the Journal.

Illustrations

Black-and-white figures (line drawings, graphs and photographs) must be suitable for high-quality reproduction. They must be no bigger than the printed page, kept to a minimum, and numbered consecutively with Arabic numerals. Legends to figures must be typed on a separate sheet. Colour illustrations can only be included at the author's expense.

Proofs and reprints

Authors will receive proofs of their papers before publication. Ten reprints of each paper will be provided free of charge.

Submission

Manuscripts should be submitted in triplicate (including all figures but not original artwork), together with a floppy diskette version of the text, to:

The Managing Editor
Journal of Science and Technology in the Tropics
C-3A-10, 4th Floor Block C, Lift No: 5
No. 1 Jalan SS20/27
47400 Petaling Jaya
Selangor Darul Ehsan
Malaysia

Manning [12]. It has been demonstrated that the primers targeted to *ompW* are better suited for species-specific identification due to the unique presence of the gene with conserved sequences in *V. cholerae* [13].

MATERIALS AND METHODS

Isolation of *V. cholerae*

A total of 5 *V. cholerae* strains isolated from both clinical and environmental sources in Osaka, were included in this study. The strains were isolated locally and kept as stock cultures. The list of strains which included O139, O1 CT-positive and CT-negative were: O139 Hiroshima, O139 Hiroshima RET$^-$, O1 no. 960852 (clinical strain), O1 no. 960951 (clinical strain) and O1 CT$^-$ no. 9612.

The isolation was performed by standard methods [14]. Cells were grown on heart infusion broth or agar plates (Difco, Detroit, USA). The O1-antigen CT-positive strains were characterized by conventional biochemical tests such as IMVic, amino acid and sugar assimilation tests (15). Biotype determination was based on haemolysis of sheep erythrocytes and Voges-Proskauer reaction.

Preparation of DNA for pulse-field gel electrophoresis

The RFLP pattern analysis for all *V. cholerae* strains were performed using PFGE. Agarose plugs containing DNA for PFGE were prepared using CHEF bacterial genomic DNA Plugs kit (Bio-Rad Laboratories, Hercules) with modifications to the manufacturer's instructions. In brief, bacterial cells were grown for 3 hours at 37°C in heart infusion broth and bacterial concentration adjusted to the concentration of McFarland 2. The bacterial cells then were inoculated into agarose blocks and bacterial genomic DNA was extracted with lysozyme and proteinase K solution. Bacterial DNA in agarose plugs were then digested with *Not*1 restriction enzyme (New England Biolabs) at 37°C overnight.

Pulse-field gel electrophoresis (PFGE)

Electrophoresis was carried out by the contour-clamped homogeneous electric field method on a CHEF-DR II system (Bio-Rad Laboratories, Richmond, California) in 1% agarose (Pulse Field Certified Agarose; Bio-Rad Laboratories, Hercules) and 0.5 X TBE buffer (44.5 mM Tris, 44.5 mM boric acid, 1 mM EDTA, pH 8.3) at 14°C for 24 h at 150 V, with the pulse time at 3-40 sec. Gels were stained with SYBR Green I nucleic acid gel stain (FMC BioProducts, Rockland, USA) for 30 min and photographed with a UV transluminator. RFLP patterns were visually analyzed.

Polymerase Chain Reaction (PCR)

Oligonucleotides were synthesized commercially by TakaraBio Inc., Shiga, Japan. All amplifications were performed on a thermocycler (Perkin Elmer). The primer pair used for *ompW* was 5'-CACCAAGAAGGTGACTTTATTGTG-3' and 5'-GAACTTATAACCACCCGCG-3' [13]. PCR amplification of target DNA was carried out according to Nandi *et al* [13] and the cool start method was used when preparing the master-mix solutions. This is to minimize the amplication of non-specific bands and to achieve more accurate amplification. PCR tubes (200 µl volume) with a reaction mixture volume of 25 µl were used. Each of the reaction mixtures contained 3 µl of template DNA (lysate) obtained by boiling for 2 min, 2.5 µl of primer (10 pmol/µl), 2.5 µl of 2.5 mM deoxynucleoside triphosphate, 0.3 µl (5 U/µl) of Taq DNA polymerase (TakaraBio Inc., Shiga, Japan), 2.5 µl of 10X reaction buffer containing 20 mM $MgCl_2$ (TakaraBio Inc., Shiga, Japan) and 11.8 µl of distilled water. The reaction mixture was subjected to an amplification of 30 cycles and consisted of three steps in the following order: denaturation of template DNA at 94°C for 30s, annealing of the template DNA at 64°C for 30s, and extension of the primers at 72°C for 30s. Before initiation of the first cycle, the reaction mixture was heated at 94°C for 5 min to allow complete denaturation of the template. PCR products were electrophoresed through 1.5% (wt/vol) agarose gel and the amplified products were stained using ethidium bromide and visualized under UV light.

RESULTS AND DISCUSSION

PFGE

A total of 5 *V. cholerae* serotypes were investigated by PFGE and the RFLP patterns analyzed. From the results obtained, there were several patterns based on *Not*1 restriction (Fig. 1). The O139 RET$^-$ strain had one extra band as compared to ordinary O139 strains (Lane 2 and 1, respectively). Different RFLP patterns of the same strain occurred by deleting certain sequence. The results also showed the consensus pattern in all strains tested.

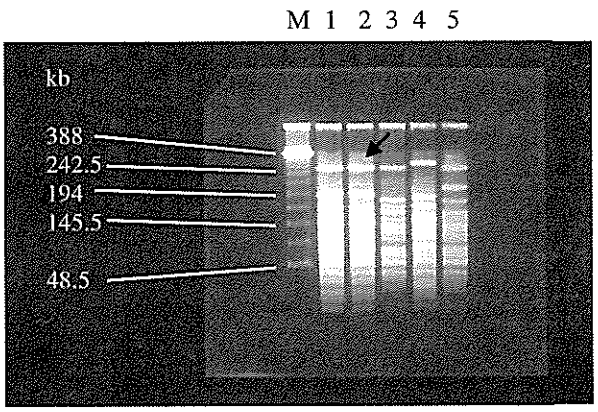

Figure 1. NotI-RFLP patterns among the five *V. cholerae* strains. Lane M, 48.5 kb lambda ladder size marker; lane 1, *V. cholerae* O139 Hiroshima; lane 2, *V. cholerae* O139 Hiroshima RET$^-$; lane 3, *V. cholerae* O1 no.960852; lane 4, *V. cholerae* O1 no.960951; lane 5, *V. cholerae* CT$^-$. ↙ Denotes extra band in *V. cholerae* O139 Hiroshima RET$^-$.

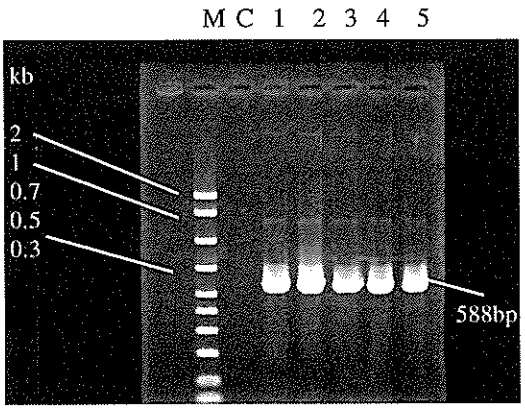

Figure 2. Results of PCR amplification obtained with bacterial strains using ompW-specific primers. Lane M, 2 kb lambda ladder size marker; lane C, negative control; lane 1, *V. cholerae* O139 Hiroshima; lane 2, *V. cholerae* O139 Hiroshima RET$^-$; lane 3, *V. cholerae* O1 no.960852; lane 4, *V. cholerae* O1 no.960951; lane 5, *V. cholerae* CT$^-$.

PCR

PCR amplification of *ompW* gene for *V. cholerae* yielded amplicons of 588 bp. From the results obtained, all *V. cholerae* strains, including the CT$^-$ strains, were positive for *ompW*-based PCR assay. This result supported the finding of Nandi *et al.* [13] in which all the *Vibrio* strains tested were positive to *ompW*. Therefore, they concluded that *ompW* gene could be used for the species-specific identification of *V. cholerae* strains. As *ompW* is a universal gene present in both CT-positive and CT-negative strains, it is not suitable to be used as a gene target for the identification of CT-positive strains.

Acknowledgements – The authors are grateful to the Japan Society for the Promotion of Science, Tokyo, Japan for sponsoring one of the authors as a visiting scientist under the General Exchange Program at the Department of Microbiology, Osaka Medical College and for funding this project.

REFERENCES

1. Tauxe R., Seminario L., Tapia R. and Libel M. (1994). The Latin American epidemic. *In* Wahcsmuth I.K., Blake P.A. and Olsvik O. (eds.) *Vibrio cholerae and Cholera:Molecular to global perspectives.* pp. 3-30. American Society for Microbiology, Washington, DC.
2. Minami A., Hashimoto S. and Abe H. (1991) Cholera enterotoxin production in *Vibrio cholerae* O1 strains isolated from the environment and from humans in Japan. *Appl. Environ. Microbiol.* **57**: 2152-2157.
3. Jeanteur D., Gletsu N., Pattur F. and Buckley J.T. (1992) Purification of *Aeromonas hydrophila* major outer membrane proteins:N-terminal sequence analysis and channel-forming properties. *Mol. Microbiol.* **22**: 3355-3363.
4. Molloy M.P., Herbert B.R., Walsh B.J., Tyler M.I., Traini M., Sanchez J.C, Hochstrasser D.F., Williams K.L. and Gooley A.A. (1998) Extraction of membrane proteins by differential solubilization for separation using two-dimensional gel electrophoresis. *Electrophoresis* **19**: 837-844.
5. Pilsl H., Smajs D. and Braun V. (1999) Characterization of colicin S4 and its receptor, *OmpW*, a minor protein of the *Escherichia coli* outer membrane. *J. Bacteriol.***181**: 3578-3581.
6. Sengupta T.K., Nandy R.K., Mukhopadhyay S., Hall R.H., Sathyamoorthy V. and Ghose A.C. (1998) Characterization of a 20-kDa pilus protein expressed by a diarrheogenic strain of non-O1/non-O139 Vibrio cholerae. *FEMS Microbiol. Lett.***160**(2): 183-189.

7. Choudry S.R., Bhadra R.K. and Das J. (1994) Genome size and restriction fragments length polymorphism analysis of *Vibrio cholera* strains belonging to different serovars and biotypes. *FEMS microbial. Lett.* **115**: 329-334.
8. Colombo M.M., Mastrandrea S., Leite F., Santona A., Uzzau S., Tapelli P., Pisano M., Rubino S, and Cappucinelli P. (1997) Tracking of clinical and environmental *Vibrio cholerae* O1 strain by combined analysis of the presence of the toxin cassette, plasmid content and ERIC PCR. *FEMS Immun. Med. Microbiol.* 19: 33–45.
9. Jiang S.C., Matte M, Matte G., Huq A. and Colwell R.R. (2000) Genetic diversity of clinical and environmental isolates of *Vibrio cholerae* determined by amplified fragment length polymorphism fingerprinting. *Appl. Environ. Microbiol.* 66: 148–153.
10. Karaolis D.K.R., Lan R. and Reeves P.R. (1995) The sixth and seventh cholera pandemics are due to independent clones separately derived from environmental, nontoxigenic, non-O1 *Vibrio cholerae*. *J. Bacteriol.* 177: 3191–3198.
11. Rivera I.G., Chowdhury M.A.R., Huq A., Jacobs D., Martins M.T. and Colwell R.R. (1995) Enterobacterial repetitive intergenic consensus sequences and the PCR to generate fingerprint of genomic DNAs from *Vibrio cholerae* O1, O139, and non-O1 strains. *Appl. Environ. Microbiol.* 61: 2898–2904.
12. Jalajakumari M.B. and Manning P.A. (1990) Nucleotide sequence of the gene, ompW, encoding a 22 kDa immunogenic outer memberane protein of *Vibrio cholerae*. *Nucleic Acids Res.* **18**: 2180.
13. Nandi B., Nandy R.K., Mukhopadhyay S., Nair G.B., Shimada T. and Ghose A.C. (2000) Rapid method for species-specific identification of *Vibrio cholerae* using primers targeted to the gene of outer membrane protein OmpW. *J. Clin. Micro.* **38**(11): 4145-51.
14. Cheesbrough M. (1985) Medical laboratory manual for tropical countries. *In* Cheesbough, M, (ed.) Tropical Health technology, Doddington. pp. 218-238.
15. Miyagi K., Nakano T., Yagi T., Hanafusa M., Imura S., Honda T., Nakano Y. and Sano K. (2003) Survey of *Vibrio cholerae* O1 and its survival over the winter in marine water of Port of Osaka. *Epidemiol. Infect.* **131**: 613-19.

Journal of Science and Technology in the Tropics (2006) **2**: 21-26

Synthesis of fatty acid alkyl esters *via* direct esterification

Cheng Sit Foon[1,2], Choo Yuen May[1]*, Ma Ah Ngan[1] and Chuah Cheng Hock[2]
[1]Engineering and Processing Research Division, Malaysian Palm Oil Board (MPOB),
6 Persiaran Institusi, Bandar Baru Bangi, 43000 Kajang, Selangor, Malaysia
[2]Department of Chemistry, Faculty of Science, University of Malaya, 50603 Lembah Pantai,
Kuala Lumpur, Malaysia
*To whom correspondence should be addressed: (e-mail: choo@mpob.gov.my)

Received 20.02.2006; accepted 10.05.2006

Abstract Fatty esters were synthesized in the present study *via* direct esterification of palm fatty acids with alkyl alcohols. The procedures for the esterification and purification of the esters are described. Generally, the alkyl alcohols used in this study can be divided into two main groups, i.e. water-miscible and water-immiscible. Based on this difference, two experimental set-ups were used whereby direct esterification involving water-immiscible alcohols was conducted using a Dean and Stark set-up while a Soxhlet set-up was used for water-miscible alcohols. Under the optimum condition established, ester conversion and yield of up to 99% and 90%, was obtained respectively in less than 5 hours reaction time.

Keywords alkyl esters – esterification – fatty acid esters – palm oil

INTRODUCTION

Esterification refers to the synthesis of esters *via* reaction between carboxylic acid with alcohols [1]. The reaction is essentially the reverse of fat splitting and may be carried out in the absence of a catalyst but a reasonable rate can only be achieved at a relatively high temperature. Strong mineral acids are normally used in the acid catalyzed esterification, particularly sulfuric acid and hydrochloric acid, although other substances such as salts, silica gel and cation-exchange resins have been used. However, for industrial processes, sulfuric acid is preferred as the hydrochloric acid is corrosive. Anhydrous hydrochloric acid may be used but side products such as the alkyl chlorides may be formed when the reaction time is prolonged. Aromatic sulfonic acids (Twitchell reagent) such as benzeno-sulfonic and p-toluene sulfonic acid catalysts have been recommended for esterifying long-chain fatty acids. In the case where no catalyst is employed in an esterification reaction, it proceeds slowly and requires higher temperature in order to attain sufficient reaction rate. Thus, generally a suitable catalyst is able to give a good conversion rate and yield. Since the reaction involves a reversible equilibrium, the reaction is normally pushed towards the products with the usage of excess reactants, i.e. either the acid or the alcohol; or the removal of the co-product (water) continuously during the reaction.

The present paper reports the preparation of a series of palm esters from palm fatty acids with carbon chain length from 8 to 18, which are finding new applications in value-added downstream products such as lubricants base oils, solvents and biodiesel.

MATERIALS AND EXPERIMENTAL PROCEDURES

Materials

Caprylic, capric, lauric, myristic, palmitic and stearic acids of 98% purity and oleic acid of 75% purity, were obtained from Southern Acid (M) Sdn. Bhd. Monohydric alcohols, namely, *n*-butanol, isobutanol, 2-butanol, isopropanol and 2-ethylhexanol were

purchased from Fluka. Polyhydric alcohols, namely, neopentyl glycol, trimethylolpropane and pentaerythritol were purchased from Merck. All alcohols used were of reagent grades.

Concentrated sulphuric acid (H_2SO_4) (98%) and *p*-toluene sulfonic (*p*-TSA) acid were purchased from Aldrich Chemical and Fluka, respectively. Toluene, dichloromethane, glacial acetic acid, diethyl ether, hexanes and thin layer chromatography (TLC) plates pre-coated with silica gel 60 F254 were purchased from Merck. Deuteriochloroform ($CDCl_3$) was from Sigma-Aldrich while anhydrous sodium sulphate (Na_2SO_4), triacontane and *N,N*-Bis (trimethylsilyl)trifluoroacetamide (BSTFA) were supplied by Fluka. Sodium hydroxide (NaOH), sodium bicarbonate ($NaHCO_3$) and molecular sieves 300 were purchased from Tokyo Chemical Inc. (TCI).

Preparation of fatty esters from water-immiscible alcohols and fatty acid

A stoikiometric mixture of fatty acid and alcohol was transferred into a 1-L three-necked round bottom flask. Additional alcohol (in one to two moles excess) and a 400 mL of solvent (toluene) were added into the reaction mixture. The reaction flask was then equipped with thermometer, magnetic stirrer, condenser, a modified Dean and Stark distillation set-up, a dropping funnel and a heating plate. The reaction mixture containing fatty acid, alcohol and toluene was then heated in an oil bath to the desired reaction temperature (120°C for monohydric alcohols and 180°C for polyhydric alcohols) with stirring to provide a homogenous reaction mixture. When the reaction mixture has reached the elevated temperature, a catalytic amount (1 weight per cent of fatty acid) of the catalyst was added slowly into it. Heating continued until the reaction is completed.

Reaction progress was monitored by the volume of water collected in the modified Dean and Stark trap. Aliquots of reaction samples were taken during the reaction in order to monitor the formation of fatty esters by thin layer chromatography (TLC), using a suitable solvent system.

After the reaction has completed, the crude reaction product was cooled to room temperature. Then, it was transferred into a round-bottom flask and subjected to rotary evaporator to remove toluene and excess alcohol as much as possible. In order to remove the catalyst used, the crude product was washed with warm distilled water until the decanted aqueous layer was neutral. Then, the product was dried with anhydrous sodium sulphate (Na_2SO_4). The hydrated Na_2SO_4 was filtered off. The dried product was then passed through a column packed with silica gel to remove any coloured or decomposed materials formed during the reaction. Unreacted fatty acid was removed by washing with sodium hydroxide (NaOH) or sodium bicarbonate ($NaHCO_3$) solutions. Traces solvent and water were further removed by a vacuum pump.

Preparation of fatty esters from water-miscible alcohols and fatty acids

A stoikiometric mixture of fatty acid (1 mole) and alcohol was transferred into a 1-L two-necked round bottom flask. An excess of 2 moles of alcohol was then added into the reaction mixture. The reaction flask was equipped with magnetic stirrer, a soxhlet containing molecular sieves in a thimble, condenser and a heating plate. The reaction mixture now containing fatty acid and alcohol was heated in an oil bath to the desired reaction temperature, with stirring to provide a homogenous reaction mixture. The temperature of the oil bath was fixed using a controlled-thermometer, which is connected to the heating plate. When the reaction mixture has reached the elevated temperature, a catalytic amount of the catalyst was added slowly into it. Heating continued for about 5 hours or until the reaction is completed. Reaction progress monitoring and purification of the product was done as described in previous section.

Gas chromatography

Reaction mixtures withdrawn for kinetics study during reactions and final products were derivatized before subjected to gas chromatography (GC) analyses. A 0.02 g sample was weighed into a 2 mL auto-sampler vial. Into this vial, a 0.2 mL of internal reference solution (0.02 g of triacontane in 50 mL dichloromethane) and 1.3 mL of Bis (trimethylsilyl) trifluoroacetamide (BSTFA) solution (8 mL of BSTFA in 50 mL dichloromethane) was added accurately by using a micropipette. The vial, capped tightly with a screw cap and septum was shaken well and then heated for two hours at 60 – 70°C for silyllation process. External standards such as fatty acids and methyl esters were also prepared in the same manner as sample preparation. The gas chromatography-flame ionization detector (GC-FID) and the temperature programme used in the analyses are similar to that described by Lau *et al.* [2].

RESULTS AND DISCUSSION

Esterification of fatty acids with mono and polyhydric alcohols

Acid-catalysed direct esterification method was employed to synthesis the fatty mono-esters and fatty polyol-esters in the present study. The reactions are depicted in the chemical equation as depicted in Figure 1. Direct esterification was the chosen method as it is the cheapest and most practical way for large-scale industrial production of esters.

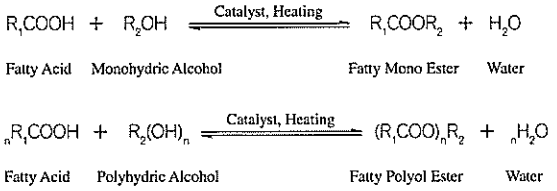

Figure 1. Esterification reaction equation for mono and polyhydric alcohols.

Researchers have pointed out that there is no universal manner in which esterification reaction can be driven to completion. The reaction will not go to completion since it involves a reversible equilibrium. However, steps were taken to ensure high conversion from reactants to products in the present study, namely, the addition of an azeotroping agent, continuous removal of water (co-product) and using excess of reactants.

The addition of an azeotroping agent, namely, toluene (400 mL per mole of fatty acid) in the present study helps to facilitate the removal of water from the reaction mixture. Addition of toluene helps the removal the of water since the boiling point of the azeotrope mixture of water and toluene is 85°C, thus, water was easier to remove and at lower temperature compared to its boiling point at 100°C.

According to the Le Chartelier Principle, large excess of one of the reactant or the removal of one of the product would drive the reaction to completion. In the present study, an excess of alcohol was used in the preparation of fatty monoesters (molar ratio of fatty acid to alcohol = 1:3). Besides using an excess of reactant, the removal of water (co-product of esterification process) was also removed continuously during the reaction. A modified Dean and Stark set-up was engaged in to shift the equilibrium towards the products.

Besides pushing the reaction equilibrium towards the products, removal of water produced along the reaction also has an added advantage. Volume of water collected from the separating funnel during the reaction also served as an indicator to the progress of reaction. The volume collected was compared to the theoretical amount by calculation.

Under the most favourable reaction condition described, high ester conversion (above 99%) was achieved for all fatty mono-esters synthesized. The respective yield of the esterification reactions are presented in Tables 1 and 2.

Table 1. Yield of fatty mono-esters from water-immiscible alcohols. (Reaction conditions: molar ratio of fatty acid:alcohol = 1:2; reaction temperature = 120°C; stirring rate = 350 rpm, catalyst (sulphuric acid concentrated) concentration = 1 wt % based on fatty acid; solvent (toluene) = 400 mL per mole of fatty acid; reaction time = 5 hours.)

Synthesized fatty esters	Yield (%)	Starting material	
		Fatty acids	Alcohol
n-butyl Caprylate	89.4	Caprylic	*n*-butanol
2-butyl Caprylate	88.8	Caprylic	2-butanol
n-butyl Caprate	85.0	Capric	*n*-butanol
2-butyl Caprate	89.4	Capric	2-butanol
n-butyl Laurate	83.6	Lauric	*n*-butanol
2-butyl Laurate	90.5	Lauric	2-butanol
n-butyl Myristate	84.3	Myristic	*n*-butanol
2-butyl Myristate	88.6	Myristic	2-butanol
n-butyl Palmitate	93.4	Palmitic	*n*-butanol
2-butyl Palmitate	93.3	Palmitic	2-butanol
n-butyl Stearate	94.3	Stearic	*n*-butanol
2-butyl Stearate	88.4	Stearic	2-butanol
n-butyl Oleate	91.4	Oleic	*n*-butanol
2-butyl Oleate	84.5	Oleic	2-butanol
2-Ethylhexyl Stearate	88.5	Stearic	2-Ethylhexanol
2-Ethylhexyl Palmitate	83.6	Palmitic	2-Ethylhexanol

Journal of Science and Technology in the Tropics (2006) 2: 21-26

Table 2. Yield for fatty mono-esters from water miscible alcohols. (Reaction conditions: molar ratio of fatty acid:alcohol = 1:3; reaction temperature = 120°C; stirring rate = 350 rpm, catalyst (concentrated sulphuric acid) concentration = 1 wt % based on wt of fatty acid; solvent (toluene) = 400 mL; reaction time = 6 hours.)

Synthesized fatty esters	Yield (%)	Starting material	
		Fatty acids	Alcohol
Methyl Caprylate	82.5	Caprylic	Methanol
Isopropyl Caprylate	84.5	Caprylic	Isopropanol
Methyl Caprate	90.7	Capric	Methanol
Isopropyl Caprate	89.8	Capric	Isopropanol
Methyl Laurate	88.9	Lauric	Methanol
Isopropyl Laurate	86.5	Lauric	Isopropanol
Methyl Myristate	92.0	Myristic	Methanol
Isopropyl Myristate	88.7	Myristic	Isopropanol
Methyl Palmitate	84.8	Palmitic	Methanol
Isopropyl Palmitate	86.5	Palmitic	Isopropanol
Methyl Stearate	90.6	Stearic	Methanol
Isopropyl Stearate	89.4	Stearic	Isopropanol
Methyl Oleate	89.6	Oleic	Methanol
Isopropyl Oleate	87.9	Oleic	Isopropanol

Table 3. Yield of fatty polyol-esters. (Reaction conditions: reaction temperature = 180°C; stirring rate = 350 rpm, catalyst (p-toluene sulfonic acid) concentration = 1 wt % based on wt of fatty acid; solvent (toluene) = 400 mL; reaction time = 5 hours; fatty acid in excess = 2 moles.)

Synthesized fatty esters	Yield (%)	Starting material	
		Fatty acids	Alcohol
Pentaerythritol Tetracaprate	79.4	Capric	Pentaerythritol
Pentaerythritol Tetracaprylate	84.5	Caprylic	Pentaerythritol
Neopentylglycol Dicaprate	90.8	Capric	Neopentyl Glycol
Neopentylglycol Dilaurate	94.8	Lauric	Neopentyl Glycol
Neopentylglycol Dioleate	88.7	Oleic	Neopentyl Glycol
Neopentylglycol Dicaprylate	89.9	Caprylic	Neopentyl Glycol
Trimethylolpropane Tricapylate	86.4	Caprylic	Trimethylolpropane
Trimethylolpropane Tricaprate	89.7	Capric	Trimethylolpropane
Trimethylolpropane Trioleate	86.8	Oleic	Trimethylolpropane

The Dean and Stark set-up was not used for esterification of fatty acids with water-miscible alcohols, namely, isopropanol. As it is miscible with water, it will be entrained out together with water formed during reaction. To overcome this, a set-up using sohxlet extractor with a thimble filled with molecular sieves 3Å was used to absorb water formed during the reaction. The molecular sieves were routinely changed every two hours to increase its efficiency.

As compared to the mono-esters, the yield for polyol-esters is relatively lower, i.e. between 79 to 94% (Table 3). More intense reaction conditions were used for the esterification reactions between palm fatty acids and polyhydric alcohols in order to achieve comparable ester conversion as the palm mono-esters. Due to the longer chain length and the more steric hindrance present in polyhydric alcohols molecules as compared to the monohydric alcohols (Figure 2), reactions involving them were conducted at a higher reaction temperature, i.e. 180°C *ca.* 160°C for the preparation of mono-esters. An excess of 2 moles of fatty acid were used for the synthesis of fatty polyol-esters to push reaction equilibrium towards reaction products.

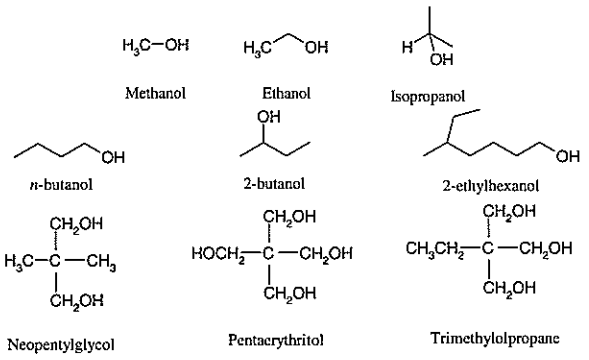

Figure 2. Molecule structures of mono and polyhydric alcohols used in the present study.

Kinetics and rate constant of esterification reaction

From the kinetics data obtained in the present study, it was found that the initial rate of direct esterification of fatty acid with alcohol was moderately fast but not as fast as that described for transesterification of crude palm oil [3]. The rate of reaction also became slower as reaction is approaching completion. A typical reaction profile for the esterification reaction is presented in Figure 3.

The observation of moderately fast reaction rate in the initial stage and a slow one when approaching completion can be explained in terms of mass transfer. When the reaction mixture consisting fatty acid, alcohol and solvent (toluene) was heated up to 120°C, fatty acid became miscible with alcohol and a single phase was formed. Mixing became insignificant and good diffusion occurred in the system. As a result, fast

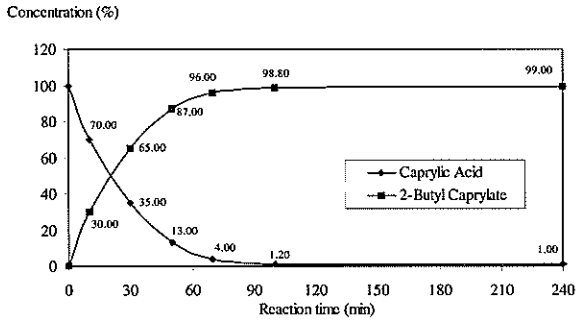

Figure 3. Reaction mixture profile during esterification of caprylic acid with 2-butanol. (Reaction conditions: molar ratio of caprylic acid: 2-butanol = 1:2; catalyst = concentrated sulphuric acid, 1 wt % based on wt of caprylic acid; Solvent = toluene, 400 mL per mole caprylic acid, temperature = 120°C; stirring rate = 350 rpm.)

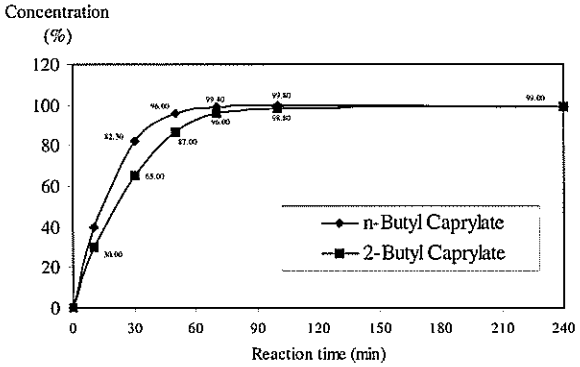

Figure 4. Ester Conversion during esterification of caprylic acid with alcohols. (Reaction conditions: molar ratio of caprylic acid:alcohol = 1:2; catalyst = concentrated sulphuric acid, 1 wt % based on wt of caprylic acid; solvent (toluene) = 400 mL per mole caprylic acid, temperature = 120°C; stirring rate = 350 rpm.)

reaction rate was obtained. Depletion of fatty acid and formation of esters as the reaction progresses results in lower diffusion and slower reaction rate.

Kinetics data are also in agreement with general knowledge that the rate of reaction is influence by the molecule structures of reactants. Figure 4 shows the percentage of ester conversion in respect to reaction time for esterification of caprylic acid with *n*-butanol and 2-butanol. Relatively, the ester conversion for *n*-butanol is higher than that of 2-butanol. High ester conversion was obtained for *n*-butanol (a primary alcohol) as it has an unbranched alkyl group that donates electrons to carbon, resulting in stronger carbon and oxygen bond. As a result, the bond between oxygen and hydrogen became weaker and more readily to dissociate from its molecule. 2-butanol (a secondary alcohol) is a bulkier molecule than *n*-butanol. Thus, under the same esterification reaction condition as *n*-butanol, a slower ester conversion is observed (Figure 3). The hindered structure of 2-butanol reduces the chances of reaction with fatty acid due to its hydroxyl group being shielded by its branched and bulky alkyl group in the molecule.

Graph of ln [concentration of reactant] as a function of time was used to obtain the order for esterification reactions in the present study. The method was based on the integrated rate laws. For first order reaction, $-kt = \ln([A]_t / [A]_o)$ where $[A]_t$ = concentration of reactant at t time, $[A]_o$ is the initial concentration and k is the rate constant [4]. According to the integrated rate law for first order reaction, $\ln [A]_t = -kt + \ln [A]_o$. The slope of linear graph $\ln [A]_t$ versus time (t) will give the k

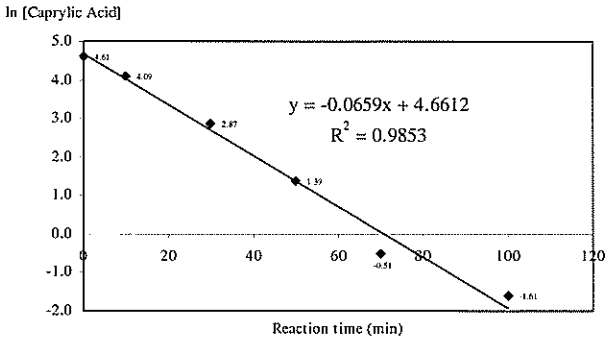

Figure 5. Graph of ln [Caprylic Acid]$_t$ versus Reaction Time for Esterification of Caprylic Acid with *n*-Butanol. (Reaction conditions: molar ratio of caprylic acid:alcohol = 1:2; catalyst = concentrated sulphuric acid, 1 wt % based on wt of caprylic acid; solvent (toluene) = 400 mL per mole caprylic acid, temperature = 120°C; stirring rate = 350 rpm.)

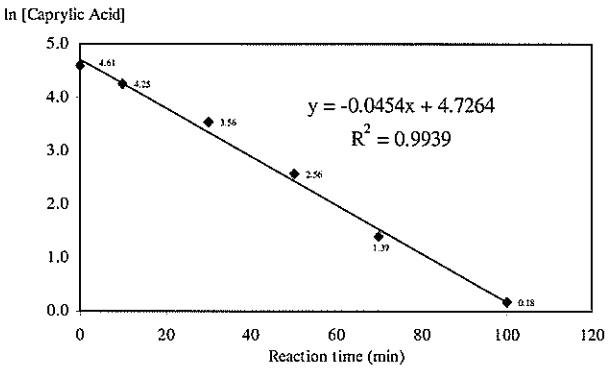

Figure 6. Graph of ln [Caprylic Acid]$_t$ versus Reaction Time for Esterification of Caprylic Acid with 2-Butanol. (Reaction conditions: molar ratio of caprylic acid:n-butanol = 1:2; catalyst = concentrated sulphuric acid, 1 wt % based on wt of caprylic acid; solvent (toluene) = 400 mL per mole caprylic acid, temperature = 120°C; stirring rate = 350 rpm.)

Table 4. Rate constant for selected esterification reactions. (Reaction conditions: molar ratio of caprylic acid:alcohol = 1:2; catalyst = concentrated sulphuric acid, 1 wt % based on wt of caprylic acid; solvent (toluene) = 400 mL per mole caprylic acid, temperature = 120°C; stirring rate = 350 rpm.)

Reaction product	Reaction order	Rate constant, k (min^{-1})	R^2
n-butyl Caprylate	1	6.59×10^{-2}	0.9853
2-butyl Caprylate	1	4.54×10^{-3}	0.9939

value. The technique of flooding, i.e. the assumption of a stoikiometric excess of all but one reactant so that effectively the concentration of only one reactant changes with time, is applied in the current study to attain the esterification reaction rate constant. As discussed in the previous section, the esterification reactions involving monohydric alcohols uses excess of the alcohols to push the equilibrium towards the products. Using the integrated laws, graphs of ln [caprylic acid]$_t$ versus t for esterification reaction of caprylic acid with *n*-butanol and 2-butanol are presented in Figures 5 and 6, respectively and their k values are summarised in Table 4.

Acknowledgement – The authors would like to thank the Director General of Malaysian Palm Oil Board (MPOB) for his permission to publish this paper.

REFERENCES

1. Solomon T.W.G. (1997) *Fundamentals of Organic Chemistry*. Fifth Edition. New York: John Wiley & Sons, Inc. p. 760.
2. Lau H.L.N., Choo Y.M., Ma A.N. and Chuah C.H. (2002) Gas Chromatography Method for Vegetable Oil and Fats. Paper presented at *2002 National Seminar on Palm Oil Milling, Refining Technology, Quality and Environment*. Kota Kinabalu, Sabah, Malaysia. 19-20 August 2002.
3. Cheng S.F., Choo Y.M., Ma A.N. and Chuah C.H. (2004) Kinetics Study on Transesterification of Palm Oil. *Journal of Oil Palm Research* **16**(2): 19-29.
4. Mahan B.M. and Myers R.J. (1987) Chemical Kinetics. In *University Chemistry*. Fourth Edition. The Benjamin / Cummings Publishing Company, Inc., USA. p. 438–497.

Journal of Science and Technology in the Tropics (2006) **2**: 27-34

Characteristic study of hot spot in the new solar furnace comprising of non-imaging focusing heliostat and parabolic reflector

K. K. Chong†, B. K. Tan and Jasmy Yunus*
Faculty of Engineering and Science, Tunku Abdul Rahman University, Off Jalan Genting Klang, 53300 Kuala Lumpur, Malaysia
*Faculty of Electrical Engineering, University of Technology Malaysia, 83000 Skudai, Johor, Malaysia
(†chongkk@mail.utar.edu.my)

Received 06.01.2006; accepted 27.04.2006

Abstract Conventional fixed-target type of solar furnace requires the size of the parabolic reflector nearly the same as that of heliostat. In contrast, the newly proposed non-imaging focusing heliostat, which can perform off-axis-focusing and sun-tracking concurrently, has significantly reduced the size of solar image during the first stage focusing and hence the required size of the parabolic reflector is also greatly reduced. Following the previous publication on the practical verification of the new solar furnace to achieve 3400°C, this paper further explores the characteristics of the new solar furnace through the theoretical study of the hot spot formed at the focusing point of the parabolic reflector. The relations of the size of hot spot and the solar concentration ratio with incidence angle, L/H_{ph} ratio of the heliostat as well as f/D ratio of the parabolic reflector are reported.

Keywords hot spot – non-imaging focusing heliostat – solar furnace – parabolic reflector – optical modeling

INTRODUCTION

Conventional fixed-target type of solar furnace comprises of two components: heliostat and parabolic reflector. The function of heliostat is to track the sun and redirect the sunlight onto a parabolic reflector located at a fixed position. While, the parabolic reflector accomplish the function of concentrating the sunlight at a focusing point to form a hot spot. In practice, some conventional heliostats are canted in order to reduce the size of solar image and hence the size of parabolic reflector, but the image size can only be partially reduced due to the effect of the off-axis aberration. As a result, the conventional solar furnaces over the world, i.e. Odeillo Solar Furnace at France and White Sands Solar Furnace at U.S. etc., are all inevitably designed in such a way that the total reflective area of the heliostat is almost the same as the aperture area of parabolic reflector [1].

In order to greatly reduce the size of parabolic reflector, non-imaging focusing heliostat was first proposed by Chen *et al.* in 2001 [2]. The newly proposed heliostat consists of many small movable mirrors arranged into M rows and N columns so that each element mirror can play the role as a single unit of heliostat. Therefore, the required size of parabolic reflector can be reduced to the size of single element mirror. The major challenge of this new proposal is how to realize the mechanical implementation for controlling all the element mirrors because of each mirror will require two-degree-of-freedom. If there are M rows and N columns of element mirrors in the heliostat frame, the total required controlling devices shall be equal to the number of $2\times M\times N$. It will be too complicated to be implemented in practice and also very costly. To overcome this problem, the spinning-elevation tracking method was explored so that the sagittal and tangential directions are always fixed with respect to the heliostat frame during sun tracking. Therefore, the movements of all the mirrors in the heliostat frame can be grouped according to a certain regulation to superpose all the mirror images into one. Due to the fact that the new heliostat is an off-axis focusing and tracking device, mirror images cannot be perfectly overlapped all the time and instead they form a certain kind of distribution pattern scattered within a

Journal of Science and Technology in the Tropics (2006) **2**: 1

Editorial

We are pleased to announce that the Academy of Sciences Malaysia (ASM) and the Confederation of Scientific and Technological Associations in Malaysia (COSTAM) will jointly publish Journal of Science and Technology in the Tropics (JOSTT) Volume 2 onwards. This is indeed a historic development and augurs well for the future, as much synergy may be derived from the wealth of scientific expertise in both organisations. We will march steadily forward to focus on scientific developments in the Tropics.

While deliberating on matters of research and development, the question of basic and applied research often surfaces for debate. Our view, in short, is that we need both and what matters most is achieving excellence in the pursuit for and achievements in scientific solutions to problems and issues in the Tropics – our special focus of interest.

It is well known that numerous problems and issues exist in the developing countries many of which are in the Tropics, demanding scientific solutions. One way is the identification and establishment of specific mission oriented research such as those conducted by the Malaysian Palm Oil Board, where both fundamental and applied approaches are brought to bear for solutions. However, there should always be room for 'blue sky' research especially at institutions of higher learning in order not to miss the gems in our gifted young. Universities must provide a highly stimulating environment for current and comprehensive intellectual development and continue to produce motivated graduates convinced with the importance of 'The Art and Science of THINKING' encompassing both the critical as well as the creative.

Professor Datuk Dr Mazlan Othman
Co-Chairman, Editorial Board

Academician Tan Sri Dr Augustine S.H. Ong
Co-Chairman, Editorial Board

small area near the focusing point. This distribution pattern of mirror images was identified as residual aberration and the detail study of its characteristic was done [3].

Two prototypes were constructed to verify the theory of non-imaging focusing heliostat and to study its applications in harnessing solar energy. The first prototype was the smallest solar furnace in the world with total collective area of 4 m^2. In our laboratory testing on the new solar furnace, the highest achievable temperature of 3400°C was recorded through the melting of pure tungsten wire [4]. Following the verification of the theory, the second prototype of new solar furnace with total collective area of 12.96 m^2 was built for the application of potatoes peeling using highly concentrated sunlight [5].

In fact, the maximum achievable solar concentration as well as the temperature of solar furnace is determined by a hot spot formed at the target point. Practically, the size of the hot spot can be maneuvered to accommodate various applications' needs. In this paper, we will study and analyze the characteristics of the hot spot for the newly proposed solar furnace using mathematical modeling method. Furthermore, the performance of solar furnace including daily and yearly changes of the hot spot size in the relation with the design parameters will also be discussed.

METHODOLOGY OF HOT SPOT ANALYSIS

In the study of residual aberration for non-imaging focusing heliostat, Chen *et al.* have developed a special methodology to analyze the daily and yearly distribution pattern of solar images for the new heliostat [3]. Following the previous study, we employed the same methodology in performing an optical modeling of non-imaging focusing heliostat and its complementary parabolic reflector as to analyze the hot spot of new solar furnace. The configuration of the new solar furnace is shown in Figure 1, where the vertex of parabolic reflector is placed at the focusing point of the heliostat and both of their optical axes are coaxial. In the optical modeling, coordinate transformation is employed to describe the movements of the heliostat frame and the associated element mirrors. Besides, ray-trace method is employed to find the intersection point between the reflected ray from the heliostat and the surface of parabolic reflector, as well as the intersection point between the reflected ray from the parabolic reflector and target plane.

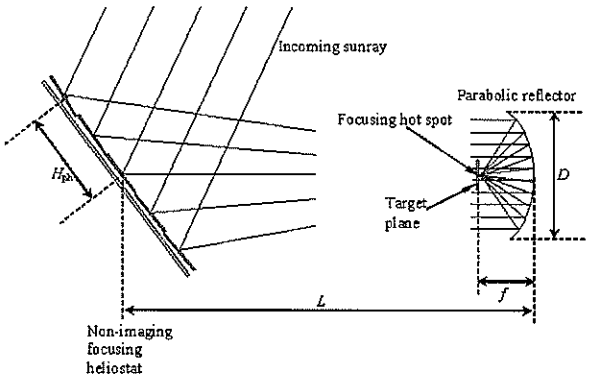

Figure 1. Configuration of the new solar furnace that consists of non-imaging focusing heliostat and a parabolic reflector.

The methodology to analyze the hot spot of the new solar furnace is divided into two stages: first stage is to model the mechanism of non-imaging focusing heliostat which performs sun tracking and sunlight focusing simultaneously; second stage is to model the parabolic reflector, which will further focus the sunlight to form a hot spot at the target plane.

To accomplish two simultaneous functions, the non-imaging focusing heliostat has to perform two different kinds of movements: global movement and local movement [4]. In the global movement, the heliostat frame will rotate with an angle ρ around the spinning-axis and with an angle θ around the elevation-axis, which are described as

$$\rho = \sin^{-1}\left\{\frac{-\sin\delta\cos\omega\sin\phi\sin\Phi+\cos\delta\sin\omega\cos\phi+\sin\delta\sin\phi\cos\Phi}{\cos\beta}\right\}, \quad (1)$$

$$\theta = \frac{\pi}{4}-\frac{1}{2}\beta, \quad (2)$$

and

$$\beta = \sin^{-1}\left\{\begin{array}{c}-\cos\delta\cos\omega(\sin\lambda\cos\Phi+\cos\lambda\cos\phi\sin\Phi)-\cos\delta\sin\omega\cos\lambda\sin\phi\\+\sin\delta(\cos\lambda\cos\phi\cos\Phi-\sin\Phi\sin\lambda)\end{array}\right\}, \quad (3)$$

where δ is the declination angle, Φ is the latitude, ω is the hour angle, ϕ is the facing angle of non-imaging focusing heliostat, and λ is the target angle of non-imaging focusing heliostat.

In the local movement, all element mirrors attached to the heliostat frame will be tilted in group manner with an angle σ for the mirrors arranged in rows and an angle γ for the mirrors arranged in columns, which are described as

$$\sigma = \frac{1}{2}tan^{-1}\left[\frac{H_z\cos\theta}{H_z\sin\theta+L}\right], \quad (4)$$

$$\gamma = \frac{1}{2}tan^{-1}\left[\frac{H_y}{L\cos\theta}\right], \quad (5)$$

where H_x is the perpendicular distance between the center of master mirror (the mirror that is located at the centre of heliostat frame) and the central line of the row where the concerned element mirror is located, H_y is the perpendicular distance between the center of master mirror and the central line of the column where the concerned element mirror is located, and L is the horizontal distance from the intersection point of spinning-axis and elevation-axis to the vertex of the parabolic reflector.

In the simulation of the hot spot at the target plane, we have made two simplifications to the methodology of optical modeling in order to reduce the computing time without much affecting on the final result. First, we assume that all the sunrays are parallel by omitting the solar disc effect where the sunrays are slightly deviated from the ideal parallel rays with maximum deviation angle of ± 4.653 mrad [6]. Second, we represent the image of each element mirror by a finite number of parallel sunray that are uniformly incident onto the element mirror in the grid form (see Fig. 2). Additionally, we also considered that all element mirrors are flat and its pivot point located at the centre of the mirror.

Prior to carry out the mathematical analysis, an initial coordinate of reflective point for the particular element mirror located at i-th row and j-th column is defined as $(H_x, H_y, H_z)_{ijop}$, where the other two subscribes o and p represent the position of the reflective point at o-th row and p-th column in the element mirror. In the following text, we call this reflective point as primary reflective point as to differentiate it from the reflective point on the parabolic reflector that will be called secondary reflective point. Fig. 2 shows that each element mirror is represented by 9 rows and 9 columns of primary reflective points and the origin of the coordinate system, **O** (0, 0, 0), is located at the centre of the heliostat frame.

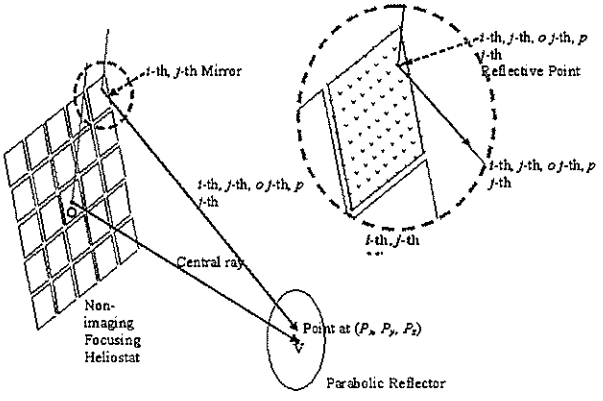

Figure 2. Schematic diagram to show how a ray that incident onto i-th, j-th, o-th, p-th reflective point located at i-th, j-th mirror and is then reflected towards the parabolic reflector. In the highlighted diagram (at the right), we represent each facet mirror by 9 rows and 9 columns of reflective points in the grid pattern.

During sun tracking, the heliostat frame initiates global movement to rotate about **O** for achieving the angles ρ and θ, while the concerned element mirror engages local movement to tilt about its pivot point for achieving the angles σ and γ. The combination of two movements will relocate the primary reflective point to a new coordinate $(H'_x, H'_y, H'_z)_{ijop}$.

The matrix for the coordinate transformations from $\mathbf{H}_{ijop} = (H_x, H_y, H_z)_{ijop}$ to $\mathbf{H'}_{ijop} = (H'_x, H'_y, H'_z)_{ijop}$ is described as

$$\mathbf{M}_{ij} = [\rho][\theta][\sigma][\gamma] \tag{6}$$

and hence we also can write it as

$$\mathbf{H'}_{ijop} = \mathbf{M}_{ij}\,\mathbf{H}_{ijop} \tag{7}$$

where

$$[\rho]=\begin{bmatrix} cos\rho & sin\rho & 0 \\ -sin\rho & cos\rho & 0 \\ 0 & 0 & 1 \end{bmatrix},\quad [\theta]=\begin{bmatrix} cos\theta & 0 & sin\theta \\ 0 & 1 & 0 \\ -sin\theta & 0 & cos\theta \end{bmatrix},$$

$$[\sigma]=\begin{bmatrix} cos\sigma & 0 & -sin\sigma \\ 0 & 1 & 0 \\ sin\sigma & 0 & cos\sigma \end{bmatrix},\quad [\gamma]=\begin{bmatrix} 1 & 0 & 0 \\ 0 & cos\gamma & -sin\gamma \\ 0 & sin\gamma & cos\gamma \end{bmatrix}$$

In ray-trace technique, we need to find the unit vector of the primary reflected ray from the heliostat in order to trace the secondary reflective point that is located on the surface of the parabolic reflector. To do so, we have to define the unit vector of incident sunray $\hat{I} = I_x\hat{x} + I_y\hat{y} + I_z\hat{z}$, which is described in terms of sun's position angles of ρ and β as

$$\begin{aligned} I_x &= cos\beta cos\rho \\ I_y &= -cos\beta sin\rho \\ I_z &= sin\beta \end{aligned} \tag{8}$$

Before sun tracking, all the element mirrors are assumed to be oriented in such a way that their normal, are pointing towards + z direction as shown in Fig. 3. Therefore, the normal of the mirror in the initial orientation can be described by unit vector $\hat{N} = \hat{z}$ or its corresponding matrix form as

Journal of Science and Technology in the Tropics (2006) 2: 27-34

$$\mathbf{N} = \begin{bmatrix} 0 \\ 0 \\ 1 \end{bmatrix} \tag{9}$$

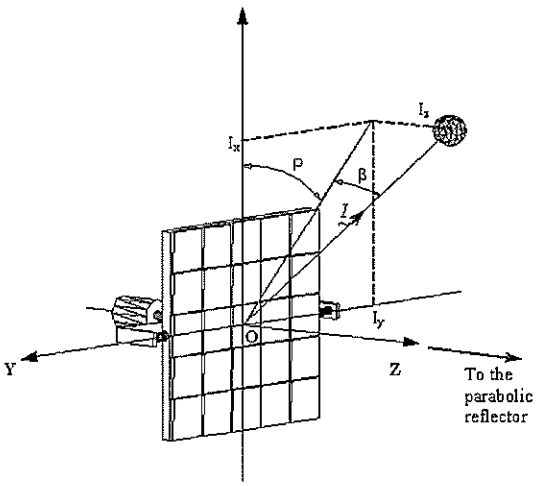

Figure 3. Schematic diagram to show the coordinate system with the origin **O** is at the intersection point of the elevation-axis and spinning-axis. Before sun tracking, all the facet mirrors are assumed to be oriented in such a way that their normal, are pointing towards + z direction.

Similar to the case of the reflective point, the initial unit vector normal, **N**, will also undergo the coordinate transformation $\mathbf{M_{ij}}$ when the element mirror performs global and local movements during sun tracking. Consequently, we will have new unit vector normal, $\hat{N}_{ijop} = N_x\hat{x} + N_y\hat{y} + N_z\hat{z}$ or its corresponding matrix form as

$$\mathbf{N_{ijop}} = \mathbf{M_{ij}}\,\mathbf{N} \tag{10}$$

Based on the unit vectors of both the incident sunray and the normal of the element mirror, the unit vector of the primary reflected ray from the heliostat $\hat{R}_{ijop} = R_x\hat{x} + R_y\hat{y} + R_z\hat{z}$ can be obtained as

$$\begin{aligned} R_x &= 2(I_xN_x + I_yN_y + I_zN_z)N_x - I_x \\ R_y &= 2(I_xN_x + I_yN_y + I_zN_z)N_y - I_y \\ R_z &= 2(I_xN_x + I_yN_y + I_zN_z)N_z - I_z \end{aligned} \tag{11}$$

Given the unit vector of the primary reflected ray and the coordinate of the primary reflective point, the line equation of the primary reflected ray can easily be derived as

$$\frac{P_x - H'_x}{R_x} = \frac{P_y - H'_y}{R_y} = \frac{P_z - H'_z}{R_z} \tag{12}$$

where (P_x, P_y, P_z) is the coordinate of the secondary reflective point located on the surface of parabolic reflector.

On the other hand, the surface equation of the parabolic reflector is written as

$$S = P_x^2 + P_y^2 + 4f(P_z - L) \tag{13}$$

where f is the focusing distance of the parabolic reflector.

To obtain the coordinate of secondary reflective point (P_x, P_y, P_z), the value of S in the eqn. (13) is first set to zero and then solved with eqn. (12).

From the eqn. (13), the unit vector normal of the parabolic reflector, $\hat{N}'_{ijop} = N'_x\hat{x} + N'_y\hat{y} + N'_z\hat{z}$, can be derived from the gradient of the surface equation and then divided by its magnitude as shown

$$\hat{N}'_{ijop} = \frac{\nabla S}{|\nabla S|} \tag{14}$$

Again, with the reflection equations similar to eqn. (11), the unit vector of the secondary reflected ray, $\hat{R}'_{ijop} = R'_x\hat{x} + R'_y\hat{y} + R'_z\hat{z}$, can be obtained as

$$\begin{aligned} R'_x &= 2(R_xN'_x + R_yN'_y + R_zN'_z)N'_x - R_x \\ R'_y &= 2(R_xN'_x + R_yN'_y + R_zN'_z)N'_y - R_y \\ R'_z &= 2(R_xN'_x + R_yN'_y + R_zN'_z)N'_z - R_z \end{aligned} \tag{15}$$

Finally, in order to determine the image point on the target plane that is placed perpendicular to the optical axis of parabolic reflector, we have to solve the line equation of the secondary reflected ray with the surface equation of the target plane. The coordinate of the image point on the target is then calculated as

$$\begin{aligned} T_x &= \frac{R'_x}{R'_z}(L - f - P_z) + P_x \\ T_y &= \frac{R'_y}{R'_z}(L - f - P_z) + P_y \end{aligned}$$

Given the coordinate of (T_x, T_y), we will be able to plot the distribution of solar images that forms the hot spot of the solar furnace on the target plane.

CHARACTERISTIC STUDY OF THE HOT SPOT

It is well known that the size of the hot spot is the key factor for the success of a solar furnace. This is because the highest achievable temperature of a solar furnace system depends on the solar concentration ratio and thus the size of hot spot. Following the results gained from previous prototypes of new solar furnaces, in this paper we would reveal the theoretical study of the new solar furnace system using the above methodology. As to relate the study with the previous practical work, we choose all the parameters of our case study to be the same as that of the first prototype of new solar furnace. In the first prototype, the non-imaging focusing heliostat consists of 25 mirrors arranged into 5 rows and 5 columns with the dimension of each element mirror as 40cm × 40cm. In addition, we assume that the new solar furnace system is located at Kuala Lumpur, Malaysia, with latitude $\Phi = 1.57°$ m, while other parameters include target angle $\lambda = 0°$, facing angle $\phi = 0°$, slant range $L = 10.0$ m as well as focusing distance of parabolic reflector $f = 15.0$ cm and its aperture size $D = 60$ cm.

Using the methodology of the hot spot analysis, the changes of solar images distribution pattern on daily and yearly basis are plotted as shown in Fig. 4 and Fig. 5 respectively. Referring to Fig. 4, the distribution pattern of the solar images is actually a distorted image of 25-mirror heliostat. Apparently, the solar image of the master mirror is perfectly collapsed into a point in as much as the sunray reflected from the master mirror is parallel and on-axis towards the parabolic reflector. Whereas for the solar image other than that of the master mirror, the image is distorted to a comet-like pattern in as much as the sunray reflected from this mirror is off-axis towards the parabolic reflector. Apart from that, the images distribution pattern is symmetric along the axis of the central column, while it is asymmetry along the axis of the center row. This asymmetrical pattern of the hot spot is caused by the tilting angles of the upper rows are greater than the tilting angles of the lower rows.

With the above parameters, the incidence angle, θ, is nearly constant in the same day but the angle ρ changes is with the local time at the rate of about 15° per hour during daily sun tracking. Hence, the distribution pattern of solar images remains unchanged during the course of the day. Fig. 4(a)-(d) illustrate how the distribution pattern rotates around the optical axis. In the yearly sun tracking, the incidence angle will vary as the declination angle of the earth changes over the

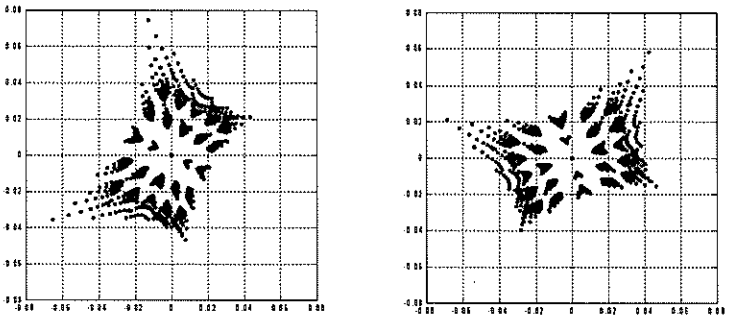

(a) Local Time: 0900 Hour

(b) Local Time: 1200 Hour

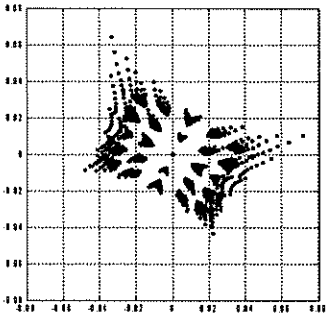

(c) Local Time: 1500 Hour

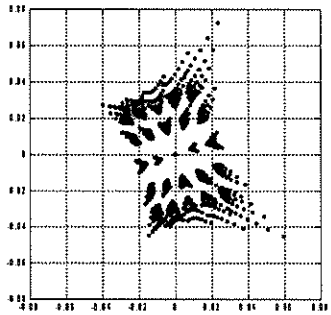

(d) Local Time: 1800 Hour

Figure 4. The distribution pattern of solar images for the new solar furnace that consists of 25-mirror non-imaging focusing heliostat and parabolic reflector. The plots show the daily changes of the hot spot pattern on 21st March for local time 0900 Hour, 1200 Hour, 1500 Hour and 1800 Hour.

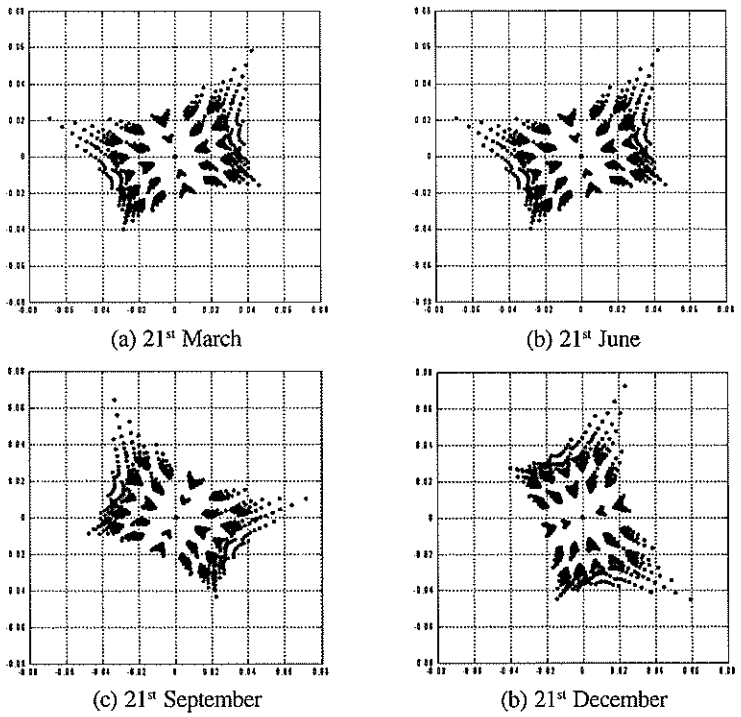

(a) 21st March (b) 21st June

(c) 21st September (b) 21st December

Figure 5. The distribution pattern of solar images for the new solar furnace that consists of 25-mirror non-imaging focusing heliostat and parabolic reflector. The plots show the yearly changes of the hot spot pattern on 21st March, 21st June, 21st September and 21st December.

year. From Fig. 5(a)-(d), the coverage area of the distribution pattern alters with the incidence angle in different months. On 21st December, the incidence angle is the largest over the year with 56.2° but the size of the hot spot is the smallest. In contrast, the incidence angle is the smallest on 21st June, with 33.9°, whilst the hot spot is the largest. This can be explained from the result of residual aberration in the first stage focusing by the heliostat [4] as higher incidence angle leads to a larger aberrant spread. This also indicates that the reflected rays from the heliostat are closer to parallel rays. For parabolic reflector, the focusing effect is better if the sunrays are more parallel relative to its optical axis. Thus, this explains why larger incidence angle leads to better overall result.

DESIGN PARAMETERS OF SOLAR FURNACE

In general, the characteristic of the hot spot can be analyzed through its relationship with three major design parameters. These parameters are incidence angle, L/H_{ph} ratio of the heliostat and f/D ratio of the parabolic reflector, where H_{ph} is the perpendicular distance between the centre of the master mirror with the centre line of the peripheral row or column. The incidence angle is considered as one of the design parameters because the range of incidence angle is determined by the orientations of the heliostat, which are the target angle, λ, and the facing angle, ϕ.

From the above plotted distribution pattern of solar images, it is obvious that they are not perfectly superposed onto each other. Instead, the sunrays reflected from all the mirrors in the heliostat frame and parabolic reflector are inevitably spread and therefore the focusing spot is aberrant. Since the aberrant spread is not uniformly distributed, we naturally approximate the size of hot spot as the rectangular area of the aberrant spread where 80% of the solar rays are confined within.

Figure 6 compares the effects of varying the L/H_{ph} ratio of the heliostat to the size of hot spot for the incidence angle of 30°. In the same graph, the average concentration ratio of the hot spot is also plotted to shows its relationship with L/H_{ph} ratio. In the design of solar furnace, the larger the L/H_{ph} ratio, the better is the average concentration, and hence the higher is the temperature obtained. This is due to the fact that the reflected rays from the heliostat will be closer to parallel rays as the ratio of L/H_{ph} is increased.

Figure 7 shows how the size of hot spot and average concentration ratio varies with f/D ratio of parabolic reflector in the design of solar furnace with condition

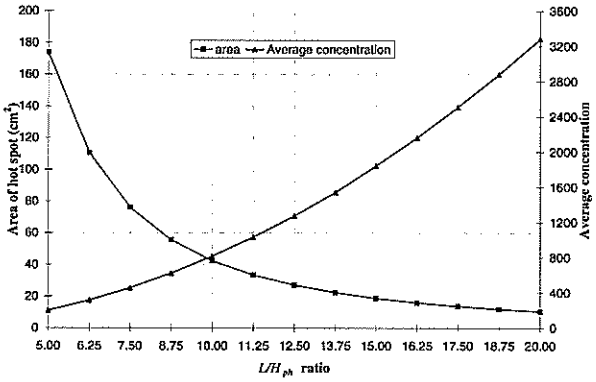

Figure 6. Graphs to show the size of hot spot and average solar concentration ratio versus the L/H_{ph} ratio, provided that incidence angle = 30° and the *f/D* of parabolic reflector = 0.5.

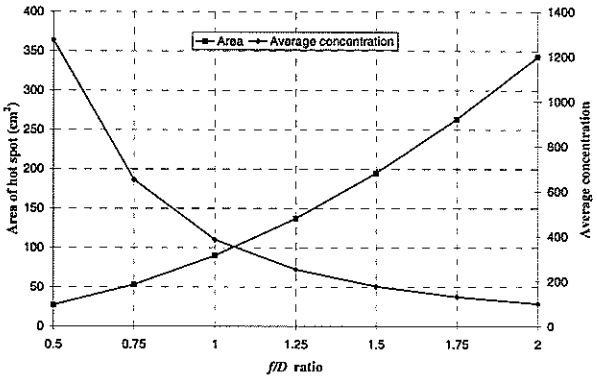

Figure 7. Graphs to show the size of hot spot and average solar concentration ratio versus the *f/D* ratio of the parabolic reflector, provided that incident angle = 30° and the L/H_{ph} of the heliostat = 10.

of incident angle = 30° and L/H_{ph} ratio = 10. In contrast to L/H_{ph} ratio of the heliostat, the smaller value of *f/D* ratio will produce higher value of the average concentration ratio.

Finally, Figure 8 reveals the relationship between the incidence angle and the average concentration ratio of the solar furnace provided that L/H_{ph} ratio = 10 and *f/D* ratio = 0.5. In common practice, most of the solar

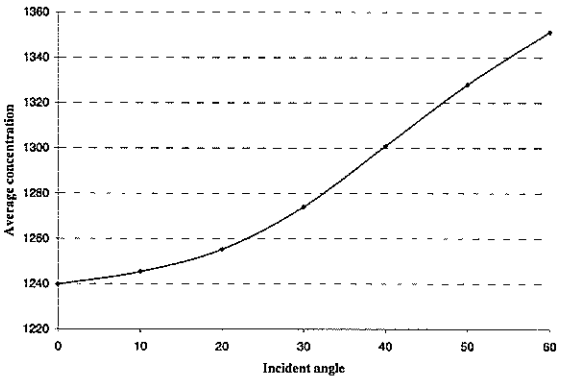

Figure 8. Graph to show the average solar concentration ratio versus the incidence angle, provided that the L/H_{ph} ratio of the heliostat = 10 and the *f/D* ratio of the parabolic reflector = 0.5.

furnace designs are not desirable to have high incidence angle as the power losses is serious due to the cosine effect. Therefore, we are only interested on the effect of the incidence angle up to 60° and it is found that the average concentration ratio is proportional to the incidence angle.

CONCLUSION

Unlike the conventional fixed-target of solar furnace, the newly proposed non-imaging focusing heliostat, which can perform off-axis-focusing and sun-tracking concurrently, has allowed a much smaller parabolic reflector to be used. In our case study, the reflective area of new heliostat is 2.0 m × 2.0 m while the aperture size of parabolic reflector is only 60 cm in diameter. In this paper, the methodology of hot spot analysis and the characteristic study of the new solar furnace were presented. In general, the size of the hot spot and hence the solar concentration ratio are proportional with incidence angle as well as L/H_{ph} ratio of the heliostat, while is inversely proportional with *f/D* ratio of the parabolic reflector.

REFERENCES

1. Kreider J. F. (1979) *Medium and High Temperature Solar Processes*. Academic Press, USA.
2. Chen Y.T, Chong K.K., Bligh T.P., Chen L.C., Yunus J., Kanna K.S., Lim B.H., Lim C.S., Alias M.A., Bidin N., Aliman O., Salehan S., Shk. Abd. Rezan S.A.H., Tam C.M. and Tan K.K. (2001) Non-imaging focusing heliostat. *Solar Energy* **71**: 155-164.
3. Chen Y.T., Chong K.K., Lim C.S., Tan B.K., Lim

B.H. and Lu Y.F. (2005) Report on the Second Prototype of Non-Imaging Focusing Heliostat and Its Application in Food Technology. *Solar Energy* **79**: 280-289.

4. Chen Y.T., Chong K.K., Lim B.H. and Lim C.S. (2003) Study of residual aberration for non-imaging focusing heliostat. *Solar Energy Materials & Solar Cells* **79**: 1-20.
5. Chen Y.T., Chong K.K., Lim C.S. et al (2002). Report of the first prototype of non-imaging focusing heliostat and it's application in high temperature solar furnace. *Solar Energy* **72**: 531-544.
6. Winter C.J., Sizmann R.L. and Vant-Hull L.L. (Eds.) (1991) *Solar Power Plants Fundamentals, Technology, Systems, Economics*. Springer-Verlag, New York.

Journal of Science and Technology in the Tropics (2006) **2**: 35-39

Synthesis and evaluation of glycerol esters

Gladys H. P. Cho [1,2], S. K. Yeong [2], T. L. Ooi [2] and C. H. Chuah[1]
[1]Department of Chemistry, Faculty of Science, University of Malaya,
50603 Kuala Lumpur
[2]AOTD-MPOB, Lot 9&11, Jalan P10/14, 43650 Bandar Baru Bangi,
Selangor Darul Ehsan
(Email: gladyschohp@yahoo.com)

Received 20.10.2005; accepted 24.03.2006

Abstract Base-catalyzed reactions of glycerol with dicarboxylic acid esters (C_4-C_9) produced a mixture of mono- and di-esterified glycerol. These esters 2,3-dihydroxy-propyl methyl succinate, 1,3-dimethoxysuccinyloxy propan-2-ol, 2,3-dihydroxy-propyl methyl glutarate, 1,3-dimethoxyglutaryloxy propan-2-ol, 2,3-dihydroxy-propyl methyl azelate and 1,3-dimethoxyazelyloxy propan-2-ol which were not reported were separated chromatographically and elucidated spectrometrically.

Keywords Diglycerol ester – dimethyl ester – glycerol – monoglycerol ester

INTRODUCTION

Glycerol is one of the oleochemicals that can be derived from oils of rapeseed [1], sunflower [2], soybean [3], crambe [4], camelina [4] and palm fruits [5]. As glycerol is the by-product in the production of biodiesel [2], we would envisage that there would be a surplus of glycerol due to the increased in demand for biodiesel. As there are limited reports in the synthesis of glycerol with short-carbon-chain dicarboxylic acid esters, the present studies on synthesis of glycerol ester by alcoholysis of glycerol with dicarboxylic acid esters (C_4–C_9) represent a contribution to this subject. It was noted that dicarboxylic glycerol ester possess properties of lubricant [6], surfactants [7] and thin film coating [8-9]. In this paper, the physical properties and potential applications of synthesized glycerol esters were evaluated.

MATERIALS AND METHODS

Materials

Glycerol with purity of 99.2 % was purchased from Fisher Chemicals. Dicarboxylic acid ester, i.e. dimethyl succinate, dimethyl glutarate, dimethyl adipate and dimethyl azelate and molecular sieves 4A were purchased from Fluka whereas potassium hydroxide was purchased from J.T.Baker. All the solvents used in LCMS were of HPLC grade.

Methods

Alcoholysis reactions were performed in a 1000 ml three-necked flask equipped with a reflux condenser, thermometer and sampling port. The reactor was immersed in a water bath and agitation was provided by a magnetic stirrer. The reaction of glycerol with dicarboxylic acid ester in the molar ratio 4:1 was carried out at 80°C, catalyzed by 0.2 wt% of potassium hydroxide (KOH) and 2 wt% of molecular sieve for 6 hours. The reaction products were washed with water and followed by extraction of glycerol esters. 100 ml of products were placed in a separating funnel and extracted with 30 ml of chloroform. The funnel was shaken for 2 minutes. The chloroform phase was collected in a 150 ml round bottom flask. The extraction was repeated twice with 30 ml of chloroform. Finally, the combined chloroform extracts were concentrated by a Rotary vacuum evaporator at 60 °C.

Analysis

IR spectrum of glycerol esters was recorded on a Nicolet magna FT-IR 550 spectrometer. GC analysis of glycerol

esters were performed on an Agilent 6890N gas chromatograph equipped with a flame ionization detector fitted with a DB Wax 30 m x 0.32 mm x 0.25 μm column. The oven temperature was programmed from 60 °C to 230 °C with increment at 2 °C/min. The injector port temperature was set at 240 °C and the detector temperature at 260 °C. GCMS was performed on an Agilent 6893 series gas chromatograph fitted with a DB Wax 30 m x 0.32 mm x 0.25 μm capillary column and temperature programming was similar to GC. LCMS was performed on PE Sciex API 100 LC/MS fitted with a SGE GL Wakosil 150 mm x 2 mm x 5 μm C-18 column. Water with 0.1 % of formic acid and methanol with 0.1 % of formic acid in ratio (55:45) was used as mobile phase for Flow Injector Analysis. Viscosity was obtained by using a common cross arm viscometer and viscosity index was calculated using ASTM method D445-88 [10] and ASTM D 2270-79 [11]. Pour points were measured by ASTM method D 97-87 [12] to an accuracy of ± 3 °C. Cloud points were determined by AOCS method Cc 6-25 [13] to an accuracy of ± 1 °C. Densities were measured by DMA 5000 Anton Paar density meter. Electrical conductivities were measured by Crison conductivity meter. The measurements of surface tension were performed by using the Sigma 70 tensiometer.

Identification of the synthesized compounds are described below.

(1) *Products identified from reaction of glycerol with dimethyl succinate*

2,3-dihydroxy-propyl methyl succinate (A) : IR ν_{max} cm^{-1}: 3408, 2953, 1727, 1641, 1433, 1217. EI-GCMS m/z (rel. int.): 189 (M^+-OH, 1), 175 (M^+-OCH_3, 5), 147 ($C_6H_{11}O_4^+$, 5), 115 ($C_5H_7O_3^+$, 100%), 59 ($C_2H_3O_2^+$, 20). APCI-LCMS m/z (rel. int.): 207 [$(M+H)^+$, 100%].

1,3-dimethoxysuccinyloxy propan-2-ol (B) : IR ν_{max} cm^{-1}: 3408, 2953, 1727, 1641, 1433, 1217. EI-GCMS m/z (rel. int.): 320 [M^+, 2], 289 (M^+-OCH_3, 5), 189 ($C_8H_{13}O_5^+$, 7), 175 ($C_7H_{11}O_5^+$, 10), 115 ($C_5H_7O_3^+$, 100%), 59 ($C_2H_3O_2^+$, 20). APCI-LCMS m/z (rel. int.): 321 [$(M+H)^+$, 100%].

(2) *Products identified from reaction of glycerol with dimethyl glutarate*

2,3-dihydroxy-propyl methyl glutarate (C) : IR ν_{max} cm^{-1}: 3443, 2951, 1726, 1640, 1444, 1216. EI-GCMS m/z (rel. int.): 220 [M^+, 3], 203 (M^+-OH, 1), 189 (M^+-OCH_3, 10), 129 ($C_6H_9O_3^+$, 100%), 101 ($C_5H_9O_2^+$, 45), 59 ($C_2H_3O_2^+$, 53). APCI-LCMS m/z (rel. int.): 221 [$(M+H)^+$, 100%].

1,3-dimethoxyglutaryloxy propan-2-ol (D) : IR ν_{max} cm^{-1}: 3443, 2951, 1726, 1640, 1444, 1216. EI-GCMS m/z (rel. int.): 289 (M^+-C(=0)OCH_3, 5), 189 ($C_8H_{13}O_5$, 7), 129 ($C_6H_9O_3^+$, 100%), 101 ($C_5H_9O_2^+$, 10), 87 ($C_4H_7O_2^+$, 11), 59 ($C_2H_3O_2^+$, 20). APCI-LCMS m/z (rel. int.): 349 [$(M+H)^+$, 100%].

(3) *Products identified from reaction of glycerol with dimethyl adipate*

2,3-dihydroxy-propyl methyl adipate (E) : IR ν_{max} cm^{-1}: 3410, 2951, 1724, 1639, 1442, 1213. EI-GCMS m/z (rel. int.): 203 (M^+-OCH_3, 5), 175 (M^+-C(=0)OCH_3, 10), 173 ($C_8H_{13}O_4^+$, 22), 161 ($C_7H_{13}O_4^+$, 15), 143 ($C_7H_{11}O_3^+$, 100%), 115 ($C_6H_{11}O_2^+$, 30), 59 ($C_2H_3O_2^+$, 21). APCI-LCMS m/z (rel. int.): 235 [$(M+H)^+$, 100%].

1,3-dimethoxyadipyloxy propan-2-ol (F) : IR ν_{max} cm^{-1}: 3410, 2951, 1724, 1639, 1442, 1213. EI-GCMS m/z (rel. int.): 345 (M^+-OCH_3, 3), 317 (M^+-C(=0)OCH_3, 7), 303 ($C_{14}H_{23}O_7^+$, 15), 143 ($C_7H_{11}O_3^+$, 100%), 115 ($C_6H_{11}O_2^+$, 40), 73 ($C_3H_5O_2^+$, 20), 59 ($C_2H_3O_2^+$, 18). APCI-LCMS m/z (rel. int.): 377 [$(M+H)^+$, 100%].

(4) *Products identified from reaction of glycerol with dimethyl azelate*

2,3-dihydroxy-propyl methyl azelate (G) : IR ν_{max} cm^{-1}: 3412, 2950, 1723, 1637, 1443, 1215. EI-GCMS m/z (rel. int.): 276 [M^+, 2], 259 (M^+-OH, 5), 217 (M^+-C(=0)OCH_3, 7), 215 ($C_{11}H_{19}O_4^+$, 15), 203 ($C_{10}H_{19}O_4^+$, 20), 185 ($C_{10}H_{17}O_3^+$, 100%), 157 ($C_9H_{17}O_2^+$, 20), 59 ($C_2H_3O_2^+$, 25). APCI-LCMS m/z (rel. int.): 277 [$(M+H)^+$, 100%].

1,3-dimethoxyazelyloxy propan-2-ol (H) : IR ν_{max} cm^{-1}: 3412, 2950, 1723, 1637, 1443, 1215. EI-GCMS m/z (rel. int.): 429 (M^+-OCH_3, 7), 401 ($C_{21}H_{37}O_7^+$, 10), 303 ($C_{14}H_{23}O_7^+$, 20), 185 ($C_{10}H_{17}O_3^+$, 100%), 157 ($C_9H_{17}O_2^+$, 20), 73 ($C_3H_5O_2^+$, 25), 59 ($C_2H_3O_2^+$, 30). APCI-LCMS m/z (rel. int.): 461 [$(M+H)^+$, 100%].

RESULTS AND DISCUSSION

Glycerol esters (**A-H**) from the reaction of glycerol with dicarboxylic acid methyl esters (dimethyl succinate,

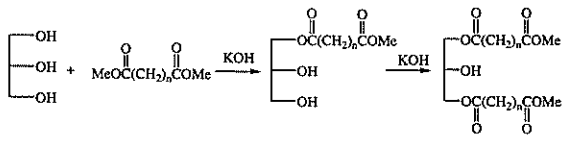

Figure 1. Schematic of synthesized mono- and di-glycerol esters (n=2,3,4,7).

dimethyl glutarate, dimethyl adipate and dimethyl azelate) were synthesized. The general scheme of synthesis is illustrated in Figure 1.

The proposed mechanism as in Figure 2 showed the reaction of the base with the alcohol (glycerol) to produce an alkoxide, (**i**) [14]. The alkoxide (**i**) will attack the carbon atom of carbonyl group in dicarboxylic acid methyl esters to generate a tetrahedral intermediate, (**ii**). The formation of glycerol monoesters is due to the intermolecular rearrangement and cleavage of methoxyl group as a leaving group. The deprotonate catalyst produce an alkoxide that regenerating the active species which is now able to react with a second molecule of the alcohol and the reaction repeated another catalytic cycle to produce di-glycerol ester.

Based on the mechanism, mono-glycerol esters were initially formed whereas di-glycerol esters were formed from the mono-glycerol esters. Therefore, we can envisage that yield of mono-glycerol esters were much higher than di-glycerol ester as shown in Figure 3. In addition, the glycerol esters formed from the reaction of glycerol-dimethyl azelate were highest

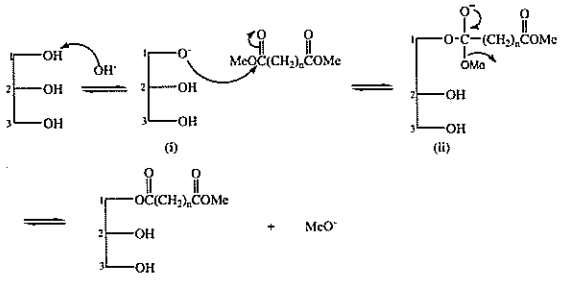

Figure 2. Proposed mechanism for the formation monoester (n=2,3,4,7).

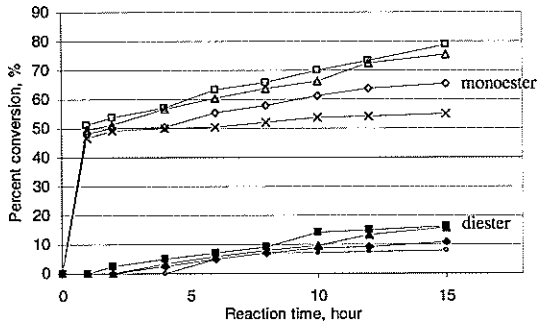

Figure 3. Percent conversion of mono- glycerol ester by glycerol with dimethyl succinate, (x); dimethyl glutarate, (◇); dimethyl adipate, (△); dimethyl azelate, (□) and di-glycerol ester by glycerol with dimethyl succinate, (o); dimethyl glutarate, (◆); dimethyl adipate, (▲);and dimethyl azelate, (■).

followed with dimethyl adipate, dimethyl glutarate and dimethyl succinate as shown in Figure 3.

IR spectrum of all compounds showed an absorption at 3408-3412 cm^{-1} that are characteristic of the OH stretching from glycerol, along with the absorption at 1723-1727 cm^{-1} that are C=O stretching for glycerol esters, 1637-1641 cm^{-1} band that are C=O stretching of dicarboxylic acid esters and 1230 cm^{-1} band that are bending of the C-O-C group in ester. The C=O stretching is useful for monitoring the formation of glycerol esters.

In the EI mass spectrum, all glycerol esters showed a characteristic fragment of $[C(=O)(CH_2)_nC(=O)OCH_3]^+$ which is the cleavage at oxygen atoms of ester bond of the glycerol ester. The fragment ions serve as primary function of depicting the types of dicarboxylic acid esters that have reacted with glycerol. The reaction of dimethyl succinate with glycerol gives fragment ions m/e 115; dimethyl glutarate with glycerol gives fragment ions m/e 129; dimethyl adipate with glycerol gives fragment ions m/e 143; and dimethyl azelate with glycerol gives fragment ions m/e 185. Identification of M^+ can be verified by the acylium ion, M^+-31, as shown in Figure 4 [15]. Formation of acylium ion was due to the loss of methoxyl group by simple α-cleavage for all the products. Another significant ion in methyl ester was m/e 59, $[CH_3OC(=O)]^+$, which is also due to the α-cleavage in ester linkage [15-16]. The fragmentation pattern of m/e 59 is shown in Figure 4.

Due to the bombardment of the molecules with 70 eV beams of electrons at EI-GCMS, only a few glycerol ester's molecular ion were obtained [15-17]. Therefore, APCI-LCMS, a soft ionization technique, was used in order to obtain the molecular ion [17-19]. In the positive ion mode, the reagent ion generally acts as an acid, donating a proton to the synthesized compounds (M) and thus producing $[M+H]^+$ as a pseudo-molecular (even electron) ions for the glycerol esters. CI-MS spectrum gave a molecular ion for compounds **A**, **B**, **C**, **D**, **E**, **F**, **G** and **H** at m/e 206, 320, 220, 348, 234, 376, 276 and 460, which correspond to the molecular formula $C_8H_{14}O_6$, $C_{13}H_{20}O_9$, $C_9H_{16}O_6$, $C_{15}H_{24}O_9$,

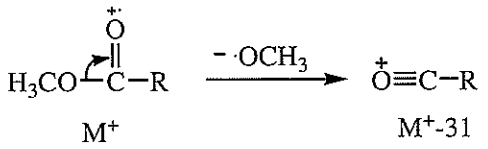

Figure 4. Simple α-cleavage of methoxyl group; where R = $(CH_2)_nO(C=O)CH_2CHOHCH_2OH$ or $(CH_2)_nO(C=O)CH_2CHOHCH_2OC(=O)(CH_2)_nC(=O)OMe$.

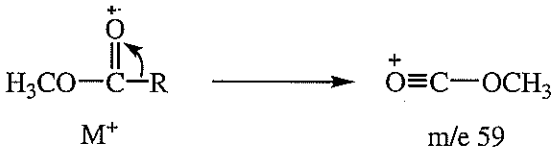

Figure 5. Formation of m/e 59; where R = $(CH_2)_nO(C=O)CH_2CHOHCH_2O$ or $(CH_2)_nO(C=O)CH_2CHOHCH_2OC(=O)(CH_2)_nC(=O)OMe$.

$C_{10}H_{18}O_6$, $C_{17}H_{28}O_9$, $C_{13}H_{24}O_6$ and $C_{23}H_{40}O_9$, respectively. As results of this, compounds 2,3-dihydroxy-propyl methyl succinate (**A**), 1,3-dimethoxysuccinyloxy propan-2-ol (**B**), 2,3-dihydroxy-propyl methyl glutarate (**C**), 1,3-dimethoxyglutaryloxy propan-2-ol (**D**), 2,3-dihydroxy-propyl methyl adipate (**E**), 1,3-dimethoxyadipyloxy propan-2-ol (**F**), 2,3-dihydroxy-propyl methyl azelate (**G**) and 1,3-dimethoxyazelyloxy propan-2-ol (**H**) were assigned based on the GCMS and LCMS.

Glycerol esters have been reported to have a direct application as non-ionic surfactant [20], emulsifying, thickening agent and as plasticizers [21]. However, we are focus on the application as lubricant or surfactant. The measurement of viscosity, viscosity index, pour point, cloud point, density, surface tension, specific gravity and electrical conductivity of the glycerol esters were summarized in Table 1. Dynamic viscosity of compounds **A**, **C**, **E** and **G** were 20, 23, 25 and 115 cP respectively. These data showed that they are possessing properties of a newtonian fluid which is similar to mineral oil and thin motor oil. Electrical conductivities of mono-glycerol esters were from 0.46 to 1.29 μS/m meet the ASTM 4865 guide (Standard Guide for the Generation and Dissipation of Static Electricity in Petroleum Fuel Systems) for lubricants. The kinematic viscosity of mono-glycerol esters is in the range from 16 to 98 cSt at 40 °C and 3 to 11 cSt at 100 °C. Compound **E** has a viscosity 3.96 cSt at 100 °C that is in the range of 2.3 to 5.4 cSt at 100 °C which was the specification for adipates that are commonly used in synthetic lubricants such as screw compressor oils, gear and transmission oils, automotive crankcase oils, and hydraulic fluids. However, VI of the mono-glycerol esters are range from 33 to 95 did not meet the specification of industrial mineral lubricating oils which normally have VI from 90 to 175. The density of compounds **A**, **C**, **E**, and **G** were more than 1 g/ml which was also out of the range of the lubricant specification (0.86 to 0.98 g/ml).

Surface tension of **A**, **C**, **E** and **G** were at a range from 29 to 30 mN/m. These values are close to the surface tension of the industrial surfactants which range from 26-28 mN/m [23]. Surface tension decreased when the carbon chain length of dimethyl ester increased. This is probably due to polarity of the molecules [24]. From the literature, mono- and di-glycerides are mild surfactants and widely used in food industries. They also can be reacted further to produce more complex products such as the phospholipids [25] which are the most common biosurfactants. Besides that, succinate glycerides can be used in the preparation of sulphosuccinates. Sulphosuccinates are used in conjugation with harsh detergents like sodium lauryl sulphate to reduce the irritation of the sulphate ester. In addition, pour point of mono-glycerol esters was range from -15 to -45 °C, and useful in cool temperature. This pour points are superior to the current surfactants (glycerol mono-oleate and glycerol mono-stearate) which have pour point 6 °C [26]. Based on the physical data of mono-glycerol ester, they can be used as a precursor for biopolymers which will benefit the surfactant industries.

Acknowledgements – We thank University of Malaya and Malaysian Palm Oil Board (MPOB) for supporting this work.

Table 1. Physical data of mono-glycerol esters.

Properties	Temperature, °C	A	C	E	G
Kinematic viscosity, cSt.	40	16.21	18.54	21.31	98.34
	100	3.22	3.52	3.96	10.95
Dynamic viscosity, cP	25	20.12	23.21	25.77	115.58
Viscosity index, VI	-	33	38	70	95
Pour point, °C	-	-42	-42	-45	-15
Cloud point, °C	-	-18	-20	-22	9
Density, g/ml	25	1.2379	1.2159	1.2094	1.1753
Specific gravity, g/ml	25	1.2416	1.2187	1.2130	1.1788
Electrical conductivity, 10^6pS/m	25	1.29	1.13	1.00	0.46
Surface tension, mN/m	25	30.70	30.50	30.30	29.51

REFERENCES

1. Dragan N., Rupert P., Manfred W. and Richard J.G. (2000) Preparation of rapeseed oil esters of lower aliphatic alcohols. *J. Am. Oil Chem. Soc* **77**: 275-280.
2. Fukuda H., Kondo A. and Noda H. (2001) Review; Biodiesel fuel production by transesterification of oils. *J. Biosci. And Bioengine.* **92**: 405-416.
3. Freedman B., Butterfield R.O., Pryde E.H. (1986) Transesterification kinetics of soybean oil. *J. Am. Oil Chem. Soc* **63**:1375-1380.
4. Georg S., Stefanie S. and Kumar D.M. (2000) Alkali catalyzed alcoholysis of crambe oil and camelina oil for the preparation of long chain esters. *J. Am. Oil Chem. Soc* **77**: 367-371.
5. Darnoko D. and Munir C. (2000) Kinetics of palm oil transesterification in a batch reactor. *J. Am. Oil Chem. Soc.* **77**: 1263-1267.
6. Feuge R.O. and Ward T.L. (1958) 1,3-Diolein and 1,3-distearin ester of fumaric, succinic and adipic acids. *J. Am. Chem. Soc.* **80**: 6338-6341.
7. Villeneuve P., Foglia T.A., Mangos T.J., and Nuñez A. (1998) Synthesis of polyfunctional glycerol esters: lipase-catalyzed esterification of glycerol with diesters. *J. Am. Oil Chem. Soc.* **75**: 1545-1549.
8. Nagata M., Kiyotsukuri T., Ibuki H., Tsutsumi N., and Sakai W. (1996) Synthesis and enzymatic degradation of regular network aliphatic polyesters. *Reactive and Functional Polym.* **30**: 165-171.
9. Kiyotsukuri T., Kanaboshi M. and Tsutsumi N. (1994) Network polyester film from glycerol and dicarboxylic acids. *Polym. Inter.* **33**: 1-8.
10. American Society for Testing Materials (1988) *Standard test method for kinematic viscocity of transparent and opaque liquids (and calculation of dynamic viscosity)*, ASTM (D445-68). ASTM, West Conshohocken, PA, pp. 168-173.
11. American Society for Testing Materials (1980) *Standard test method for calculating viscosity index from kinematic viscosity at 40 and 100°C*, ASTM (D2270-79). ASTM, West Conshohocken, PA, pp. 277-283.
12. American Society for Testing Materials (1989) *Standard test method for pour point of petroleum oils*, ASTM (D 97-87). ASTM, West Conshohocken, PA, pp. 1-8.
13. American Oil Chemical Society (1993) *Cloud point test*, AOCS(Cc 6-25).
14. Roberto A.R. and Rita H.R. (1974) Preparation of benzoate esters of tertiary alcohols by transesterification. *J. Org. Chem.* **39**: 855-856.
15. McLafferty F.W. and Tureèek F. (1993) Interpretation of mass spectra. In: *Mass spectra of common compound classes* pp. 200. University science books, United states.
16. William M. (2000) Technique of combined GCMS-Application in organic analysis. In: *The relationship of components of a mass spectrometer to the requirements of GCMS analysis* p. 198. John Wiley & Sons, United States.
17. Brondz I. (2002) Review Development of fatty acid analysis by high performance liquid chromatography, gas chromatography, and related techniques. *J. Chimica Acta,* **465**: 1-37.
18. Kudo K., Tsuchihashi H. and Ikeda N. (2003) Review Meeting challenges in forensic toxicology in Japan by liquid chromatography mass spectrometry. *J. Chimica Acta,* **492**: 83-104.
19. Mehlis B. and Kertscher U. (1997) Liquid chromatography mass spectrometry of peptides of biological samples. *J. Chimica Acta,* **352**: 71-83.
20. Lauridsen J.B. (1976) Food emulsifiers: Surface activity, edibility, manufacture, composition and application. *J. Am. Oil Chem. Soc.*, **53**: 400-407.
21. Bent F.A. and Marple K.E. (1946) Polyvinyl acetal plasticized with a diglycerol ether. *US patent*, 2 393 513.
22. American Society for Testing Materials (1988) *Standard Guide for the Generation and Dissipation of Static Electricity in Petroleum Fuel Systems*, ASTM 4865. ASTM, West Conshohocken, PA, pp.323-326.
23. Jönsson B., Lindman B., Holmberg K. and Kronberg B. (1999) Introduction to surfactants. In: *Surfactants and polymers in aqueous solution*. John Wiley & Sons England. pg 1-30.
24. Bell A. and Birdi K.S. (1984) Aqueous solution properties of a fatty dicarboxylic acid hydrotrope. In: *Structure/performance relationships in surfactants*. American chemical society, Washington.
25. Coupland K. (1992) Surfactants in lipid chemistry-Recent synthetic, physical and biodegradative studies. In: *Natural base surfactants-Some aspects of their chemistry and uses* pp.158. Edited by Tyman J.H.P., Royal society of chemistry, Cambridge.
26. Jerven D. (2002) Biodegradable base oils and other Radia Oleochemicals for the lubricant industry. In: *Handbook of Oleon*. Oleon, France.

Journal of Science and Technology in the Tropics (2006) **2**: 41-43

On a modification of the Numerov algorithm to solve the Schrödinger equation

Bernardine Renaldo Wong
Quantum Scattering Theory Group, Institute of Mathematical Sciences, Faculty of Science, University of Malaya,50603 Kuala Lumpur, Malaysia
(Email: bernardr@um.edu.my)

Received 20.10.2005; accepted 24.3.2006

Abstract We implement a modification of the Numerov method to numerically solve the time-independent Schrödinger equation in one dimension. We show that this modification, suggested by Zongcheng Wang (2005), significantly improves on the calculation of the wave-function as compared to the traditional Numerov algorithm.

Keywords Numerov algorithm – time-independent Schrödinger equation

INTRODUCTION

The time-independent Schrödinger equation (TISE) is a fundamental equation in non-relativistic quantum mechanics. Because analytical solutions are available for only a few families of potentials, the TISE often needs to be solved numerically. There are many approaches; see, for example, the recent papers of Simos [1] and Vanden Berghe *et al.* [2] One useful algorithm has been that of Numerov [3] which has found wide application. Very recently, Wang [4] has reported on a modification, called the P-stable Numerov method. Wang showed that this modification resulted in a 10- to 500-fold improvement in the evaluation of the bound-state eigen-energies, and a 5000- to 10^6-fold improvement in the eigen-energies of resonant states for a potential of a Woods-Saxon form. However, Wang did not explicitly show in his paper how the generation of the wave-function was improved by the modification. Hence, in this paper, I wish to investigate the P-stable Numerov method by numerically solving the TISE for the simple harmonic oscillator potential, whose wave-functions and eigen-energies are known analytically.

NUMERICAL SOLUTIONS OF THE TISE

The time-independent Schrödinger equation (in one dimension) can be written as

$$\psi''(x) = F(x)\psi(x), \tag{1}$$

where is the wave-function and is a function whose specific form depends on the potential function used. Wang [4] has derived the following P-stable Numerov formula:

$$\psi_{k+2} = \left[\left(\alpha_s + \frac{5h^2}{6}F_{k+1}\right)\psi_{k+1} - \left(1 - \frac{h^2}{12}F_k\right)\psi_k\right] \bullet \left(1 - \frac{h^2}{12}F_{k+2}\right)^{-1}, \tag{2}$$

where α_s is a position-dependent parameter defined as

$$\alpha_s = \frac{5h^2}{6}|F_{k+1}| + 2\left(1 + \frac{h^2}{12}|F_{k+1}|\right)\cos\left(h\sqrt{|F_{k+1}|}\right), \quad F_{k+1} \le 0 \tag{3a}$$

and

$$\alpha_s = 2, \quad F_{k+1} > 0. \tag{3b}$$

Here, h refers to the spatial step-size. Equation (3a) is the P-stable modification to the Numerov method. It is applicable in the classically-allowed region, and slightly modifies the oscillatory character of the wave-function. In the traditional Numerov method, α_s is always equal to 2. In the classically-forbidden region, there is no departure from the traditional Numerov method. Both the traditional and the P-stable Numerov formulas share the same local truncation error, i.e., $O(h^6)$.

We apply the P-stable Numerov method, as well as the traditional approach, to the simple harmonic oscillator problem. Here, the TISE takes the form (with respect to the dimensionless coordinate z)

$$\psi''(z) = \left(A - z^2\right)\psi(z). \tag{4}$$

The conditions necessary for an acceptable wave-function, i.e. a continuous wave-function and first-derivative for all values of z, constrain the values of parameter A and, hence, the eigen-energy. Specifically, the eigen-energies E_N and parameter A are given by

$$E_N = \left(N - \frac{1}{2}\right)\hbar\omega, \qquad A = 2N - 1. \tag{5}$$

Here, $\hbar\omega$ is twice the zero-point energy (which we may arbitrarily fix in our calculation), and the bound states are labeled by $N \in \{1, 2, 3, \cdots\}$. Equation (4) can be solved analytically and its (un-normalized) solution is

$$\psi(z) = e^{-z^2/2}\, H_{N-1}(z), \tag{6}$$

where H denotes the Hermite polynomials.

RESULTS AND DISCUSSION

We generate the wave-function $\psi(z)$ numerically using the traditional, as well as the P-stable method, which is then compared to the analytical formula given by (6). In this calculation we set $\hbar\omega = 10$ and generate $\psi(z)$ from left to right in the region $-1.1\, z_0 \le z \le 1.1\, z_0$, where the classical turning point is $z_0 = \sqrt{A}$. With this choice of z, the calculation begins (and ends) in the classically-forbidden regions. The spatial step-size is computed using $h = 2.2\, z_0 / (npts - 1)$, where *npts* refer to the number of equally-spaced points in the region. As a representative case, we choose $N = 7$ and $npts = 101$ in this calculation.

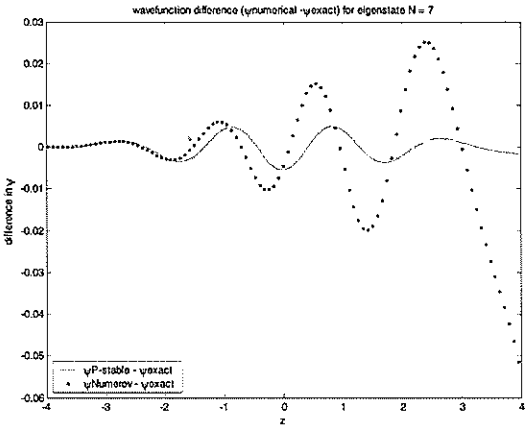

Figure 1. Difference in the wave-functions generated using the traditional Numerov formula (dotted line) and the P-stable method (full line), with respect to the analytical formula for eigenstate N=7.

In Figure 1, the full line (dotted line) shows the difference between the numerically-generated wave-function using the P-stable method (traditional Numerov method) and the analytical solution given by (6). The classically-allowed region is defined by $|z| \le 3.606$ and step-size used is $h = 0.0793$.

The analytical wave-function (not shown) has 6 nodes. Figure 1 shows the wave-function difference oscillating about zero for both methods. However, it is clear that the oscillation worsens as z increases for the traditional Numerov method. On the other hand, in the P-stable method, the oscillation is markedly reduced so that the difference is very small when the classically-forbidden region is reached. If the calculation is repeated using a smaller step size, say with *npts* = 151, the magnitude of the wave-function difference is reduced by roughly a factor of 5 but the oscillation pattern remains identical to that shown in Figure 1. This suggests that, all else being equal, the P-stable modification to the Numerov method will yield substantially better wave-functions than the traditional algorithm.

The superiority of the P-stable method over the traditional one becomes even more striking for higher eigen-energy bound-states. For example, if the calculation is repeated using $N = 15$ and *npts* = 201 as shown in Figure 2, it is clear that the wave-function

difference due to the P-stable method is smaller that that of the traditional method by approximately one order of magnitude. Hence, the P-stable modification to the Numerov method yields much more accurate wave-functions as the number of oscillations in the classically-allowed region increases.

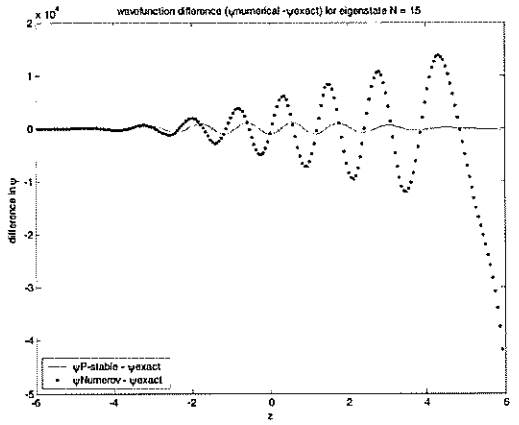

Figure 2. Difference in the wave-functions generated using the traditional Numerov formula (dotted line) and the P-stable method (full line), with respect to the analytical formula for the eigenstate N=15.

CONCLUSION

We have explicitly shown that the P-stable Numerov algorithm is a significant improvement over the traditional Numerov method. Although both methods share the same local truncation error the P-stable method ensures that oscillatory part of the wave-function, generated in the classically-allowed region, is generated more accurately than previously achieved using the traditional Numerov method. The superiority of the P-stable method is evident especially when the number of oscillations in the wave-function increases. Hence, the P-stable Numerov algorithm should become the method of choice in the numerical solution of second-order ordinary differential equations, in general, and the time-independent Schrödinger equation, in particular.

Acknowledgement – The support of the Ministry of Science, Technology and Innovation, Malaysia, via IRPA Grant No. 09-02-03-1011 is gratefully acknowledged.

REFERENCES

1. Simos T.E. (1999) Explicit eighth order methods for the numerical integration of initial-value problems with periodic or oscillating solutions. *Comput. Phys. Comm.* **119**: 32-44.
2. Vanden Berghe G., De Meyer H., Van Daele M., Van Hecke T. (1999) Exponentially-fitted explicit Runge-Kutta methods. *Comput. Phys. Comm.* **123**: 7-15.
3. Noumerov B.V. (1923) *Publ. Observ. Cent. Astrophys. Russ.* **2**: 188.
4. Wang Z. (2005) A new effective algorithm for the resonant state of a Schrödinger equation. *Comput. Phys. Comm.* **167**: 1-6.

Journal of Science and Technology in the Tropics (2006) **2**: 45-49

Fabrication and results of materials experiment in space on SUNSAT

R. Abd-Shukor, Mazlan Othman*, Hasan Adli Alwi, Mohamed Deraman and Ahmad Zaharim Abd Aziz
School of Applied Physics, Universiti Kebangsaan Malaysia, 43600 Bangi, Selangor, Malaysia
*National Space Agency, Ministry of Science, Technology and Innovation, 62250 Putrajaya, Malaysia

Received 14.12.2005; accepted: 27.04.2006

Abstract This paper reports on the fabrication and the results from a material experiment performed on SUNSAT. The electrical resistance of a YBCO superconductor and a glassy carbon material were measured for a period of about 2 years in the low-earth orbit SUNSAT. The stability of a constant current source constructed for the experiment was also monitored and was found to remain stable during the two-year period despite the variation in the temperature of the satellite's interior. Our results also indicate that oxygen in the YBCO lattice structure remains stable in space environment during the period of study. This study also shows that the glassy carbon material is also stable during the two-year period.

Keywords materials in space – SUNSAT

INTRODUCTION

An experimental study on the effect of space conditions on two advanced materials was initiated in 1996 as a joint project between School of Applied Physics, Universiti Kebangsaan Malaysia (UKM), National Space Agency, Malaysia and the University of Stellenbosch, South Africa. The objective of this experiment was to study the effect of microgravity, space radiation and condition on two materials: high temperature superconductor, and glassified carbon prepared form oil palm empty fruit bunches. In addition, the stability of a current source was also tested.

The experiment essentially consists of two modules weighing 28 g. The materials for testing were placed on the exterior while the electronic module was placed in the interior. Both modules were fabricated at UKM. SUNSAT, a low earth satellite with orbit altitude of 600-840 km, was designed and built by the Faculty of Engineering, University of Stellenbosch, South Africa. The weight of the satellite is 64 kg with dimension 450 mm × 450 mm × 600 mm. Apart from carrying experiment modules from Malaysia, this satellite also carries instruments for remote sensing, sun's sensors and others. SUNSAT was launched from Vandenberg Air Force Base in California USA on 23 February 1999.

OVERVIEW OF THE MATERIALS AND EXPERIMENT MODULES

Materials: Superconductor and Glassy Carbon

A superconducting material can carry electricity without any resistance at low enough temperature. This material can be potentially used in systems for satellite communications. The superconductor used for this experiment is $YBa_2Cu_3O_{7-d}$ (YBCO) and the structure is shown in Figure 1. The preparation method of the YBCO was described elsewhere [1]. The oxygen content is important in the superconducting and electrical property of the YBCO because it can affect the density of charge carriers. Hence variation in the electrical resistance reflects the oxygen content of the material.

The glassy carbon used in this experiment was prepared from oil palm empty fruit bunches [2]. Oil palm empty fruit bunches is a potentially valuable starting material for manufacturing solid carbon products, which are widely used in the field of

electrical engineering because they are inexpensive and available in very large quantities as a waste material from palm oil mills. In this context it was therefore important to study the electrical properties of carbon prepared from empty fruit bunches. As a light material and good electrical conductors it can also be potentially used in space applications.

The diameter of the YBCO and glassy carbon samples is 13 mm and 10 mm, respectively. The samples were mounted on the sample module and the resistance measurements were obtained by the two-point contact measurement as discussed below.

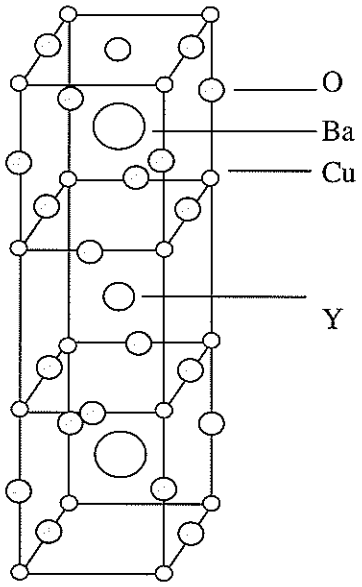

Figure 1. Structure of the $YBa_2Cu_3O_{7-d}$ superconductor.

Electronic and Sample Modules

Figure 2 shows the electronic and sample modules used in the experiment. The electronic module consists of a commercially available FET 2N3819 which provides a constant current to a ±1 % tolerance, metal-film resistance R_c of 100 Ω and a standard platinum resistor temperature sensor as shown in Figure 3.

The resistance of platinum sensor at room temperature is 110 Ω and it increases with temperature. The temperature sensor and the sample module were attached at the external of the satellite and exposed to the space environment with expected temperature variations between -30 °C and +60 °C whilst the electronic module was attached at the internal [3, 4]. The resistance of the materials was determined from the voltage difference across the samples and the constant current 1.38 mA applied (Fig. 4). The overall mass of both modules is 28 g.

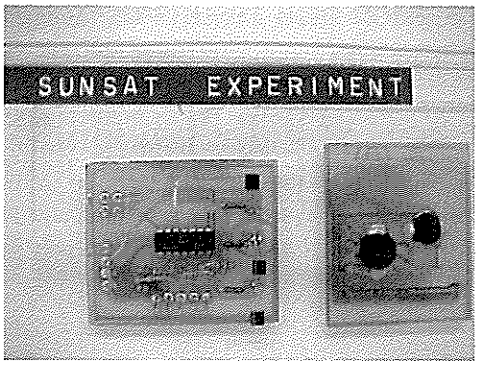

Figure 2. Photograph of the electronic and sample modules.

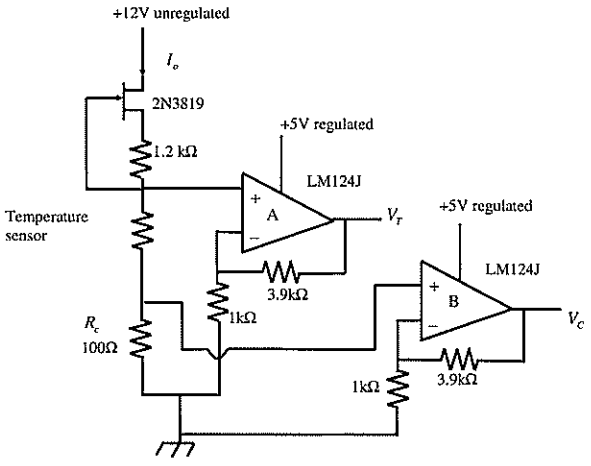

Figure 3. The circuit diagram of the module of the constant current source.n A platinum resistor temperature sensor was used to measure the external temperature of the satellite.

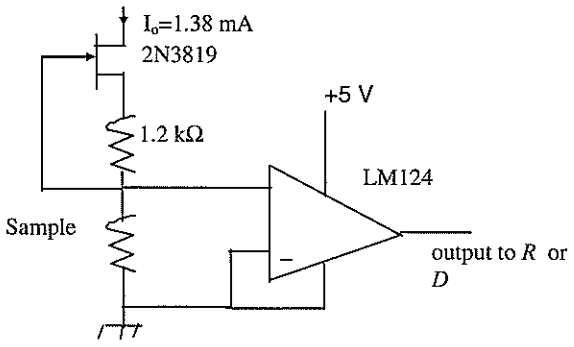

Figure 4. Circuit diagram of module to measure the electrical resistance of the samples.

Table 1. Current I_o from the 2N3819FET with variation in the internal and external temperatures of the satellite.

Date	$I_o \pm 0.04$ mA	Internal Temperature (°C)	External Temperature (°C)
May 6, 1999	1.38	-	-15 to 60
June 7, 1999	1.38	17 to 23	-15 to 60
April 2, 2000	1.38	28 to 32	-10 to 60
May 5, 2000	1.38	32 to 36	10 to 50

RESULTS AND DISCUSSION

The stability of 2N3819 FET as a constant current source for space applications has been monitored. Our data indicate that it performed reasonably well in space in space environment (Table 1). The long-term current level is constant even though the internal temperature of the satellite is increasing. This indicates that the FET can provide a steady current for an internal temperature variations between 17 °C and 36 °C. Our result can be useful in designing circuit for constant current source with stability of about 3 %. The requirements in space applications are varied and very specific [5,6]. In applications where a higher current resolution is required, a higher bit A/D converter should be considered.

Figure 5 shows the typical variation of resistance of YBCO with temperature for three-earth orbit cycles as well as the temperature of the sample. The time interval between successive peaks in the figure is about 100 minutes which is equivalent to one earth orbit cycle. The satellite also rotates about its axis five times for every earth-orbit cycle and the several smaller temperature peaks in between the larger peaks is due to this rotation.

The normal state resistance of $YBa_2Cu_3O_{7-d}$ is very sensitive to the oxygen content [7]. For example the resistivity of $YBa_2Cu_3O_{6.3}$ (non-superconducting) is several orders of magnitude higher than $YBa_2Cu_3O_7$ (superconducting). A rise in resistance of the YBCO sample indicates among others the amount of oxygen that left the sample. Figure 4 shows a typical resistance

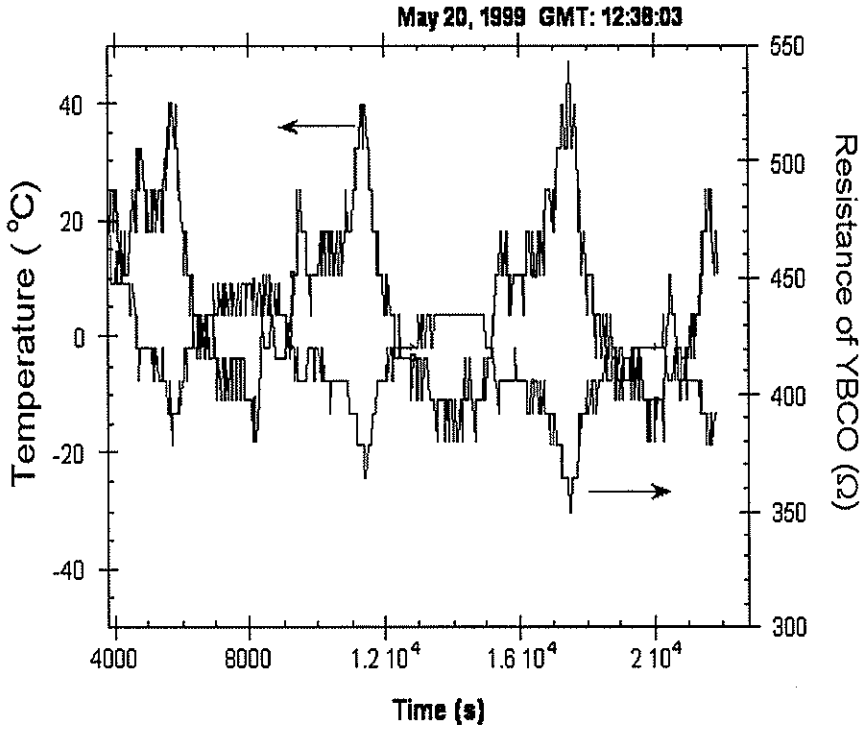

Figure 5. Variation of YBCO resistance with temperature in three earth-orbit cycles.

Journal of Science and Technology in the Tropics (2006) **2**: 3-7

Conversion of palm oil to medium-chain-length polyhydroxyalkanoates by bacteria isolated from oil palm estate soil

Pui-Hong Wong and Irene K. P. Tan*
Institute of Biological Sciences, University of Malaya, 50603 Kuala Lumpur, Malaysia

*Corresponding author's email: itan@um.edu.my

Abstract A *Pseudomonas* CN selective medium was used to isolate pseudomonad bacteria from soils taken from an oil palm plantation. The isolates were screened for the ability to metabolise palm oil and to synthesise polyhydroxyalkanoates (PHA). Each of the isolates was cultured in a nitrogen-limiting medium containing 0.5% w/v crude palm olein (CPO) as the sole carbon source. Cells from the positive cultures were stained with Nile Blue A to detect the presence of intracellular PHA. Out of 19 isolates obtained from the *Pseudomonas* CN selective medium, only two, namely MH1 and MH2, could produce PHA from CPO. Grown in shake flasks at 30°C for 48 hr, MH1 produced 1.3 g/L of dry biomass of which 10.8% was PHA, whereas MH2 produced 2.6 g/L of dry biomass of which 18.3% was PHA. The extracted PHA formed a sticky yellowish transparent film at room temperature. Nuclear magnetic resonance spectrometry and gas chromatography confirmed that the material produced by MH1 and MH2 was PHA_{MCL} containing 3-hydroxyoctanoate (55 mol%) and 3-hydroxydecanoate (33 mol%) as the predominant monomers. Differential scanning calorimetry showed that both the polymers had low crystallinity, and gel permeation chromatography showed that they had low molecular mass and a polydispersity of 1.7. In this study, a simple method based on liquid-liquid separation was developed to remove oily impurities from the extracted PHA.

Keywords liquid-liquid separation – medium-chain-length PHA – palm oil – *Pseudomonas*

INTRODUCTION

Petrochemical plastics, in various forms, have many industrially-useful properties such as inertness to chemical reactions, durability, impermeability to water and air, lightweight, mechanical strength, elastomeric, and transparent. However, the many types of single-use disposable plastic products are now one of the biggest environmental pollutants. This and the finite amount and rapid depletion of petroleum deposits have prompted a global search for alternative materials which have the useful properties of plastics but with additional important traits such as degradability to harmless components, as well as to be synthesised from renewable resources. Bacterial polyhydroxyalkanoates (PHA) have all the traits of an environmentally-friendly plastic material but the cost of production is very much higher than that of petrochemical plastics. Therefore, an important focus in PHA research is in reducing the cost of production. Plant oils are especially suited for the production of the medium-chain-length PHA (PHA_{MCL}), a copolyester in which the monomeric composition is related to the carbon source fed to the bacteria. However, not many PHA-producing bacteria could metabolise palm oil directly; the triglycerides have to be saponified to fatty acids before they could be used as an effective carbon source.

In view of the close association between plant oils and PHA_{MCL} synthesis, the objective of this study is to specifically isolate palm oil-utilising, PHA_{MCL}-producing *Pseudomonas* species from oil palm estate soil.

MATERIALS AND METHODS

Source of indigenous bacteria

Soil samples, from ground surface to a depth of 5 cm, were collected from three sites in an oil palm plantation

curve at various temperatures. There is no observable change in the resistance throughout the two-year period. This indicates that the material is stable against space environment. This also indirectly indicates that the oxygen is stable in the YBCO crystal lattice.

Figure 6 shows the resistance of glassy carbon against variation in temperature. The resistance remained constant at 14 Ω throughout the two-year period. This is somewhat expected as carbon is generally a stable material.

It is interesting to investigate further the effect of space environment on the YBCO superconductor especially in the geosynchronous orbit where most communication satellites operate. Satellites in the geosynchronous orbit will also experience low temperature (about 80 K) which is lower than the critical temperature of most high temperature superconductors such as the YBCO material. A four-point probe measurement instead of two-point probe measurement will give absolute value of the resistivity instead of resistance value in this study. This will in turn gives quantitative value of the oxygen content in the YBCO. In addition, the effect of space environment for more than two years is also useful in deciding whether these materials can be used in longer space missions.

In conclusion, we have investigated the stability of YBCO ceramics and glassy carbon in space environment on SUNSAT and found that these two materials are stable against environment during the two years period. The stability of 2N3819 FET as a constant current source for space applications has also been monitored and found to be suitable for space applications.

Acknowledgements – We thank Prof. Jan J. du Plessis, Dept. of Electrical and Electronic Engineering, University of Stellenbosch, South Africa for offering us to participate in the SUNSAT program. We also thank Malaysia Airline and the Malaysian Ministry of Science, Technology and Innovation for their support. We acknowledge Mr. Niki Steenkamp, University of Stellenbosch and Mohd. Rosli Kaskandar (UKM) for their kind assistance.

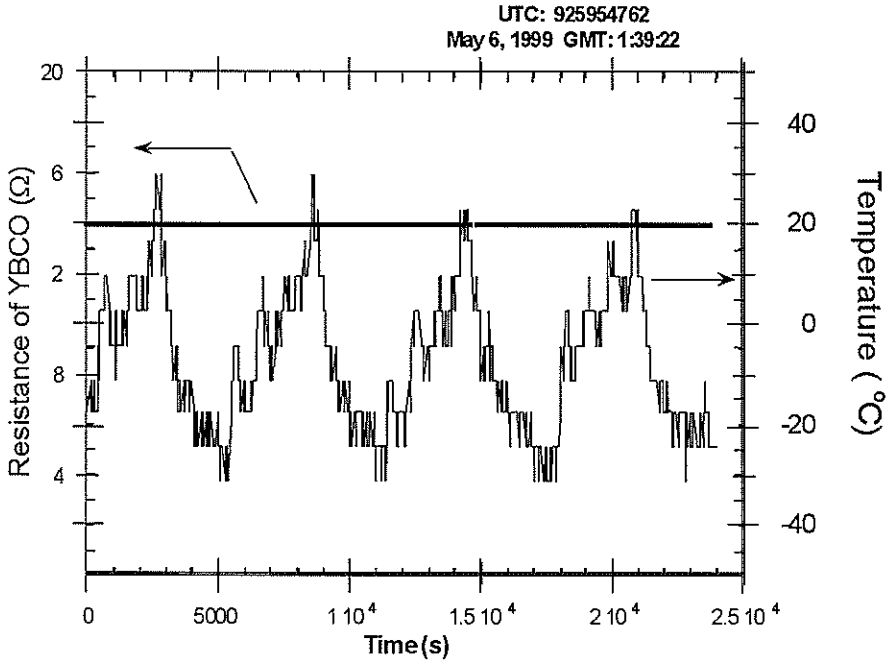

Figure 6. Variation of resistance of glassy carbon with temperature in four earth-orbit cycles.

REFERENCES

1. R. Abd-Shukor, App. Phys. Comm. 13(3&4): 323 (1993)
2. M Deraman, J. Phys. D: Appl. Phys. 27: 1060 (1994)
3. H. A. B. Alwi, R. Abd-Shukor, M. Othman, 2001. Singapore J. of Phys., 17 (1): 47 (2001).
4. Hasan Adli Alwi, Roslan Abd. Shukor, Ahmad Zaharim Abd Aziz, Mazlan Othman, Mohamad Deraman. Kajian Bahan Superkonduktor dan Karbon Glasi di Angkasa Bersama Mikrosatelit SUNSAT. Prosiding PERFIK 2000 (R .Abd-Shukor & S.V. Muniandy,ed.) pg. 315 (2000)
5. E. Polturak, G. Koren, M. Ayalon, I. Flohr, R. Wallen, M. Guelman, Appl. Phys. Lett., **75(9)**, 1293(1999).
6. S.A. Wise, R.M. Amundson, P. Hopson Jr., J.W. High, N.M.H. Kruse, E.H. Kist, IEEE Trans. Appl. Superconductivity, **5(2)**, 1545(1995)
7. M. P. Fontana, C. Paracchini, C. Paris De Renzi and P. Podini F. Licci, F. C. Matacotta, Solid State Comm. **69 (6):** 621 (1989)

Journal of Science and Technology in the Tropics (2006) **2**: 51-57

Synthesis and liquid crystalline properties of bis[((*p*substitutedphenylimino) methyl)phenyl]decyl and dodecyl ethers

Guan-Yeow Yeap[1], Moi-Me Chong[1], Atsuko Ono[2], Masato M. Ito[3], Hirononi Nakai[3], Shigeki Sanehisa[3] and Yoshiyuki Nakamura[4]

[1]Liquid Crystals Research Laboratory, School of Chemical Science,
Universiti Sains Malaysia, 11800 Minden, Penang, Malaysia
[2]Materials and Structures Laboratory,
Tokyo Institute of Technology, Yokohama, 226-8503 Japan
[3]Faculty of Engineering, Soka University, Hachioji, Tokyo 192-8577 Japan
[4]Research Laboratory of Resources Utilization,
Tokyo Institute of Technology, Yokohama, 226-8503 Japan

Received 20.02.2006; accepted 01.03.2006

Abstract Two series of dimer liquid crystals of Schiff base ethers 1,10- and 1,12-bis[((p-substituted-phenylimino)methyl)phenyl]decyl and dodecyl possessing different substituents of H, Br, Cl, OH, CH_3, and C_2H_5 were isolated and characterized. The aromatic mesogenic units attached with the para-substituent were connected to the flexible spacer of either decyl or dodecyl carbon chains at the para position. Majority of the title compounds thus obtained are monotropic exhibiting nematic mesomorphism. Whilst the compound possessing a spacer with carbon number 10 and a terminal Br atom exhibits both nematic and smectic phases, its analogue with greater carbon number of 12 in the spacer perturbed the liquid crystalline behaviour. The compound with OH as substituent upon heating shows pseudomorphism of nematic phase prior to the melting.

Keywords liquid crystalline properties – dimer – Schiff base ethers – pseudomorphism

INTRODUCTION

Investigation on dimer or twin liquid crystals has received growing interests among material chemists aiming at studying the influence of various parameters associated with the nature or the conformation of the molecule in mesophase. The length and the parity of the connecting spacer have once been reported as influential towards the phase transitional properties of the dimers, trimers and main chain liquid crystal polymers [1-7]. The recent study based on theoretical model revealed that the alternation in isotropization temperatures and their respective entropy changes have been ascribed to the different number of conformers with parallel orientations of the mesogenic units for odd and even dimers. In this regards, the dimers connected with an even spacer, more parallel orientations of the mesogenic groups are possible than for dimers connected by an odd spacer.

Since then the effort in seeking for liquid crystal with enhanced thermal stability have been intensified by forming the molecule with different shape which encompasses H-shaped liquid crystals [8, 9] and T-shaped liquid crystals [10]. In recent years, the unprecedented mesomorphic properties of non-linear mesogenic units has also been found on banana-shape liquid crystals which exhibits novel and fascinating liquid crystalline phases due to their bent shapes [11-13].

For the present study, we synthesize two series of dimer liquid crystals wherein the mesogenic units derived from various substituted Schiff bases were connected by $-(CH_2)_{10}-$ and $-(CH_2)_{12}-$, respectively. The substituents of different electronegativities residing at the *para* position in these molecules are bromine, chlorine, hydroxyl, methyl and ethyl groups.

EXPERIMENTAL

Materials

4-hydroxybenzaldehyde, 1,10-dibromodecane, 1,12-dibromododecane, aniline, 4-bromoaniline, 4-chloroaniline, 4-hydroxyaniline, 4-methylaniline and 4-ethylaniline were directly used without further purification.

Methods

CHN microanalyses were performed by 2400 and 2400 LS series II CHNS/O microanalyzer. IR spectra were recorded using a Perkin Elmer 2000 FTIR Spectrophotometer in frequency range 4000-400 cm^{-1}. The spectra of the compounds were measured in thin film sandwiched between two zinc selenide (ZnSe) windows. ^{1}H and ^{13}C spectra were recorded on a Bruker 400Mhz Ultrashield™ FT-NMR Spectrometer using $CDCl_3$ as a solvent and TMS as an internal standard.

The thermal behaviour of the title compounds were analyzed through the determination of transition temperatures by using Shimadzu DSC-50 calorimeter with a flow of dry nitrogen as a purge gas for the samples and reference cells at a heating and cooling rates of 5°Cmin^{-1} and -5°Cmin^{-1}, respectively. The temperature range 30°C to 220°C was employed throughout the study. A polarizing microscope and a Mettler FP52 hot stage were used for the texture observation over different mesophasic regions.

Synthesis of bis(p-benzalidene)decyl ethers

1,10-bis(p-benzalidene)decyl ether, **1a**. A mixture containing 4-hydroxybenzaldehye (6.5 g, 53 mmole) and potassium carbonate (8.7 g, 63 mmole) was heated in DMF (100 mL). 1,10-dibromodecane (7.5 g, 25 mmole) was then added dropwise into the mixture. The resulting solution was heated and stirred at 120°C for 12 hours. After cooling, the diluted HCl was added to the solution. The light brownish precipitate was filtered and recrystallized with ethanol. Yield 80%. m.p.81-83°C. IR (ZnSe), 2930 cm^{-1} (C-H aliphatic), 1687 cm^{-1} (C=O), 1265 cm^{-1} (C-O).

1,12- bis(p-benzalidene)dodecyl ether, **1b**. The same procedure as described above was repeated but 1,10-dibromodecane was replaced by 1,12-dibromododecane (10.3 g). Yield 78%. m.p.79-81°C. IR (ZnSe), 2930 cm^{-1} (C-H aliphatic), 1687 cm^{-1} (C=O), 1265 cm^{-1} (C-O).

Synthesis of 1,10-bis[((*p*-substituted-phenylimino) methyl)phenyl]decyl and 1,12-bis[((*p*-substituted-phenylimino)methyl)phenyl]dodecyl ethers

1,10-bis[(phenylimino)methyl]phenyl]decyl ether, **2a**. **1a** (2.6 g) and aniline (0.3 g) in a ratio of 2.1 to 1 were dissolved in ethanol before being heated at 60°C for 3 days. The resulting solution was cooled down whereupon precipitate formed. The light brownish powder was filtered and washed with ethanol. The solid thus obtained was subsequently recrystallized from chloroform. Yield 71%. Anal: Calc for $C_{36}H_{40}O_2N_2$: C 81.17, H 7.57, N 5.26. Elementary analysis: Found, C 81.16, H 7.46, N 5.17. IR (ZnSe) cm^{-1}: 2937.0, 2852.3 (C-H aliphatic), 1605 (C=N), 1246 (C-O); ^{1}H-NMR ($CDCl_3$) δ ppm: 8.40 (s, 1H, CH=N), 7.84, 7.00 (d, aromatic ring), 4.04 (t, O-CH_2) and 1.39-1.87 (C-H aliphatic chains); ^{13}C-NMR ($CDCl_3$) δ ppm: 162.34 (C_{Ar}-O), 159.7 (C=N), 152.9 (C_{Ar}-N), 115.2-130.8 (C_{Ar}-H), 68.7 (CH_2-O), 26.3-29.7 (C-H).

The other dimer liquid crystals within the same series were prepared following similar procedure of which **1a** was reacted with the substituted anilines (i.e. 4-bromoaniline, 4-chloroaniline, 4-hydroxyaniline, 4-methylaniline and 4-ethylaniline). The products thus synthesized were abbreviated as **3a-7a**, respectively. The similar synthetic method was applied to the **b** series wherein the spacer by $-(CH_2)_{10}-$ is replaced by $-(CH_2)_{12}-$. The products obtained for the latter series were abbreviated as **2b-7b**. The subsequent reactions leading to the formation of all title compounds (**2a-7a** and **2b-7b**) were shown in Figure 1.

The analytical results for the above mention compounds are listed as follows:

(a) *1,10-bis[(p-bromophenylimino)methyl]phenyl] decyl ether*, **3a**. Yield 77%; Anal: Calc for $C_{36}H_{38}O_2N_2Br_2$: C 62.62, H 5.55, N 4.06. Found: C 62.60, H 5.25, N 3.96. IR (ZnSe) cm^{-1}: 2937, 2852 (C-H aliphatic), 1606 (C=N), 1251 (C-O) ; ^{1}H-NMR ($CDCl_3$) δ ppm: 8.36 (s, 1H, CH=N), 7.85, 7.07 (d, aromatic ring), 4.04 (t, O-CH_2) and 1.37-1.87 (C-H aliphatic chains); ^{13}C-NMR ($CDCl_3$) δ ppm: 162.0 (C_{Ar}-O), 159.0 (C=N), 153.0 (C_{Ar}-N), 115.2-132.4 (C_{Ar}-H), 68.81 (CH_2-O), 26.3-29.7 (C-H).

(b) *1,10-bis[(p-chlorophenylimino)methyl]phenyl] decyl ether*, **4a**. Yield 81%; Anal: Calc for $C_{36}H_{38}O_2N_2Cl_2$: C 71.87, H 6.37, N 4.66. Found: C 71.91, H 6.17, N 4.43. IR (ZnSe) cm^{-1}: 2943, 2853 (C-H aliphatic), 1603 (C=N), 1250 (C-O); ^{1}H-NMR ($CDCl_3$) δ ppm: 8.37 (s, 1H, CH=N), 7.86, 7.00 (d, aromatic ring), 4.04 (t, O-CH_2) and 1.37-1.87 (C-

H aliphatic chains); ^{13}C-NMR ($CDCl_3$) δ ppm: 162.2 (C_{Ar}-O), 159.3 (C=N), 152.9 (C_{Ar}-N), 115.3-132.6 (C_{Ar}-H), 68.6 (CH_2-O), 26.2-29.4 (C-H).

(c) *1,10-bis[(p-hydroxyphenylimino) methyl]phenyl] decyl ether*, **5a**. Yield 81%; Anal: Calc for $C_{36}H_{40}O_4N_2$: C 76.56, H 7.14, N 4.96. Found: C 76.32, H 7.09, N 4.79. IR (ZnSe) cm^{-1}: 3437 (O-H), 2931, 2852 (C-H aliphatic), 1608 (C=N), 1250 (C-O); ^{1}H-NMR ($CDCl_3$) δ ppm: 8.40 (s, 1H, CH=N), 7.85, 7.00 (d, aromatic ring), 4.03 (t, O-CH_2) and 1.35-1.88 (C-H aliphatic chains); ^{13}C-NMR ($CDCl_3$) δ ppm: 162.2 (C_{Ar}-O), 159.3 (C=N), 152.9 (C_{Ar}-N), 115.3-132.6 (C_{Ar}-H), 68.6 (CH_2-O), 26.2-29.4 (C-H).

(d) *1,10-bis[(p-methylphenylimino)methyl]phenyl] decyl ether*, **6a**. Yield 81%; Anal: Calc for $C_{38}H_{44}O_2N_2$: C 81.39, H 7.91, N 4.99. Found: C 80.84, H 8.01, N 4.70. IR (ZnSe) cm^{-1}: 2937, 2850 (C-H aliphatic), 1607 (C=N), 1248 (C-O); ^{1}H-NMR ($CDCl_3$) δ ppm: 8.40 (s, 1H, CH=N), 7.85,7.00 (d, aromatic ring), 4.03 (t, O-CH_2) and 1.35-1.88 (C-H aliphatic chains); ^{13}C-NMR ($CDCl_3$) δ ppm: 162.2 (C_{Ar}-O), 159.3 (C=N), 152.9 (C_{Ar}-N), 115.3-132.6 (C_{Ar}-H), 68.6 (CH_2-O), 26.2-29.4 (C-H).

(e) *1,10-bis[(p-ethylphenylimino)methyl]phenyl]decyl ether*, **7a**. Yield 81%; Anal: Calc for $C_{40}H_{48}O_2N_2$: C 81.59, H 8.22, N 4.76. Found: C 81.45, H 8.13, N 4.68. IR (ZnSe) cm^{-1}: 2935.8, 2852.6 (C-H aliphatic), 1606 (C=N), 1249 (C-O) ; ^{1}H-NMR ($CDCl_3$) δ ppm: 8.41 (s, 1H, CH=N), 7.86, 6.97 (d, aromatic ring), 4.03 (t, O-CH_2) and 1.28-1.86 (C-H aliphatic chains); ^{13}C-NMR ($CDCl_3$) δ ppm: 162.2 (C_{Ar}-O), 159.1 (C=N), 150.6 (C_{Ar}-N), 115.2-130.7 (C_{Ar}-H), 68.7 (CH_2-O), 26.3-29.8 (C-H).

(f) *1,12-bis[(phenylimino)methyl]phenyl]dodecyl ether*, **2b**. Yield 70%; Anal: Calc for $C_{38}H_{44}O_2N_2$: C 81.39, H 7.91, N 5.00. Found: C 80.77, H 7.92, N 4.86. IR (ZnSe) cm^{-1}: 2937, 2850 (C-H aliphatic), 1607 (C=N), 1247 (C-O) ; ^{1}H-NMR ($CDCl_3$) δ ppm: 8.40 (s, 1H, CH=N), 7.87, 7.18 (d, aromatic ring), 4.06 (t, O-CH_2) and 1.36-1.86 (C-H aliphatic chains); ^{13}C-NMR ($CDCl_3$) δ ppm: 162.4 (C_{Ar}-O), 159.8 (C=N), 152.9 (C_{Ar}-N), 115.2-130.8 (C_{Ar}-H), 68.7 (CH_2-O), 26.3-29.8 (C-H).

(g) *1,12-bis[(p-bromophenylimino)methyl]phenyl] dodecyl ether*, **3b**. Yield 76%. Anal: Calc for $C_{38}H_{42}O_2N_2Br_2$: C 63.52, H 5.89, N 3.90. Found: C 63.61, H 6.75, N 3.83. IR (ZnSe) cm^{-1}: 2935, 2850 (C-H aliphatic), 1606 (C=N), 1249 (C-O) ; ^{1}H-NMR ($CDCl_3$) δ ppm: 8.36 (s, 1H, CH=N), 7.85, 7.06 (d, aromatic ring), 4.03 (t, O-CH_2) and 1.35-1.86 (C-H aliphatic chains); ^{13}C-NMR ($CDCl_3$) δ ppm: 162.6 (C_{Ar}-O), 160.1 (C=N), 151.9 (C_{Ar}-N), 115.2-132.5 (C_{Ar}-H), 68.7 (CH_2-O), 26.3-29.8 (C-H).

(h) *1,12-bis[(p-chlorophenylimino)methyl]phenyl] dodecyl ether*, **4b**. Yield 80%. Anal: Calc for $C_{38}H_{42}O_2N_2Cl_2$: C 72.48, H 6.72, N 4.45. Found: C 72.22, H 6.44, N 4.31. IR (ZnSe) cm^{-1}: 2936, 2852 (C-H aliphatic), 1606 (C=N), 1250 (C-O); ^{1}H-NMR ($CDCl_3$) δ ppm: 8.36 (s, 1H, CH=N), 7.85, 7.12 (d, aromatic ring), 4.03 (t, O-CH_2) and 1.35-1.86 (C-H aliphatic chains); ^{13}C-NMR ($CDCl_3$) δ ppm: 162.7 (C_{Ar}-O), 160.1 (C=N), 151.9 (C_{Ar}-N), 115.3-130.9 (C_{Ar}-H), 68.7 (CH_2-O), 26.3-29.8 (C-H).

(i) *1,12-bis[(p-hydroxyphenylimino)methyl]phenyl] dodecyl ether*, **5b**. Yield 81%; Anal: Calc for $C_{38}H_{44}O_4N_2$: C 76.99, H 7.48, N 4.73. Found: C 76.11, H 7.64, N 4.50. IR (ZnSe) cm^{-1}: 3436 (O-H) , 2932, 2851 (C-H aliphatic), 1609 (C=N), 1251 (C-O); ^{1}H-NMR ($CDCl_3$) δ ppm: 8.40 (s, 1H, CH=N), 7.85, 7.00 (d, aromatic ring), 4.03 (t, O-CH_2) and 1.35-1.88 (C-H aliphatic chains); ^{13}C-NMR ($CDCl_3$) δ ppm: 162.2 (C_{Ar}-O), 159.3 (C=N), 152.9 (C_{Ar}-N), 115.3-132.6 (C_{Ar}-H), 68.6 (CH_2-O), 26.2-29.4 (C-H).

(j) *1,12-bis[(p-methylphenylimino)methyl]phenyl] dodecyl ether*, **6b**. Yield 81%; Anal: Calc for $C_{40}H_{48}O_2N_2$: C 81.59, H 8.22, N 4.76. Found: C 82.22, H 8.38, N 4.76. IR (ZnSe) cm^{-1}: 2937, 2850 (C-H aliphatic), 1607 (C=N), 1249 (C-O) ; ^{1}H-NMR ($CDCl_3$) δ ppm: 8.40 (s, 1H, CH=N), 7.86, 7.00 (d, aromatic ring), 4.03 (t, O-CH_2) and 1.36-1.88 (C-H aliphatic chains); ^{13}C-NMR ($CDCl_3$) δ ppm: 162.2 (C_{Ar}-O), 159.3 (C=N), 152.9 (C_{Ar}-N), 115.3-132.6 (C_{Ar}-H), 68.6 (CH_2-O), 26.2-29.4 (C-H).

(k) *1,12-bis[(p-ethylphenylimino)methyl]phenyl] dodecyl ether*, **7b**. Yield 81%; Anal: Calc for $C_{42}H_{52}O_2N_2$: C 81.77, H 8.50, N 4.54. Found: C 81.74, H 8.82, N 4.50. IR (ZnSe) cm^{-1}: 2936, 2850 (C-H aliphatic), 1607 (C=N), 1248 (C-O) ; ^{1}H-NMR ($CDCl_3$) δ ppm : 8.41 (s, 1H, CH=N), 7.86, 6.97 (d, aromatic ring), 4.03 (t, O-CH_2) and 1.29-1.86 (C-H aliphatic chains); ^{13}C-NMR ($CDCl_3$) δ ppm: 162.4 (C_{Ar}-O), 159.1 (C=N), 150.2 (C_{Ar}-N), 115.2-130.7 (C_{Ar}-H), 68.7 (CH_2-O), 26.4-29.8 (C-H).

RESULTS AND DISCUSSION

Synthesis and molecular formula determination

The synthetic methods for the preparation of **1a-7a** and **1b-7b** were carried out according to the similar manner as shown in Figure 1. The CHN microanalytical data are agreeable with the empirical formula for all derivatives in **a** and **b** series.

IR spectroscopy

The characteristic absorption band, which can be assigned to the stretching vibration of C=O bond in **1a** and **1b** appears at 1687 cm^{-1}. However, this band is not observed in their derivatives (**2a-7a** and **2b-7b**). A broad band assignable to the OH in the starting material of 4-hydroxybenzaldehyde is found to be absent in the IR spectra of the intermediary compounds **1a** and **1b.** The IR analytical data of all the title compounds sandwiched in zinc selenide windows show a band at a frequency within the range of 1603-1609 cm^{-1}. This observation could be due to the stretching vibration of imine C=N group in **2a-7a** and **2b-7b** leading to the assumption that the formation of Schiff bases in these derivatives is viable following the steps as depicted in Figure 1.

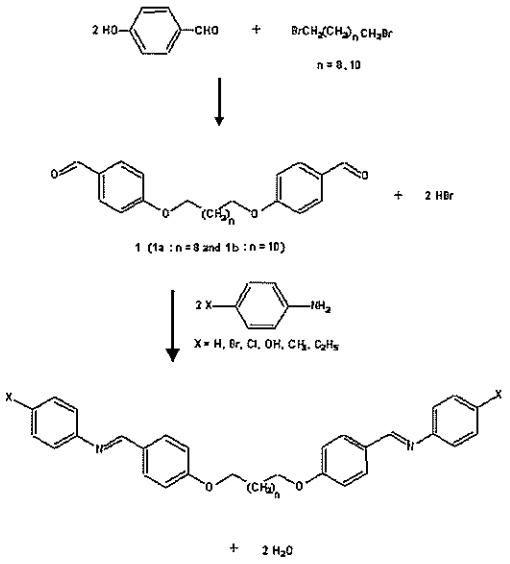

Compound	n	X
2a	8	H
2b	10	H
3a	8	Br
3b	10	Br
4a	8	Cl
4b	10	Cl
5a	8	OH
5b	10	OH
6a	8	CH_3
6b	10	CH_3
7a	8	C_2H_5
7b	10	C_2H_5

Figure 1. Synthetic routes toward the formation of 1,10-bis(*p*-benzalidene)decyl ether (**1a**), 1,12 bis(*p*-benzalidene)dodecyl ether (**1b**) and their derivatives (**2a-7a** and **2b-7b**).

^1H and ^{13}C NMR spectroscopy

The molecular structure of all the title compounds in solution can also be substantiated by the ^1H NMR spectra. The resonances and the pattern of the diagnaostic peaks are similar among these compounds. The inspection from NMR data shows that the methylene protons adjacent to the -OCH_2- group appear as a quintet at 1.87 ppm and the remaining protons as a broad multiplet at 1.37 ppm [14]. The presence of a decyl group in **3a** can be evident from the appearance of a triplet at 4.04 ppm indicating the presence of –OCH_2- group [14, 15]. The aromatics protons in compound **3a** appear as two doublets with their resonances observed at 7.07 and 7.85 ppm [16, 17] suggesting the symmetrical environment for these two sets of protons. The resonance due to the azomethine proton appears as a singlet at 8.36 ppm [18]. The assignment based on the ^{13}C-NMR spectrum of **3a** is also consistent with its postulated structure. The chemical shift at 68.81 ppm indicates the presence of carbon in alkoxyl fragment of O-CH_2. The resonances for the remaining carbon chains were observable within the chemical shift of δ = 26.3-29.7 ppm. Whilst the peaks assignable to the aromatic carbon appear at the range of δ = 115.2-132.4 ppm, the signal ascribed to the azomethine carbon (C=N) is observed at 159.0 ppm. The structural characteristic as inferred from ^1H and ^{13}C NMR spectra for all compounds **2a-7a** and **2b-7b** were found to be in agreement with the molecular structure as illustrated in the analytical results.

Thermal and optical behaviour

The phase transitions of the two homologous series of compounds **2a-7a** and **2b-7b** were investigated by DSC technique as described in the experimental section. The phase transition termperatures and the enthalpies for these series as inferred from the DSC data are presented in the respective Tables 1 and 2.

Inspection from Tables 1 and 2 indicates that compounds **2a** and **2b** upon heating exhibit a clear

isotropic melting from crystalline state at 152°C and 150°C, respectively. Upon cooling they undergo crystallization at respective temperature of 128°C and 127°C.

Compounds **6a**, **6b** and **7b** are monotropic liquid crystals with entalpy changes (ΔH) falling within a range of 13-17 Jg^{-1}. These compounds show only the nematic phase owing to the increased molecular flexibility of the dimer. However, the members **3a**, **4a** and **7a** exhibit enantiotropic nematic phase during both heating and cooling cycles. The rationale behind the emergence of enantiotropic properties of **3a**, **4a** and **7a** in comparison with **6a**, **6b** and **7b** is not clear. Although the electronegativity arising from the halogen atom of either Br and Cl in respective compound **3a** and **4a** for which the spacer consists of 10-carbon chain can be considered as one of the contributing factors towards promoting the nematic phase, but the increase of carbon number to 12-carbon in the spacer has perturbed the stability of this mesophase as those observed for **3b** and **4b**.

Table 1. Phase transitions and transition enthalpy changes for compounds **2a-7a** upon heating and cooling. Cr: crystal, N: nematic, SmA: smectic A, I: isotropic.

Compound	Phase transitions/C (corresponding enthalpy changes/Jg^{-1})
2a	Cr 152 (159) I
	I 128 (125) Cr
3a	- 141 (8) Cr 172 (92) N 173 (10) I
	I 180 (10) N 178 (7) SmA 168 (83) Cr
4a	Cr 164 (108) N 173 (10) I
	I 176 (13) N 163 (100) Cr
5a	- 183 (27) Cr 202 (132) I
	I 174 (119) Cr
6a	Cr 158 (148) I
	I 154 (14) N 151 (136) Cr
7a	Cr 148 (98) N 154 (13) I
	I 154 (12) N 141 (93) Cr

Table 2. Phase transitions and transition enthalpy changes for compounds **2b-7b** upon heating and cooling. Cr: crystal, N: nematic, I: isotropic.

Compound	Phase transitions/C (corresponding enthalpy changes/Jg^{-1})
2b	Cr 150 (166) I
	I 127 (150) Cr
3b	- 170 (3) Cr 178 (121) I
	I 176 (131) Cr 169 (7) -
4b	Cr 172 (140) I
	I 170 (148) Cr
5b	- 178 (54) Cr 194 (117) II 158 (84) Cr
6b	Cr 159 (172) II 155 (17) N 135 (131) Cr
7b	Cr 145 (145) II 142 (13) N 138 (138) Cr

This phenomenon can be exemplified by compound **4a** wherein the cooling cycle led to the formation of a nematic phase with a schlieren texture (Fig. 2a) which turns into crystal phase at 163°C. However, the compound **4b** upon cooling undergoes crystallization at 170°C without experiencing the transformation via intermediary mesophase.

Observation under polarized microscope upon cooling the compounds **6a**, **6b**, **7a** and **7b** also exhibit schlieren nematic texture prior to the crystallization. For compounds **6a**, **6b** and **7b**, the mesophases are observed only during the cooling cycle. As for compound **7a**, the nematic phase is observed when this compound is treated on the slide wherein the polarized light is passed through over heating and cooling processes. This phenomenon can be ascribed to the tendency of the spacer as that reported for compounds **3** and **4** of which the 12-carbon perturbed the formation of nematic phase when the temperature of the compound is gradually increased. In contrary to compound **7a**,

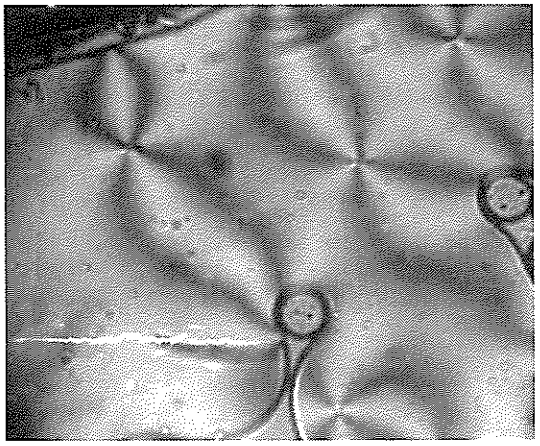

(a)

(b)

Figure 2. Optical photomicrographs of (a) compound **4a** at 174°C, and (b) compound **3a** at 172°C.

compound **7b** upon heating reaches the isotropization at 145°C without the formation of mesophase.

Another notable feature observed in each of the compounds **3a**, **3b**, **5a** and **5b** is the appearance of an endotherm below the transition temperature of Cr-N or Cr-I at 141°C, 170°C, 183°C and 178°C, respectively. Observation upon compounds **3a** and **3b** under polarized light have found that the phase for which the transition temperatures occurred before the isotropic melting are featureless mesomorphs. However, the gradual lowering of temperature enables the compound **3a** to transform into a nematic phase with a threaded schlieren texture before changing to the smectic mesophase with the latter mesophase possesses larger thermal stability. The appearance of smectic phase around 178°C has been confirmed by repeating the cooling cycle on the same compound **3a** for which both the focal-conic and psuedoisotropic textures were observed. This phenomenon suggested that the molecular packing of this compound (**3a**) with Br substituent upon cooling exhibits an orthogonal arrangement of SmA (Fig. 2b).

Further investigation upon compounds **5a** and **5b** wherein an endotherm appeared in each compound before the melting process has been observed under polarized microscope. Surprisingly, even though these compounds upon cooling have not given evidence of mesophase but the reverse thermal process has clearly shown an existence of a pseudomorph of the nematic phase which resembles the *Grandjean* terxture [19-21]. The occurrences of this mesophase in **5a** and **5b** before melting can be rationalized by the presence of intermolecular hydrogen bonding which leads to the increase of melting point.

CONCLUSION

Two series of new dimeric liquid crystals have been synthesized and characterized. The presence of substituents (Br, Cl, OH, CH_3 and C_2H_5) at the *para* position in the terminal aniline fragments has led to the formation of symmetrical structure with liquid crystalline properties. Upon cooling these compounds exhibit nematic and also smectic phases except the compound with OH substituent which shows pseudomorphism of nematic phase before melting.

Acknowledgement – The main author (G.Y.Yeap) is grateful to the Universiti Sains Malaysia and the Malaysian Government for the financial support under IRPA (EA) Grant No. 305/PKIMIA/612923. G.Y.Yeap and M.M.Ito also wish to thank Soka University for supporting this project under the ORP program.

REFERENCES

1. Marcelis, A.T.M., Koudus, A. and Sudholter, E.J.R. (1994) Odd-even effects in the optical properties at chiral twin liquid-crystalline cholesteryl ω-(cyanobiphenyloxy)alkanoates. *Recl. Trav. Chim. Pays-Bas*, **113**: 524.
2. Marcelis, A.T.M., Koudijs, A. and Sudhoelter, E.J.R. (1995) Odd-even effects in the thermotropic and optical properties of three series of chiral twin liquid crystals. *Liq.Cryst.*, **18**: 843.
3. Marcelis, A.T.M., Koudijs, A. and Sudhoelter, E.J.R. (1995) Odd-even effects in the thermotropic and optical properties of chiral triplet liquid crystals. *Liq.Cryst.*, **18**: 851.
4. Luckhurst, G.R. (1995) Liquid crystal dimers and oligomers: experiment and theory. *Macromol.Symp.*, **96**: 1.
5. Blatch, A.E., Fletcher, I.D. and Luckhurst, G.R. (1997) Symmetric and non-symmetric liquid crystal dimers with branched terminal alkyl chains: racemic and chiral. *J.Mater.Chem.*, **7**: 9.
6. Imrie, C.T. and Luckhurst, G.R., 1998, *Handbook of Liquid Crystals*, Vol. **2B**, edited by Demus, D., Goodby, J., Gray, G.W., Spiess, H.W. and Vill, V. (Weinheim: Wiley-VCH), p. 801.
7. Imrie, C.T. (1999) Liquid crystal dimers. *Structure and Bonding*, **95**: 150.
8. Weissflog, W., Demus, D., Diele, S., Nitschke, P. and Wedler, W. (1989) From laterally branched mesogens to novel twin molecules. *Liq.Cryst.*, **5**: 111.
9. Huh, S.M. and Jin, J.I. (1998) H-Shaped dimeric LC compounds : Synthesis and thermotropic properties of alpha, omega-bis[2,5-bix(4 ethoxyphenoxycarbonyl)-phenoxy]alkanes. *Liq.Cryst.*, **25**: 285.
10. Lee, J.W., Piao, X.L., Yun, Y.K., Jin, J.I., Kang, Y.S. and Zin, W.C., (1999) Synthesis and liquid crystalline

properties of T-shaped dimesogenic compounds. *Liq.Cryst.*, **26**: 1671.
11. Akutagawa, T., Matsunaga, Y. and Yashuhara, K. (1994) Mesomorphic behavior of 1,3-phenylene bis[4-(4-alkoxyphenyliminomethyl)benzoates] and related compounds. *Liq.Cryst.*, **17**: 659.
12. Pelzl, G., Diele, S., Jakli, A., Lischka, Ch. and Weissflog, W. (1999) Helical superstructures in a novel smectic mesophase formed by achiral banana-shaped molecules. *Liq.Cryst.*, **26**: 135.
13. Lee, C.K. and Chien, L.C. (1999) First observation of double-twisted helical structure in a banana-shaped achiral molecule. *Liq.Cryst.*, **26**: 609.
14. Kawamura, K., Kikuchi, T. and Koide, N. (1998) Mesomorphic properties of side chain type polyethers containing metal (salts. *Mol. Cryst. Liq. Cryst.*, **318**: 87.
15. Espinet, P., Perez, J., Marcos, M., Ros, M.B., Serrano, J.L., Barbera, J. and Levelut, A.M. (1990) Synthesis, characterization and X-ray studies of nonplanar mesogens: carboxylato-bridged orthopalladated azine complexes. *Organomet.*, **9**: 2028.
16. Espinet, P., Lalinde, E., Macros, M., Perez, J. and Serrano, J.L. (1990) Liquid crystals based on ortho-palladated azines. *Organomet.*, **9**: 555.
17. Akiyama, E., Kawamura, K. and Mihara, T. (1998) Influence of the spacer structure on liquid-crystallinity and dielectric behavior of polyacrylates having p-cyanophenyl benzoate group in the side chain. *Mol. Cryst. Liq. Cryst.*, **318**: 307.
18. Yeap, G.Y. and Ishizawa, N. (1998) New tin-Schiff's base materials : Coordination chemistry and single crystal structure determination. *Mol. Cryst. Liq. Cryst.*, **318**: 253.
19. Irvin, B.W. (1967) Gel formation and spherulite production in the mesomorphic melts of cholesterol esters. *J. Colloid Interface Sci.*, **23**: 221.
20. Chistyakov, I.G. and Gusakova, L.A. (1969) Textures of cholesterol-type liquid crystals. *Sov. Phys. Kristallografiya*, **14**: 153.
21. Merritt, W.G., Cole, G.D. and Walker, W.W. (1971) The polymorphic and mesomorphic behaviour of four esters of cholesterol (cholesterol ester polymorphic and mesomorphic behaviour, using DSC, X-ray powder diffractometry and position annihilation techniques). *Mol. Cryst. Liq. Cryst.*, **15**: 105.

(Felda Palm Industry Sdn. Bhd., Bentong, Pahang, Malaysia). Site A was around young oil palm trees, Site B was around mature oil palm trees, and Site C was where harvested oil palm fruit bunches were always stacked to await collection for transport to the mill.

Isolation of *Pseudomonas* strains

One gram of soil was placed in 200 mL of sterilised *Pseudomonas* CN medium [1] and incubated with shaking, 240 rpm, at 30°C in an orbital shaker. After 3 days, loopfuls of cultures were taken and dilution-streaked on *Pseudomonas* CN agar plates. Bacterial colonies appeared in the plates after 3 to 7 days of incubation at 30°C. Selected colonies were purified by repeat dilution-streaking on fresh *Pseudomonas* CN agar plates. Colony morphology of the isolates on *Pseudomonas* CN agar plates was recorded.

Screening for palm oil-utilising and PHA-producing bacteria

Each isolate was first grown in a nutrient-rich medium [2] to generate large amount of cells which were subsequently transferred to a nitrogen-limiting E2 medium [3] containing 0.5% w/v crude palm olein (CPO) as the sole carbon source. Those isolates which grew in CPO were stained with Nile Blue A to detect for the presence of intracellular PHA [4]. Positively-stained isolates were later identified by using the BIOLOG Microstation System equipped with MicroLog3 4.01C programme.

PHA production

PHA production was conducted using shake-flasks, 240 rpm and 30°C. Cells were first cultured in a nutrient-rich medium to produce large amount of biomass. When the culture attained an optical density of 0.5 at 660 nm, the cells were harvested by centrifugation at 5500 rpm for 15 minutes at 20°C, washed with sterile 0.85% saline solution and transferred aseptically to a nitrogen-limiting E2 medium containing 0.5% w/v CPO as the sole carbon source. After 48 hr, the cells were harvested by centrifugation, washed and dried in a hot-air oven to constant weight.

PHA extraction

PHA was extracted from dry cells using chloroform extraction and was subsequently precipitated with methanol. The precipitate was re-dissolved in a minimal amount of chloroform and methanol-precipitated again as a means to purify the extracted PHA [3]. The precipitated PHA was eventually dried in a 50°C vacuum oven and weighed.

Analysis of PHA

The molecular structure of the PHA was analysed by 400-MHz ^{1}H and 100-MHz ^{13}C nuclear magnetic resonance (NMR) spectrometry. The monomer composition of the PHA was determined by gas chromatography (GC) [5]. 3-hydroxyalkanoic acid methyl ester standards (C8, C10, C12, C14 and C16) were used to determine the respective retention times and to quantify the individual monomeric units of the PHA. The glass-transition temperature (T_g), melting temperature (T_m) and enthalpy of fusion (ΔH_m) of the PHA were analysed with a differential scanning calorimeter. The molecular weight distribution of the PHA was determined with a Gel Permeation Chromatograph. 2 mg PHA was dissolved in 1 ml tetrahydrafuran, filtered through a 0.45μm filter and injected into a GMHXL column (30 cm by 7.8 mm internal diameter) maintained at 40°C. Calibration was performed with polystyrene standards of low polydispersity.

RESULTS AND DISCUSSION

Isolation and screening for palm oil-utilising PHA producers

The soil in some parts of the oil palm plantations may contain higher levels of oils and lipids due to seepage from damaged fruits. Microbial communities could evolve in such soil whereby the oil would be utilised by some species for growth and metabolism, including the ability to synthesise PHA. This was the reason why soil samples from oil palm plantation were chosen as a source of bacteria for this study. During the isolation process using *Pseudomonas* CN medium, 19 pure bacterial isolates were selected: 3 from Site A, 9 from Site B and 7 from Site C. Only five of these isolates (one from Site B and four from Site C) grew well in the CPO medium, and only two of them, namely MH1 and MH2 (both from Site C), were positively-stained with Nile Blue A (Table 1). This means that MH1 and MH2 are able to grow and accumulate PHA in medium containing CPO as the sole carbon source. Therefore, it was envisaged that palm oil-metabolising bacteria could have evolved in such soils.

Journal of Science and Technology in the Tropics (2006) **2**: 59-63

Microwave-assisted preparation of sodium silicate from coal fly ash as silica source

Rose Aini Kamarudin[1], Halina Misran[1] and Ramesh Singh[2]
[1]Department of Engineering Sciences & Mathematic, College of Engineering
Universiti Tenaga Nasional, Km 7, Jalan Kajang-Puchong
43009 Kajang, Selangor, Malaysia
[2]Department of Mechanical Engineering, College of Engineering
Universiti Tenaga Nasional, Km 7, Jalan Kajang-Puchong
43009 Kajang, Selangor, Malaysia

Received 10.2.2006; accepted 19.5.2006

Abstract Thermal fusion reaction between coal fly ash, a waste product which has an abundant source of silica from coal powered power station, and sodium hydroxide at 550°C has been the standard procedure to prepare sodium silicate performed by researchers working with this waste material. Sodium silicate is a versatile starting material for the preparation of zeolites and other mesoporous materials such as MCM-41. A faster method to prepare sodium silicate is reported in this paper. The fusion reaction between coal fly ash and sodium hydroxide was performed in a domestic microwave oven and the reaction was completed within minutes to afford sodium silicate as shown by XRD studies. An SEM micrograph of the microwave assisted fusion product showed larger spherical agglomerates of sodium silicate and sodium aluminosilicate compared to those obtained from the thermal fusion reaction at 550°C.

Keywords coal fly ash – sodium silicate – microwave

INTRODUCTION

Coal fly ash (CFA) is derived from the minerals found in coal during its combustion. Coal combustion method contributes approximately 37 % of the total electricity production in the world [1]. Pulverized coal injected into the furnace undergoes combustion with pre-heated air in coal fired power stations which resulted in CFA as a by-product. During coal combustion, the minerals partially melt to form fly ash particles in which the crystalline phases such as quartz and mullite remained in the core while the glass phase comprised aluminosilicates cover the surface.

The glass phase plays an important role in the zeolite formation because of its high solubility in alkaline solution. The thermal fusion of coal fly ash and sodium hydroxide has been the standard method to prepare sodium silicate [2]. Coal fly ash and sodium hydroxide (CFA: NaOH = 1 : 1.2 by weight) was heated in a furnace at 550°C for 1 hour to obtain a fused mass. The fused mass based on its XRD is found to be sodium silicate.

Sodium silicate is an important starting material and a source of soluble silica for the preparations of zeolites such as faujasite, zeolite P, zeolite X, hydroxysodalite [3-5] and mesoporous materials such as MCM-41 [6,7]. Zeolites have wide applications amongst which include adsorbents, reaction catalysts, catalyst support and filtering agents [8-16]. Recently, microwave assisted zeolite synthesis has been reported in the literature [17]. However, till date there has been no report in the literature on the microwave assisted synthesis of sodium silicate.

A proposed reason for this is the one-step thermal fusion method reported in the literature has been successfully and widely used by researchers in converting quartz and mullite found in silica into the

more soluble form of sodium silicates and other aluminosilicates [18]. Hence there is no strong reason to find an alternative method to prepare sodium silicate.

This paper reports the results of our attempt to synthesize sodium silicate using a domestic microwave oven. Using the microwave assisted method the reaction time was significantly reduced from 60 minutes to 2 minutes. The shortening of reaction time proves attractive for efficient industrial production.

EXPERIMENTAL PROCEDURE

Materials

CFA used in this study was obtained from Kapar Power Station which belonged to the National Electricity Board of Malaysia. Sodium hydroxide of analytical grade from Merck was used without further purification. The chemical composition of CFA is shown in Table 1.

Table 1. Chemical composition (wt %) of as-received CFA.

Oxide	wt %
SiO_2	65.7 ± 0.02
Al_2O_3	15.5 ± 0.01
Fe_2O_3	15.7 ± 0.01
K_2O	1.43 ± 0.01
CaO	1.16 ± 0.01
TiO_2	0.34 ± 0.01
MnO	0.09 ± 0.01
Na_2O	0.03 ± 0.01

Microwave assisted reaction of CFA and NaOH

Sodium hydroxide (2.2 g) was ground in a mortar and pestle until fine. CFA was dried overnight in an oven at 120 °C before use. 2.0 g of CFA was then added to the NaOH powder and the mixture was ground further to mix both starting materials together. The mixture was transferred to a porcelain crucible, covered and then heated for 2 minutes at 450 Watts in a domestic microwave oven.

The above reaction was repeated with various other combinations of CFA to NaOH as shown in Table 2. Ratios between CFA : NaOH from 1 : 1.1 up to 1 : 1.8 were attempted. It must be noted at this point that the optimum ratio between CFA and NaOH used in the thermal fusion method reported in the literature is 1 : 1.2 [7].

Table 2. Various ratios of CFA to NaOH (irradiation time 2 minutes).

Reaction	Mass of CFA (g)	Mass of NaOH (g)	CFA:NAOH
1	2.0	2.4	1 : 1.2
2	2.0	2.9	1 : 1.4
3	2.0	3.2	1 : 1.6
4	2.0	3.6	1 : 1.8

Characterization

X-ray diffraction patterns of the products were recorded on an automatic diffractometer Rigaku Geiger-Flex using CuK_a radiation (30 kV, 20 mA) for 2q angles from 10-80 degrees (sintered CFA with/without alkali additive). The particle morphologies were observed by a Scanning Electron Microscope (SEM) of Phillips X2500, JEOL JSM 6300 and LEO 1450 VP with acceleration voltage of 20 kV. The samples were deposited on a carbon tape mounted on a sample holder sputtered with 60 nm thickness of gold.

RESULTS AND DISCUSSION

When CFA and NaOH of various ratios from 1:1 to 1:1.8 were subjected to microwave radiation for 2 minutes, the product obtained in each case was gray in colour. The products from the reactions of CFA : NaOH of mass ratios 1:1.1 - 1:1.4 were friable/powdery in texture. However, the products obtained from the reactions of CFA : NaOH of mass ratios 1:1.6 - 1:1.8 were hard and removing them from the crucibles proved to be difficult when on a number of occasions the crucibles cracked before all the product could be removed from them. Thus it can be concluded from these observations that as the amount of NaOH in the reaction mixture increased, the hardness of the fused product also increased. It is worth noting at this stage that the thermal fusion reaction carried out at 550 °C for 1 hour also produced a gray coloured powdery product.

X-ray diffraction patterns

The X-ray diffraction pattern of as-received CFA exhibits mullite and quartz as the major crystalline phases and aluminosilicate glass as an amorphous phase (Fig. 1a). The XRD patterns of the fused products from the various ratios of CFA : NaOH (1:1.1 - 1:1.8) are shown in Figures 1b – 1f. Products from the CFA : NaOH = 1:1.1 and 1:1.2 reactions are observed to have similar XRD patterns where the major phase observed

is due to sodium silicate. The disappearance of both quartz and mullite peaks in the fused products indicated that silica in its crystalline form had reacted with NaOH to form soluble sodium silicate species.

However, as the ratio of CFA : NaOH increased (1:1.4 - 1:1.8), the XRD patterns of the products showed the presence of other peaks in addition to those due to sodium silicate. The additional peaks observed are indicative of the presence of mixed phases although the major phase was still due to sodium silicate.

The XRD pattern for the product obtained from the microwave assisted fusion reaction of CFA and NaOH (ratio 1:1.2) was compared with that of the product using the thermal fusion method (Fig. 2). It is observed that the peaks present in the XRD pattern of the sodium silicate produced from the thermal fusion method are present in the product from the microwave-assisted reaction. This implied that the microwave assisted fusion reaction between CFA and NaOH has been successful and that the major product obtained is sodium silicate together with faujasites. The fusion reaction using the domestic microwave oven is thirty times faster compared to the thermal fusion reaction (2 minutes versus 60 minutes).

Morphology

The SEM image of as-received CFA is shown in Figure 3a. The as-received CFA exhibited a number of smooth spherical particles of cenosphere morphology interspersed with aggregates of crystalline compounds. The spherical particles with diameter less than 20 μm which are smooth and glassy are the amorphous aluminium silicate. The crystalline compounds observed are mullite and quartz. The images of both the microwave assisted fused CFA and thermally fused CFA are shown in Figures 4b and 4c respectively. Both images exhibit amorphous spherical agglomerates of sodium silicate and sodium aluminosilicate with the agglomerates from the microwave assisted reaction being much larger. No compound of distorted octahedron morphology corresponding to faujasites was observed in the SEM image of the product from the microwave assisted reaction. However, faujasite peaks were observed in the XRD of the product from the microwave assisted reaction. The larger agglomerates observed in the SEM image of the microwave assisted product could be due to fast melting of the silica when the microwave oven was turned on. This is in contrast with the thermal assisted reaction where the silica melted slowly as the temperature increased hence resulting in smaller agglomerations. Because of the larger agglomerations produced in the microwave assisted reaction, crystalline faujasites of distorted octahedron morphology formed may be hidden by them.

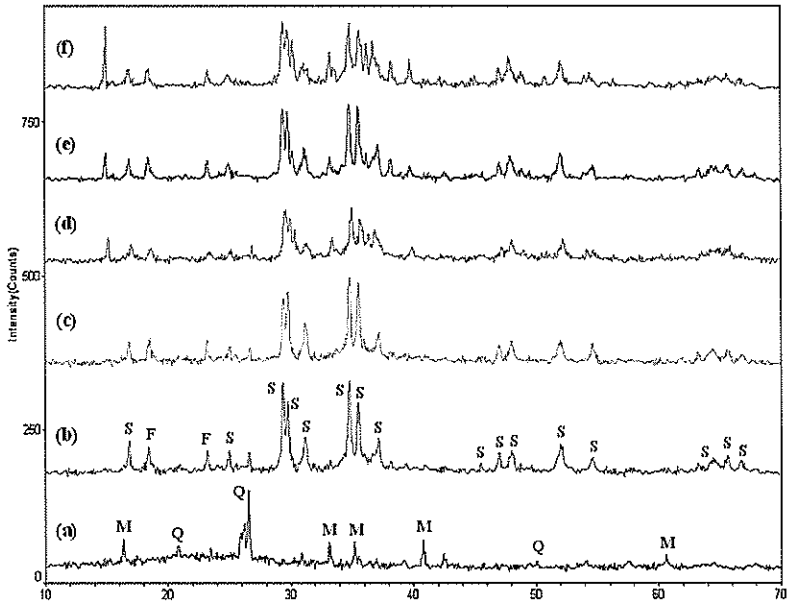

Figure 1. XRD images of (a) as-received CFA, (b) CFA:NaOH = 1:1.1, (c) CFA:NaOH = 1:1.2, (d) CFA:NaOH = 1:1.4, (e) CFA:NaOH = 1:1.6, and (f) CFA:NaOH = 1:1.8. M = Mullite; Q = Quartz; S = Sodium silicate; F = Faujasite.

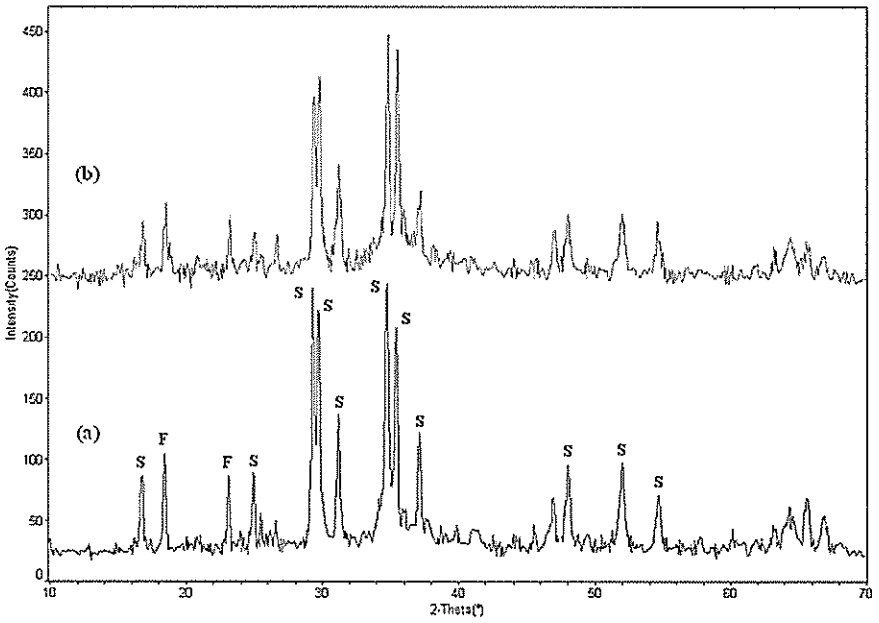

Figure 2. XRD image of product from (a) thermal reaction at 550°C (ratio CFA : NaOH = 1 : 1.2) and (b) microwave-assisted reaction (ratio CFA : NaOH = 1 : 1.2). S = Sodium silicate; F = Faujasite.

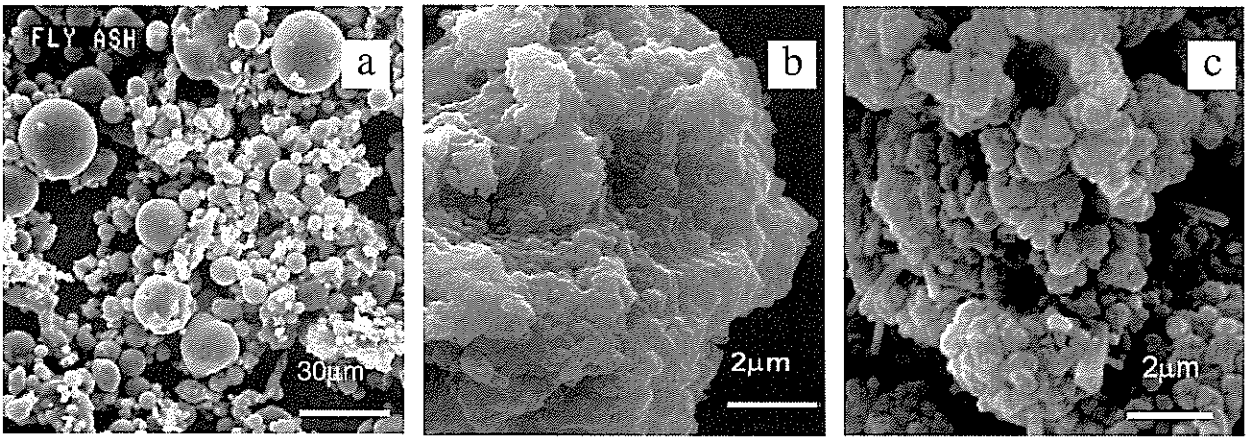

Figure 3. SEM images of (a) as received CFA, (b) microwave assisted fused CFA, (c) fused CFA at 550 °C.

CONCLUSIONS

In this study, sodium silicate was successfully prepared from CFA, a waste material from coal fired power plant, using a domestic microwave oven. Based on the similarity of the XRD patterns of the products between the microwave assisted and the thermal assisted fusion reactions, it can be concluded that sodium silicate was successfully prepared when the ratio of CFA : NaOH were.1 : 1.1 and 1: 1.2 and the exposure time to microwave irradiation of 2 minutes were used. The microwave assisted procedure is faster with the fusion reaction completed in just 2 minutes compared to 60 minutes using the sintering procedure. Ongoing work on the preparation of mesoporous materials from the microwave assisted fused CFA will be reported in the future.

Acknowledgements – The authors thank SIRIM Berhad, UKM and UNITEN for various assistance rendered.

REFERENCES

1. Zevenbergen C., Bradley J.P., Reeuwijk L.P.V., Shyam A.K., Hjelmar O. and Comans R.N.J. (1999) *Environ. Sci. Technol.* **33**: 3405.
2. Prashant K., Nawal M., Yasunori O., Kazuo Y and Tsuneji S. (2001) *J. Mater. Chem.* **11**: 3285.
3. Mouhtaris T., Charistos D., Kantiranis N., Fillipidus A., Kassoli-Fournaraki A. and Tsirambidis A. (2003) *Microporous and Mesoporous Mat.* **61**: 57.
4. Chang H.L. and Shis W.L. (1998) *Ind. Chem. Res.* **37**: 71.
5. Chang H.L. and Shis W.L. (2000) *Ind. Chem. Res.* **39**: 4185.
6. Kumar P., Mal N., Oumi Y., Sano T. and Yamana K. (2002) *Studies in Surface Sci. and Catalysis* **141**: 159.
7. Chang H-L., Chun C-M., Aksay I.A. and Shih W-H. (1999). *Ind. Chem. Res.*, **38**, 973.
8. Beck, J.S., Vartulli, J.C., Roth, W.J., Leonowicz, M.E., Kresge, C.T., Schmitt, K.D., Chu, C.T.-W., Olson, D.H., Sheppard, E.W., McCullen, S.B., Higgins, J.B., Schlenker, J.L. (1992), *J. Am. Chem. Soc.*, **114**, 10834.
9. Yanagisawa, T., Shimizu, T., Kuroda, K., Kato, C. (1990) *Bull. Chem. Soc. Jpn.* **63**: 988.
10. Inagaki, S., Fukushima, Y., Kuroda, K. J. (1993) *Chem. Comm.* 680.
11. Inagaki, S., Koiwai, A., Suzuki, N., Fukushima, Y., Kuroda, K. (1996) *Bull. Chem. Soc. Jpn.* **69**: 1449.
12. Prasad, P.N. (1991) *Polymer* **32**: 1746.
13. Avnir, D., Levy, D., Reisfeld, R. (1984) *J. Phys. Chem.* **88**: 5956.
14. Tanaka, H., Takahashi, H., Tsuchiya, J. (1989) *J. Non-Cryst. Solids.* **109**: 164.
15. Pang, Y., Samoc, M., Prasad, P.N. (1991) *J. Chem. Phys.* **94**: 5282.
16. C. Wang, B., Wilkes, G.L. (1994) *J. Macromol. Sci. Pure Appl. Chem.* **A31**: 249.
17. Inada M, Tsujimoto H, Eguchi Y, Enomoto N and Hojo J. (2005) *Fuel* **84**: 1482-1486.
18. Shigemoto M, Hayashi H. and Miyaura K. (1993) *J. Mater. Sci.* **28**: 4781-4786.

Journal of Science and Technology in the Tropics (2006) **2**: 65-74

Application of two-level full factorial design to lactic acid production using immobilized *Lactobacillus delbrueckii* from pineapple waste

Ani Idris[a]*, Suzana Wahidin[a] and M.Y. Noordin[b]
[a]Department of Bioprocess Engineering, Faculty of Chemical and Natural Resoources Engineering, Universiti Teknologi Malaysia , 81310 UTM, Skudai, Johor Bahru, Johor, Malaysia
[b]Department of Manufacturing and Industrial Engineering, Faculty of Mechanical Engineering, Universiti Teknologi Malaysia , 81310 UTM, Skudai, Johor Bahru, Johor, Malaysia
*E-mail: ani@fkkksa.utm.my

Abstract The use of pineapple waste for lactic acid production was investigated using immobilized *Lactobacillus delbrueckii* subsp. *delbrueckii* ATCC 9646 under anaerobic conditions. The two-level full factorial method has been employed to study the factors affecting lactic acid production and to determine the optimum conditions for its maximum production. The factors considered include initial pH, temperature, Na-alginate concentration, inoculums size and bead diameter whilst the response variable is lactic acid production. The experimental results indicate that bead diameter is the most significant factor that influences lactic acid production, followed by Na-alginate concentration, temperature and initial pH. A maximum lactic acid yield of 94.8% is obtained using 1 mm diameter immobilized beads consisting of 2 % Na-alginate concentration at initial pH 6.5 and temperature 37 °C.

Keywords lactic acid – immobilized – *Lactobacillus delbrueckii* – two-level full factorial design – fermentation

INTRODUCTION

The fermentative production of lactic acid must be cost-competitive with chemical synthesis. Fermentation media can represent almost 30% of the cost for microbial fermentation [1]. General media used for growth of lactic acid bacteria are not economically attractive because of their expensive nutrients such as yeast extract and peptone [2]. New low-cost media for lactic acid fermentation are needed to enhance the economics of lactic acid production by lactic acid bacteria. Currently, lactic acid production through free cell fermentation provides about 50% of the world supply, but the productivity is very low in conventional batch processes. However by employing cell immobilization method that provides high density can increase the productivity. Immobilized cell systems offer the advantages of high volumetric productivity than batch fermentation system, the possibility of continuous operation and higher stability [3]. The immobilized preparation can then be reused either in batch or in a continuous system and hence diminished the cost of the process. For immobilized cell system, for instance, dilution rates, which far exceed the growth rate of the cells, can be used without risk of cell washout, as would occur in the comparable free cell system. Immobilized cells exhibit many advantages over free cells, such as relative ease of product separation, reuse of biocatalysts, high volumetric productivity, improved process control and reduces susceptibility of cell contamination [4].

Several authors have studied lactic acid production by immobilized organisms using whey, starch, cane molasses, beet molasses and synthetic medium containing lactose and glucose as substrate. Kanwar *et al.* [5] produced lactic acid from cane molasses in continuous culture by free and Ca-alginate immobilized *Sporolactobacillus cellulosolvens* whilst Goksungur and Guvenc [3] produced lactic acid from beet molasses by immobilized *Lactobacillus delbrueckii*. Yan *et al.* [6] produced lactic acid from enzyme-thinned starch with immobilized *Lactobacillus amylovorus*. No work

has yet been done using fruits wastes such as pineapple waste which has high glucose content as the substrate.

In view of these, emphasis is being placed towards producing lactic acid from pineapple waste, focusing on the effects of various factors such as initial pH, temperature, cultivate size, Na-alginate concentration, bead size and substrate concentration since they are known to influence the fermentation process. In most fermentation studies, such as that by Goksungur and Guvenc [3], factors such as bead size, Na-alginate concentration and substrate concentration are studied using the one factor at a time experimental approach. Kanwar *et al.* [5], studied effects of pH and substrate concentration with free and immobilized cell fermentation using a similar approach which can be time consuming and exorbitant in cost. In this study, the two-level full factorial method involving 5 factors is used to investigate the effect of initial pH, temperature, cultivate size, Na-alginate concentration, bead diameter on the resulting lactic acid production. Such statistical experimental design allows planning of experiments so that the appropriate data can be analysed by statistical methods, resulting in valid and objective conclusions. Additionally, the optimum conditions can be accurately determined within the calculated confidence level and relationships will be quantified using mathematical modeling.

MATERIALS AND METHODS

Full factorial design method

Factorial design is a collection of mathematical and statistical techniques that are useful for the modeling and analysis of problems in which a response of interest is influenced by several variables. Factorial designs are used primarily for screening significant factors but can also be used sequentially to model and refine a process. Its purpose is to eliminate non significant factors so that efforts may be concentrated upon the important ones. In this study we utilized the two-level full factorial design, where the dependent variable, lactic acid concentration, was assigned at two levels.

A full factorial design (FFD) investigates all possible combinations of value of each experimental factor. It allows the independent estimation of the signals associated with each factor and with each combination of factors (interactions) and also provides good estimates of experimental error or noise. It has been widely used in the development of physical and biotechnology process because it provides data to (a) estimate linear, curvature and interaction effects of the variables studied, (b) significant effect, and (c) generate statistically valid mathematical models which can be utilized for graphic interpretation of the process under study [7].

The version 6 of Design Expert software was used to develop the experimental plan for factorial design. The same software was also used to analyze the data collected. The data collected must be analyzed in a statistically sound manner using regression, whereby an observed, empirical variable (response) is approximated based on a functional relationship between the estimated variable, y_{est} and one or more regressor or input variable $x_1, x_2, \ldots\ldots, x_i$. The least square technique is being used to fit a model equation containing the said regressors or input variables by minimizing the residual error measured by the sum of square deviations between the actual and estimated responses. The calculated coefficients or the model equation need to however be tested for statistical significance.

Liquid pineapple waste treatment

The liquid pineapple waste contained undissolved and suspended particulate matter that might interfere with the fermentation process and thus must be removed. The solution was boiled for 5 minutes resulting in flocculation of particulates and these settled rapidly upon cooling to room temperature. The particulate was then separated by centrifugation for 15 minutes at 4000 rpm. The clear supernatant was filtered using Whatman no. 54 filter paper under vacuum and stored at –18°C.

Strain and culture media

The microorganism used in this study was *Lactobacillus delbrueckii* subsp *delbrueckii* ATCC 9649 supplied from Deutsche Sammlung Von Mikroorganismen Und Zelkulturen GmbH, Braunschweig, Germany. The strain was maintained at 4°C on MRS agar. The composition for 1L MRS medium are as follows: 5g yeast extract; 5g meat extract; 10g peptone; 2g K_2HPO_4; 5g diammonium citrate; 20g glucose; 2g sodium acetate; 0.58g $MgSO_4.7H_2O$; 0.25g $MnSO_4.4H_2O$ and 1ml Tween-80.

Cell immobilization

Lactobacillus delbrueckii cells grown in a 25 cm^3 MRS broth (Oxoid) was mixed with an equal volume (1:1, v/v) of Na-alginate (Sigma, A-2033) solution. A 50 cm^3

aliquot of alginate-cell suspension was added drop wise to 1000 ml of 0.2 M $CaCl_2$ by a peristaltic pump. The alginate drops solidified upon contact with $CaCl_2$, forming beads thus entrapping bacteria cells. The beads were allowed to harden for 30 minutes. The beads were then washed with sterile physiological solution (0.85% NaCl) to remove excess calcium ions and cells. The beads were incubated overnight in the population medium at 45 °C overnight and the beads were stored at 4 °C before being used.

Analytical methods

Lactic acid and glucose concentrations were determined by HPLC. For lactic acid, a 250 mm x 4.6 mm ID Spherisob Octyl Column manufactured by Waters was used with a UV detector. The wavelength used in the UV detector is in the region of 210 nm. The adsorbed substances were eluted with 0.2 M H_3PO_4 at flow rate of 0.5 ml/min at room temperature. For glucose, a 4 mm diameter, 300 mm long ID m Bondapak/ Carbohydrate column manufactured by Waters with RI detector were used. The carrier solution used was acetonitrile:water (80:20) at a flow rate 1.0 ml/min at room temperature. The concentration of living cells entrapped in Ca-alginate beads was determined by dissolving three beads in 10 ml of 0.3 M sodium citrate solution (adjusted to pH 5.0 with 1 M citric acid) for 20 minutes with continuous stirring at room temperature. For determining the cell number entrapped in Ca-alginate beads and leaked cells from the gel beads, bacterial counts were done by plating on MRS agar and incubating them at 37 °C for 48 hours.

Experimental plan design approach

In this study, the substrate concentration is fixed, since the maximum amount of glucose in the pineapple waste is only 31.3g/L. The five parameters studied are Na-alginate concentration, initial pH, temperature, cultivate size and bead diameter while the corresponding response variable investigated is lactic acid production.

Since there are many parameters involved, a screening process is performed so as to determine the best or optimal setting for these factors and indicate whether or not curvature exists in the responses. The design has coded levels for each of the factors. There are numerous construction methods for numerous types of designs. In choosing a screening method there are five main factors to consider. Each of the five factors are represented by two levels namely a high level denoted by (+) and a low level designated by (-) as shown in Table 1. A two level design is used because of its ease of interpretation and their effectiveness.

The variables used in this study and their variation limits were initial pH 4.5 to 6.5; temperature at 37 °C to 50 °C; Na-alginate concentration 2% to 8% w/v; cultivate size 5% to 15% and bead diameter 1.0 mm to 5.0 mm. The normalized (coded) dimensionless variables employed having variations limit (-1, 1) were defined as A (coded temperature), B (coded pH), C (coded Na-alginate concentration), D (coded bead diameter) and E (coded cultivate size).

Temperature is one of the important factors affecting fermentation process. The effect of temperature on the production of lactic acid has only been studied in a few reports. In most cases batch fermentations were conducted at 35°C to 45°C. In this study, the submerged fermentation is set at 37°C for the lower level and 50°C for the upper level. A study by Hofvendahl and Hagerdal [8] has revealed that the optimal temperatures were 37°C and 40°C for maximum lactic acid production and yield respectively. Mostafa [9] in his studies of lactic acid from whey with agar immobilized cells in a packed tubular reactor obtained the maximum percentage of lactic acid of 2.75% at 40°C. Zayed and Winter [10] reported the optimum lactic acid concentration was 12 g/L at 30°C. Although there have been studies reported on the effect of temperature on the production of lactic acid, they used different substrates such as beet molasses and whey.

The fermentation pH is either set at the beginning or left to decrease due to acid production or it is controlled by base titration. Hofvendahl and Hagerdal

Table 1. The low and high levels for the factors affecting the immobilized cell.

Factor	Units	Low level (-1)	High level (+1)
Temperature (A)	°C	37	50
Initial pH (B)		4.5	6.5
Na-alginate concentration (C)	(w/v) %	2.0	8.0
Bead diameter (D)	mm	1.0	5.0
Cultivate size (E)	g	5.0	15.0

Table 1. Bacterial isolates selected from *Pseudomonas* CN medium and screened for the ability to grow in CPO as the sole carbon source and produce PHA from CPO.

Soil	No. isolates selected	Isolates that could grow in CPO medium	Isolates that produce PHA
A: around young oil palm trees	3	0	0
B: around mature oil palm trees	9	1	0
C: under stacks of oil palm fruit bunches	7	4	2 (MH1 & MH2)

Table 2. Amount of biomass and PHA produced by MH1 and MH2 when grown for 48 hours in nitrogen-limiting medium containing 0.5% w/v CPO.

Isolate	Biomass (CDW, g/L)	PHA (g/L)	PHA Content (% CDW)
MH1	1.3 ± 0.1	0.14 ± 0.07	10.8
MH2	2.6 ± 0.2	0.48 ± 0.01	18.5

CDW = cell dry weight

MH1 and MH2 are both gram-negative and rod-shape (general characteristics of the genus *Pseudomonas*). The Biolog Microstation System indicated that MH1 had 65.6% similarity to *Pseudomonas aeruginosa*, and MH2 had 77.3% similarity to the same species. As there was less than 80% similarity to the standard strain of *Pseudomonas aeruginosa*, it would be prudent for the moment to name MH1 and MH2 as *Pseudomonas* sp.

Cell growth and production of PHA

Table 2 shows the amount of biomass and PHA produced by MH1 and MH2 when grown with CPO as the sole carbon source for 48 hr. In early studies conducted by this laboratory, *Pseudomonas putida* PGA1 (not an indigenous bacterial isolate) produced 3.0 g/L biomass comprising 37% PHA_{MCL} with saponified palm kernel oil as the sole carbon source [6]. The palm kernel oil had to be saponified before feeding to *P. putida* PGA1 because the bacteria could not metabolise the triglyceride. A technique was then developed by this laboratory to specifically isolate bacteria that could metabolise palm oil to produce PHA [7]. As a result of this, FLP1, a bacterial strain isolated from palm oil mill effluent was obtained, and it metabolised crude palm oil to produce 4.2 g/L biomass of which 50% was poly(3-hydroxybutyrate), a short-chain-length PHA.

Removal of oily impurities from the extracted PHA

The polymers produced by both MH1 and MH2 were sticky in nature and, when air-dried, the polymers formed slightly yellowish transparent films which were oily. The oiliness might be due to the presence of remnant CPO from the culture broth which adhered to the PHA during the extraction process. In order to reduce the amount of these oily impurities, a simple method based on liquid-liquid separation was developed. The extracted oily PHA film was first dissolved in a minimal amount of chloroform. This chloroform solution (containing the dissolved PHA) was added drop-wise into a rapidly-stirred methanol-distilled water mixture (1:2 v/v) in a conical flask, then left to stand for several minutes for phase separation. The chloroform settled at the bottom of the conical flask while the methanol-distilled water solution was on top. An oily layer was found on the surface of the methanol-distilled water layer. The bottom chloroform layer was removed from the conical flask by using a long-tip Pasteur pipette, then it was added drop-wise into a fresh rapidly-stirred methanol-distilled water solution. This procedure was repeated until no more oily deposits were seen on the surface of the methanol-distilled water layer. The bottom chloroform layer was then pipetted out and added drop-wise into 10 volumes of rapidly-stirred methanol to allow the PHA to precipitate.

[8] reported the optimal initial pH for lactic acid production varies between pH 5 and pH 7. His work revealed that 81 g/L and 49 g/L of lactic acid were produced at pH 5 and pH 7 respectively. Studies by Mostafa [9] have revealed that initial pH 6.5 of fermentation medium produced highest lactic acid of 1.58%. Zayed and Winter [10] in their study on batch and continuous production of lactic acid from salt whey using free and immobilized cultures of *Lactobacilli* revealed that optimum initial pH was between 6 to 7. The highest lactic acid was produced with 62.3 g/L at initial pH 6.5. Investigation on lactic acid production by Senthuran *et al.* [11] showed that productivity was highest at initial pH 6.5 when using hydrolyzed whey protein. The productivity decreased for successive batches in immobilized cell at initial pH 5.5. It was reported at initial pH 7.0 and above the product yield dropped significantly. In this study, the initial pH is set with a lower level of pH 4.5 and an upper level of pH 8.5.

Bead diameter is another factor that affects the lactic acid fermentation using immobilized *Lactobacillus delbrueckii.* Goksungur and Guvenc [3] in his early studies used various Ca-alginate bead sizes ranking from 1.3 to 3.2 mm diameter. It was reported that the highest lactic acid production was obtained with cell entrapped in the 1.3 to 1.7mm Ca-alginate bead. Abdel-Naby *et al.* [12] reported maximum lactic acid was produced with cell entrapped in 2.0mm Ca-alginate bead. In this study, the cells were entrapped in 1.0mm Ca-alginate bead for the lower level and 5.0mm Ca-alginate bead for the upper level.

Besides varying the Ca-alginate bead diameter, Na-alginate concentration is also varied. In this study, the Na-alginate is set with a lower level of 2.0% w/v and an upper level of 8.0%w/v. Goksungur and Guvenc [3] reported that maximum lactic acid production, 5.93% was obtained with beads prepared at 2.0% w/v of Na-alginate concentration. Abdel-Naby *et al.* [12] investigated lactic acid by Ca-alginate immobilized lactic acid and determined the maximum lactic acid production with beads containing 3.0% Na-alginate concentration and obtained lower yields with beads made of 4.0 and 6.0% alginate due to diffusion problem.

The inoculums size is normally in the range of 3.0% to 15% (v/v) of the culture volume [12] for free cell fermentation. Studies by Atkinson and Mavituna [13] the inoculum volume is usually about 5 to 10% (v/v) of the fermentation broth volume. It was reported that 5.0% of inoculum size produced highest lactic acid production. In this study, the inoculum size used is 5.0g bead for the lower level end and 15.0g bead for the upper level. The cell concentration (cfu) immobilized in 1 bead and the weight of 1 bead can be determined. Thus by varying the weight of beads the inoculum size is varied. In our study the inoculum size is reflected in terms of the weight of beads. Thus the 5 g bead and 15.0g bead represents the lower and higher inoculum sizes respectively.

Experimental conditions

A total of 34 experiments were carried out under anaerobic conditions as outlined in Table 2. The two-level full factorial design (2^5) was used to determine the significant factors affecting lactic acid production in shake flask fermentation by immobilized *Lactobacillus delbrueckii* onto pineapple waste medium. This design consists of 34 experiments runs with 32 factorial runs and two replicates of the center point. Each run corresponds to a set of values for the factors at which a measurement of the response, which is lactic acid production, is to be made.

RESULTS

The results from the fermentation trials performed as per the experimental plan are also presented in Table 2. The response variable results were input into the Design Expert software for further analysis as described in the following section.

Effects half normal probability plot

The factorial model was selected using the effects half normal probability plot. Generally, the model consists of main and interaction effects that are significant. The combination of the pure error effects and the main and interaction effects produce the half normal probability plot as shown in Figure 1. The significant effects show up as outliers in the upper right hand section of the plot. These are selected as one moves from the right to left along the ordered effects. The pure error points together with the insignificant effects should fall in a line near the zero effect level.

In this study, the significant effects such as bead diameter (D), Na-alginate concentration (C), temperature (A), pH (B), the interaction between Na-alginate concentration and bead diameter (CD), pH and bead diameter (BD) and temperature and bead diameter (AD) tend to have a normal distribution centered at their respective large effect value while the insignificant

Table 2. Experimental design layout and results.

Run	Factors					Response
	A: Temp °C	B: pH	C: Na-alginate conc. % w/v	D: Bead diameter, mm	E: Cultivate size, g	Lactic acid production, %
1	37	4.5	2	1	5	89.7
2	50	4.5	2	1	5	79.4
3	37	6.5	2	1	5	94.8
4	50	6.5	2	1	5	85.3
5	37	4.5	8	1	5	76.1
6	50	4.5	8	1	5	69.3
7	37	6.5	8	1	5	87.1
8	50	6.5	8	1	5	74.5
9	37	4.5	2	5	5	78.9
10	50	4.5	2	5	5	65.3
11	37	6.5	2	5	5	91.4
12	50	6.5	2	5	5	76.1
13	37	4.5	8	5	5	61.3
14	50	4.5	8	5	5	41.7
15	37	6.5	8	5	5	71.3
16	50	6.5	8	5	5	60.3
17	37	4.5	2	1	15	90.1
18	50	4.5	2	1	15	80.1
19	37	6.5	2	1	15	93.5
20	50	6.5	2	1	15	91.3
21	37	4.5	8	1	15	81.3
22	50	4.5	8	1	15	78.1
23	37	6.5	8	1	15	90.9
24	50	6.5	8	1	15	74.8
25	37	4.5	2	5	15	79.9
26	50	4.5	2	5	15	67.4
27	37	6.5	2	5	15	88.7
28	50	6.5	2	5	15	77.9
29	37	4.5	8	5	15	57.8
30	50	4.5	8	5	15	39.4
31	37	6.5	8	5	15	73.9
32	50	6.5	8	5	15	56.4
33	43.5	5.5	5	3	10	89.3
34	43.5	5.5	5	3	10	93.8

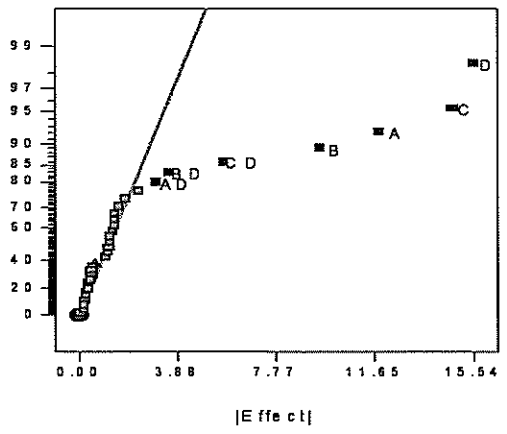

Figure 1. The half-normal probability plot of lactic acid production: A: temp, B: pH, C: Na-Alg, D: bead diam, E: cultivate.

effects such as cultivate size (E) and other interactions tend to have a normal distribution centered near zero.

Quantitatively, the half normal plot could be used to rank the order of factors according to its significance. Thus, based on Figure 1, it could be seen that bead diameter (D) has the largest effect followed by Na-alginate concentration (C), temperature (A) and pH (B). This is because bead diameter (D) has the largest absolute value show up as outliers in the upper right hand section of the graph and the square-dot for bead diameter (D) is the farthest away from the zero value. The interactions such as Na-alginate concentration-bead diameter (CD), temperature-bead diameter (AD) and pH-bead diameter (BD) are also significant and should be included with the main effects.

ANOVA analysis

An ANOVA table is commonly used to summarize the tests performed such as the test for significance of the regression model, and test for lack of fit. Table 3 shows the ANOVA table for the full factorial model for lactic acid fermentation. The model, F value of 96.61 implies that the model is significant. There is only a 0.01% chance that a model with F value this large could occur due to noise.

A value of <0.0001 for the "Prob. > F" value shown in Table 3 indicates a value of very much less than 0.05, which implies that the model is significant, and this is desirable as it indicates that the terms in the model have a significant effect on the response. In a similar manner the main effect of temperature (A), pH (B), Na-alginate concentration (C), bead diameter (D), and the two-level interaction of temperature-bead diameter (AD), pH-bead diameter (BD) and Na-alginate-bead diameter (CD) are significant model terms. Other model terms are not significant. These insignificant model terms can be removed and may result in an improved model [14]. The curvature F value of 53.46 implies there is significant curvature (as measured by difference between the averages of the factorial points) in the design space. There is only a 0.01% chance that a curvature F value this large could occur due to noise. A significant curvature may indicate that the design is in the region of an optimum [11].

The lack of fit value is tested against the pure error to see if the model adequately fits the response data model. In this study the lack of fit F value of 0.86 implies that the lack of fit is insignificant relative to the pure error. This is desirable as we want a model that fits.

The R^2 value is high (0.9644), close to 1, which is desirable. Since this value is very close to 1, it is concluded that the important effects identified explained most of the variability. The predicted R^2 is in reasonable agreement with the adjusted R^2. The adjusted R^2 value is particularly useful when comparing models with different number of terms. If there are many terms in the models and the sample size is not very large, the adjusted R^2 maybe noticeably smaller than the R^2. Adequate precision compares the range of the predicted values at the design points to the average predicted error. Ratios greater than 4 indicate adequate model discrimination. In this particular case the value is well above 4. The final empirical model in terms of coded factors is listed as follows:

Lactic aid production = 75.75 - 5.92A + 4.76B - 7.36C - 7.77D - 1.50AD + 1.76BD - 2.86CD

While the following equation is the final empirical models in terms of actual factors:

Lactic aid production = 105.381 - 0.564 * Temp + 2.128 * pH -1.026 * Na - alginate conc. - 1.315 * bead diameter - 0.115 * temp * bead diameter - 0.476 * Na - alginate conc. * bead diameter + 0.878 * pH * bead

Table 3. Analysis of variance (ANOVA) for the selected linear model.

Source	Sum of Squares	DF	Mean Square	F Value	Prob > F
Model	5944.49	7	849.21	96.61	< 0.0001 *significant*
A	1121.01	1	1121.01	127.53	< 0.0001
B	725.81	1	725.81	82.57	< 0.0001
C	1734.60	1	1734.60	197.34	< 0.0001
D	1931.31	1	1931.31	219.72	< 0.0001
AD	72.00	1	72.00	8.19	0.0084
BD	98.70	1	98.70	11.23	0.0026
CD	261.06	1	261.06	29.70	< 0.0001
Curvature	469.91	1	469.91	53.46	< 0.0001
Residual	219.75	25	8.79		
Lack of Fit	209.62	24	8.73	0.86	0.7077 *insignificant*
Pure Error	10.13	1	10.13		
Cor Total	6634.16	33			

Std. Dev.	2.96	R-Squared	0.9644
Mean	76.68	Adj R-Squared	0.9544
C.V.	3.87	Pred R-Squared	0.9377
PRESS	413.17	Adeq Precision	33.844

Model plot

(i) One-factor effect plots

The one factor effects graph shows the linear effect of changing the level of a single factor. It is constructed by predicting the responses for the low (-1) and high (+1) levels of a factor under consideration. Figure 2(a) to (d) show the one factor effect graphs for the various significant main effects identified. The magnitude of the effect estimates show that the bead diameter (D) is by far the most important factor. Na-alginate concentration (C) plays the next most important factor followed by temperature (A) and pH (B). Additionally the steepness of the graph also indicates the significance of the factors. Three of the effect estimates (A, C and D) are negative whilst the effect estimate B is positive. If only these main effects are to be considered for maximizing lactic acid production then factors A, C and D would be set to the low level (-1), while factor B would be set to the high level (+). Since factor E is not significant the level to be used is not important. Therefore select a level that would bring benefit to the experimenter

(ii) Interaction plot

Two factor interactions can have an important effect on the relationship between the response and the experimental factors. Figures 3a to 3c show the results of the contribution of the interaction effect between the temperature-bead diameter (AD), Na-alginate concentration-bead diameter (CD) and pH-bead diameter (BD) respectively. An interaction plot graphically shows the presence or absence of a two-factor interaction between two experimental factors. Interaction is present when the response is different depending on the settings of the two factors and the plot will show two non parallel lines.

In a factorial design the estimate of the two factor interaction effect is the average of the runs in which both factors are extreme (high-high and low-low) minus the average of the runs in which the factor level are mixed (high-low and low-high). This is the same as taking the difference of the averages of diagonal corners in the square plot. If there is no two-factor interaction this difference is zero (except for experimental error) because the two diagonal have symmetric changes in the factor levels. This is equivalent to the lines in the interaction plot being parallel.

All the interaction graphs of the significant two level interaction terms are shown in Figures 3(a) to 3(c). From the graphs plotted it can be seen that the effect of the two factor interactions is not very strong. The relatively small F value obtained for the various two factor interactions compared to the main effects further confirmed the weak two factor interactions. In this particular instance, consideration of the two factors interaction would yield similar settings as proposed when considering only main effects.

DISCUSSION

The effect of the bead diameter and Na-alginate concentration mostly cause the variation in the production of lactic acid. Thus in immobilization cell fermentation these two factors played an important role in determining the production of lactic acid. A one mm diameter bead diameter is favourable compared to larger diameter beads because nutrients and substrate can penetrate through the thin walls of the small diameter

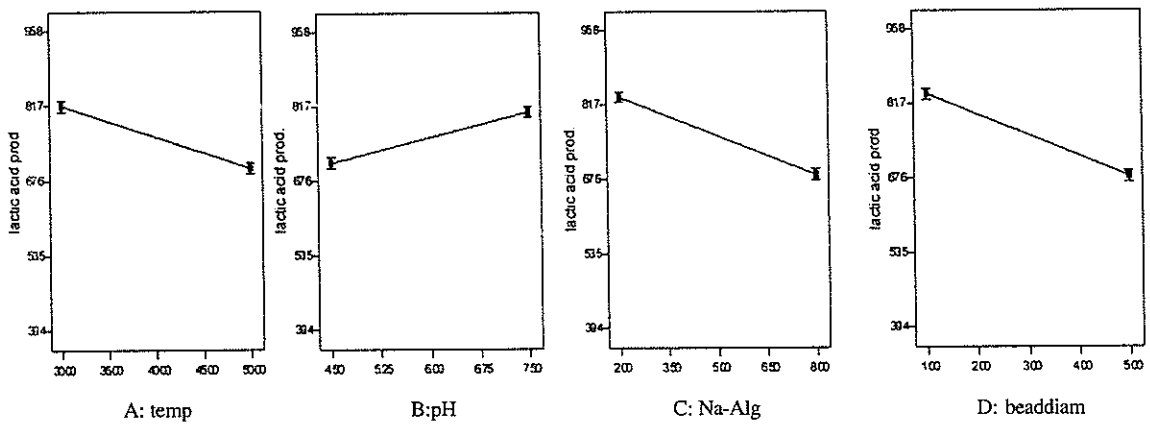

Figure 2. One-factor effects plot for the various significant main effects during lactic acid production.

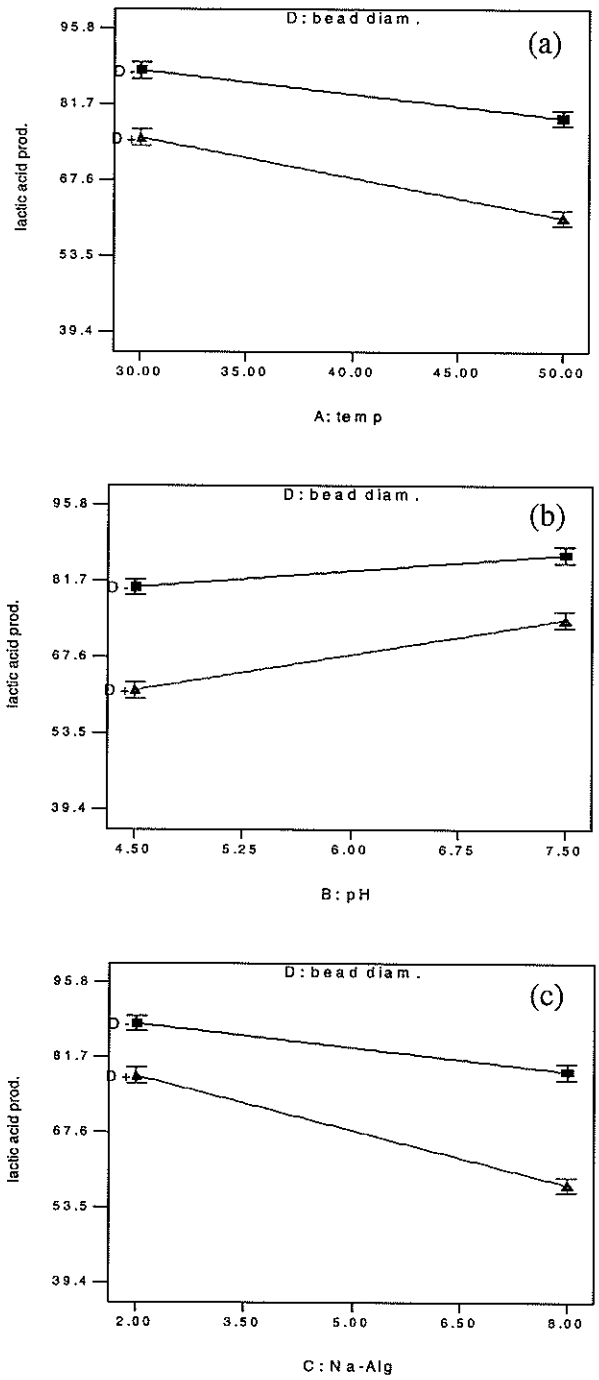

Figure 3. Interaction graph of various significant two-factor interaction terms during lactic acid production (a) temperature and bead diameter interaction (b) pH and bead diameter interaction and (c) Na-alginate and bead diameter interaction.

bead, thus ensuring ample supply of food for the *Lactobacillus delbrueckii* and with less resistance. This promotes the growth of cell mass thus producing higher amounts of lactic acid production. However the large diameter beads 5 mm in diameter house more cells and probably has thicker walls which do not allow easy access of nutrients and substrates to diffuse through thus hinder cell mass growth and results in a reduced amount of lactic acid production. The results seem to have some similarities to the work of Goksungkur and Guvenc [3] who found that the optimum bead diameter for glucose utilization is between 1.5 to 2 mm and as the bead diameter increases the glucose utilization decreases. This view was also shared by Abdel-Naby *et al.* [12] who had studied the effect of bead diameter for lactic acid production and found the optimum lactic acid yield was obtained using a 2mm bead diameter. Lactic acid production is reduced as bead diameter continues to increase.

Experimental analysis also revealed that the variation in the lactic acid production is contributed to Na-alginate concentration. For this study Na-alginate concentration seems to be the second most important factor that must be considered during the fermentation process. The Na-alginate concentration levels in this study was set to two levels, 2% being the lower limit and 8% being the upper limit. From the one factor plot it is observed that the 2% Na-alginate concentration gives higher production of lactic acid compared to the 8% Na-alginate concentration. This is explained by the fact that when the Na-alginate concentration is increased to 8%, the thickness of the membrane capsule decreases [15], and this is presumably due to the fact that on increasing the number of biopolymer molecules per unit solution, the binding sites for Ca^{2+} ions also increases. As a result a more densely cross-linked gel structure will probably form and consequently it will have a smaller thickness. The dense membrane is expected to create diffusion resistance through the beads which will result in lower product formation as nutrients and substrates are restricted to diffuse easily to the *Lactobacillus delbrueckii* cells. Thus high concentration of Na-alginate results in a less porous gel which consequently decreases the production of lactic acid. At this juncture, its optimum concentration has yet to be determined but the low concentration Na-alginate is observed to produce higher lactic acid probably due to less crosslinking of the alginate molecules taking place forming less densely packed three-dimensional lattice from the outermost layer to the core of the drop resulting

in easy diffusion of nutrients through the porous beads. Similar results were reported by Najafpour *et al.* [16] in ethanol production and Bandi *et al* [17] in neomycin production when using calcium alginate matrices.

The other factors, which contribute to variation in the experimental data, are temperature and initial pH in order of importance. The rate of lactic acid formation depends also on the temperature and initial pH. *Lactobacillus delbrueckii* which is a mesophilic bacteria seems to grow very well at 37°C compared to the higher temperatures thus resulting in high lactic acid production. These results are different to those reported by Goksungur and Guvenc [18] who used beet molasses as the substrate for their lactic acid production. They obtained the highest yield at 45°C and this might be due to the different substrate and strain used in lactic acid fermentation process. Initial pH of 6.5 is also suitable for *Lactobacillus delbrueckii* resulting in high cell mass and high production of lactic acid. It is possible that the lower initial pH brought too much stress on the organism metabolic abilities. The bacteria, *Lactobacillus delbrueckii* seems to grow well in a neutral environment with an initial pH of 6.5. An environment, which is too acidic, is not conducive for lactic acid production. These results seem to be in agreement with those obtained by Goksungur and Guvenc [18] where optimum initial pH of 6.5 is obtained using beet molasses.

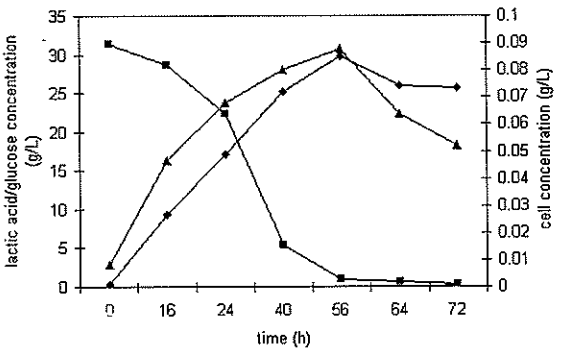

Figure 4. Relationships between cell concentration (▲), glucose consumption (■) and lactic acid production (◆) versus fermentation time.

Submerged fermentation or batch fermentation of pineapple waste to lactic acid by immobilized *Lactobacillus delbrueckii* was studied in 34 runs of experiment as a function of temperature, pH, inoculum size, bead diameter and sodium alginate concentration. In this study, from the 34 runs of experimental design, run 3 which was performed at 37°C, initial pH of 6.5, bead size 1 mm and 2% w/v Na-alginate concentration gave the maximum production of lactic acid. The relationship between cell concentrations, glucose consumption and lactic acid production versus fermentation time for run 3 is depicted in Figure 4. The result indicates that the lactic acid production depends on the microbial growth or cell concentration. Increase in microbial growth or cell concentration promotes lactic acid production. This means that there is a parallel relationship between cell and lactic acid concentration. Biosynthesis of lactic acid was carried out during the growth phase of the microorganisms. Maximum viable cell number (43.3×10^5) cfu/ml was observed after 56 hours of fermentation. As expected the glucose concentration reduces indicating substrate utilization during fermentation and there was an increase in growth of *Lactobacillus delbrueckii* which then promotes lactic acid production. The concentration of glucose reduces gradually during the first 24 h but then fell rapidly during the next 16 h of fermentation, after which it slowly decreased owing to rapid increase of lactic acid concentration. When the maximum concentration of lactic acid was attained, almost 97% of glucose had been converted to lactic acid. The results obtained in this study once again showed that the immobilized system is capable of producing higher amounts of lactic acid compared to free cell systems [19].

Acknowledgements – This work is financially supported by Ministry of Science, Technology and Environment, Malaysia through the IRPA funding vote no. 75089 and 74263.

REFERENCES

1. Miller T.L. and Churchill B.W. (1986) Substrates for large-scale fermentations, In Demain A.L. and Solomon D.C. (ed.) *Manual of industrial microbiology and biotechnology* pp.127-140. American Society for Microbiology, Washington, D. C
2. Mercier P., Yerushalmi L., Rouleau D. and Dochain D. (1992) Kinetics of lactic acid fermentation

on glucose and corn by *Lactobacillus Amylophilus*. *J. Chem. Tech. Biotechnol.* **55**: 11-121.

3. Goksungur Y. and Guvenc U. (1999) Production of lactic acid from beet molasses by calcium alginate immobilized *L. delbrueckii* IFO 3202 Batch and Continuous. *J. Chem. Eng. Biotechnol.* **74**: 131-136.
4. Goksungur Y. and Guvenc U. (1999) Batch and continuous production of lactic acid from beet molasses by *Lactobacillus delbrueckii*. *J. Chem. Tech. Biotechnol.* **69**: 399-404.
5. Kanwar S.S., Chadha B.S., Tewari H.K. and Sharma V.K. (1995) Short communication: Continuous production of lactic acid from molasses by free and immobilized *Sporoclactobacillus* cellulosolvents. *World J. Microbiol. Biotechnol.* **11**: 687 – 688.
6. Yan J., Bajpai R., Iannoti E., Popovic M. and Mueller R. (2001) Lactic acid fermentation from enzyme-thinned starch with immobilized *Lactobacillus amylovorus*. *Chem. Biochem. Eng.* **5**(2): 59-63.
7. Montgomery D.C. (2002) *Design And Analysis of Experiments*. 5th ed. John Wiley and Sons Inc., New York.
8. Hofvendahl K. and Hagerdal B.H. (1997) L-Lactic acid production from whole wheat flour hydrolysate using strain of *Lactobacilli* and *Lactococci*. *Enzyme Microb. Technol.* **20**(3): 303-307.
9. Mostafa N.A. (1996) Production of lactic acid from whey with agar immobilized cells in a continuous packed tubular reactor. *Energy Conversion Management* **37**(3): 253-260.
10. Zayed G. and Winter J. (1995) Batch and continuous production of lactic acid from salt whey using free and immobilized cultures of *Lactobacilli*. *Applied Microbiol. Biotechnol.* **44**: 362-366.
11. Senthuran A., Senthuran V., Rajni H. and Mattiasson B. (1999) Lactic acid production by immobilized *lactobacillus casei* in recycle batch reactor: A step toward optimization. *J. Biotechnol.* **73**(1): 61-70.
12. Abdel-Naby M., Mok K. and Lee C. (1992) Production of organic acid from enzymatic hydrolyzate of starch by immobilized lactic acid bacteria. *UNIDO Proceedings* 227-243.
13. Atkinson B. and Mavituna F. (1991) *Biochemical engineering and biotechnology handbook*. 2nd Ed. Stockton Press, New York.
14. Haaland P.D. (1993) *Experimental Design in Biotechnology*. Marcel Dekker Inc., New York.
15. Blandino A., Macias M. and Cantero D. (1999) Formation of calcium alginate gel capsules: Influence of sodium alginate and calcium chloride concentration on gelation kinetics. *J. Biosci. Bioeng.* **88**(6): 686-689.
16. Najafpour G., Habibollah Younesi and Ku Syahidak Ku Ismail (2004) Ethanol fermentation in an immobilized cell reactor using *Saccharomyces cerevisiae*. *Bioresource Technology* **92**(3): 251-260.
17. Bandi S., Kunamneni A. and Poluri Ellaiah (2003) Investigation on neomycin production with immobilized cells of *Streptomyces marinensis* Nuv-5 in calcium alginate matrix. *AAPS Pharm. Sci. Tech.* **4**(4) Article 57.
18. Goksungur Y. and Guvenc U. (1997) Batch and continuous production of lactic acid from beet molasses by *Lactobacillus Delbrueckii*. J. Chem. Eng. Biotechnol. **69**: 399-404.
19. Idris A., Suzana W. and Mat H.B. (2003) Lactic acid fermentation from pineapple waste using free and immobilized *Lactobacillus delbrueckii* atcc 9646. *Water Environment Management Series*.213-219.

Although this method could remove most of the oily impurities from the PHA, there are drawbacks, e.g. the method is tedious and would not be suitable for use in large scales. Furthermore, some low molecular weight PHA might be lost when they separate into the methanol-water layer from the chloroform layer. Therefore, more efficient oil-removal methods need to be developed if CPO is to be used as the sole carbon source for the production of PHA_{MCL} by MH1 and MH2. The studies in this report were conducted in the form of a batch culture in shake flasks, and the initial CPO concentration was 0.5% w/v. At higher production scales using vessel bioreactors, a fed-batch system whereby the carbon source is fed intermittently, is used to increase biomass and PHA productivities (unpublished data). By this fed-batch system, the problem of remnant oil occurring in the broth at the time of cell harvest might not arise.

Another way to avoid the adherence of remnant oil, glycerol or fatty acids to the extracted PHA would be to wash the cells well to remove these oily deposits before the PHA is extracted. However, much care needs to be exercised because solvents used at this stage to remove oily deposits from the cells might also remove the intracellular PHA should the cells break during the washing process.

PHA characterisation

The ^1H NMR spectra of the PHA extracted from MH1 and MH2 were similar to one another, and they closely resembled the PHA spectrum produced by *Pseudomonas* sp. Strain NCIMB40135 cultivated on glucose [8]. Likewise, the ^{13}C NMR spectra of the PHA from MH1 and MH2 were identical, each having 10 major peaks corresponding to the carbon

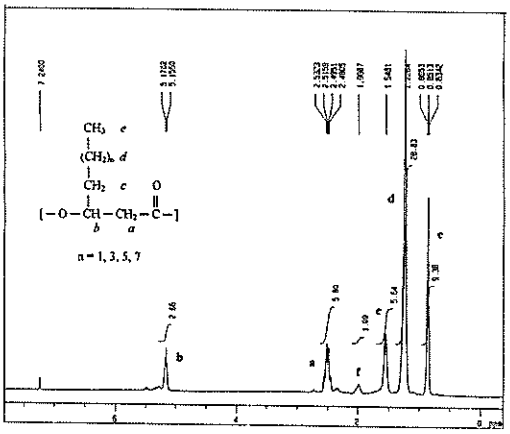

Figure 1. 400-MHz ^1H NMR spectrum of the PHA extracted from MH2 grown with CPO as the sole carbon source.

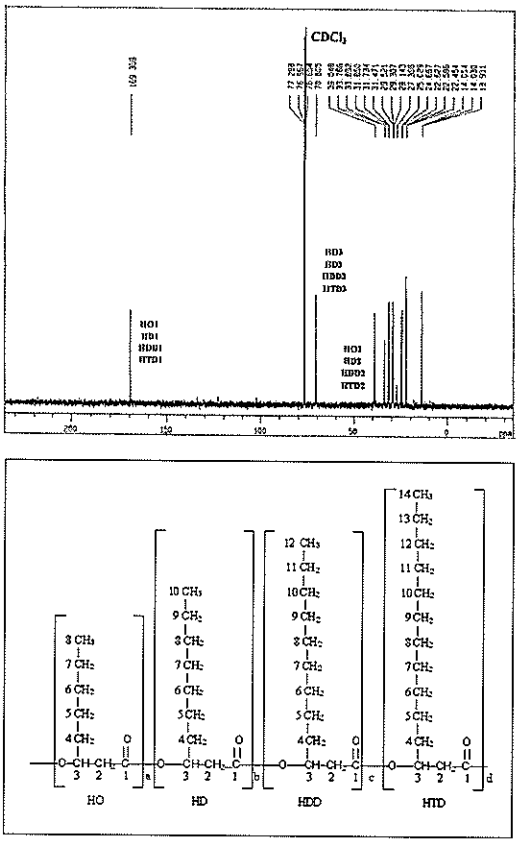

Figure 2. 100-MHz ^{13}C NMR spectrum of the PHA extracted from MH2 grown with CPO as the sole carbon source.

atoms of the monomer units. By referring to the reported chemical shift data [5], the various peaks could be identified as belonging to the monomer units of 3-hydroxyoctanoate (C_8), 3-hydroxydecanoate (C_{10}), 3-hydroxydodecanoate (C_{12}) and 3-hydroxytetradecanoate (C_{14}). The ^1H and ^{13}C NMR spectra of the PHA produced by MH1 and MH2 thus indicate that they are PHA_{MCL}. Figure 1 shows the ^1H NMR spectrum while Figure 2 shows the ^{13}C NMR spectrum of the PHA extracted from MH2.

GC analysis revealed that 3-hydroxyoctanoate and 3-hydroxydecanoate were the predominant monomers in the PHA produced by MH1 (56.3 mol % C8 and 33.4 mol % C10) and MH2 (54.0 mol % C8 and 33.5 mol % C10). C12, C14 and C16 monomeric units were also detected but they were in much lower proportions (Table 3). This lends further support that the PHA produced by MH1 and MH2 are PHA_{MCL}. As the sole carbon source was CPO, the precursors for the various monomeric units were very likely even carbon-number fatty acid intermediates arising from the β-oxidation of fatty acids [3]. The high proportions of C8 and C10 monomeric units suggest that the

Table 3. Chemical properties of PHA extracted from MH1 and MH2 grown in nitrogen-limiting medium containing 0.5% w/v CPO as the sole carbon source.

Isolate	Chemical properties of PHA										
	Monomer composition (mol%)					Thermal Properties			Molecular Mass		
	C8	C10	C12	C14	C16	T_m (°C)	H_m (J/g)	T_g (°C)	M_w	M_n	M_w/M_n
MH1	56.3	33.4	7.4	0.9	2.0	41.22	12.11	-35.74	50,167	28,988	1.73
MH2	54.0	33.5	8.6	1.4	2.5	41.86	9.64	-35.91	67,430	37,612	1.79

PHA synthase for the biosynthesis of PHA_{MCL} has higher affinity for these two precursors [9]. The major fatty acids in CPO are palmitic acid ($C_{16:0}$), oleic acid ($C_{18:1}$) and linoleic acid ($C_{18:2}$) [10], and these could be β-oxidised to the C8 and C10 intermediates which are then used by the PHA synthase to polymerise into PHA_{MCL}.

When the purified PHA from MH1 and MH2 were analysed by differential scanning calorimetry, both the polymers have T_g values around -35°C and a very small melting peak around 41°C. They exhibited low crystallinity as reflected in ΔH_m which were 12.11 J/g for MH1 and 9.64 J/g for MH2 respectively (Table 3). Both the polyesters can therefore be considered as elastomers at room temperature.

From the gel permeation chromatograph data, the PHA produced by MH1 has a number-average molecular mass (M_n) of 28,988 and a weight-average molecular mass (M_w) of 50,167, while the PHA produced by MH2 has a M_n of 37,612 and a M_w of 67,430. The polydispersity of both PHAs was around 1.7 (Table 3).

Acknowledgements – This study was funded by the Malaysian Ministry of Science, Technology and Innovation, under the Intensification of Research in Priority Areas (IRPA) programme, grant no. 09-02-03-0372. CPO was kindly given by Southern Acids (M) Ltd., Klang, Selangor, Malaysia.

REFERENCES

1. Atlas, R.M. (1993) *Handbook of Microbiological Media.* CRC Press Inc.
2. Doi, Y., Nakamura, Y., Soga, K. (1989) ^{1}H and ^{13}C NMR analysis of poly(β-hydroxybutyrate) isolated from *Bacillus megaterium. Macromol.* **19**: 1274-1276.
3. Lageveen, R.G., Huisman, G.W., Preusting, H., Ketelaar, P., Eggink, G., Witholt, B. (1988) Formation of polyesters by *Pseudomonas oleovorans* : Effect of substrates on formation and composition of poly-(R)-3-hydroxyalkanoates and poly-(R)-3-hydroxyalkenoates. *Appl. Environ. Microbiol.* **54**: 2924- 2932.
4. Ostle, A.G., Holt, J.G. (1982) Nile Blue A as a fluorescent stain for poly--hydroxybutyrate. *Appl. Environ. Microbiol.* **44**: 238-241.
5. Huijberts, G.N.M., van de Wal, H., Wilkinson, C., Eggink, G. (1994) Gas-chromatographic analysis of poly(3-hydroxyalkanoates) in bacteria. *Biotechnol. Technol.* **8**: 187-192.
6. Tan, I.K.P., Sudesh, K., Theanmalar, M., Gan, S.N., Gordon III, B. (1997) Saponified palm kernel oil and its major free fatty acids as carbon substrates for production of polyhydroxy-alkanoates in *Pseudomonas putida* PGA1. *Appl. Microbiol. Biotechnol.* **47**: 207-211.
7. Alias, Z., Tan, I.K.P. (2005) Isolation of palm oil-utilising, polyhydroxyalkanoate (PHA)-producing bacteria by an enrichment technique. *Bioresource Technol.* **96**: 1229-1234.
8. Haywood, G.W., Anderson, A.J., Dawes, E.A. (1989) A survey of the accumulation of novel polyhydroxyalkanoates by bacteria. *Biotechnol. Lett.* **11:** 471-476.
9. Ashby R.D. and Foglia T.A. (1998) Polyhydroxyalkanoates synthesis from triglycerides substrates. *Appl. Microbiol. Biotechnol.* **49**: 431-437.
10. Iftikhar, A. (1984) Significance of palm oil and palm stearin as fatty raw materials for soap. *PORIM Occassional Paper No. 13*, Palm Oil Research Institute of Malaysia, pp 3-9.